This project has received funding from the European Union's Horizon Europe Programme

SAMPLEIV [EASA.2020.FC05]

[DELIVERABLE 3: DATA REPORT]

Improving nvPM sampling and measurement system uncertainties

An Agency of the European Union

Disclaimer

Funded by the European Union. Views and opinions expressed are however those of the author(s) only and do not necessarily reflect those of the European Union or the European Union Aviation Safety Agency (EASA). Neither the European Union nor EASA can be held responsible for them.

DELIVERABLE NUMBER AND TITLE:	SAMPLEIV, D3
CONTRACT NUMBER:	EASA.2020.FC05
CONTRACTOR / AUTHOR:	Dr's E. Durand (Cardiff University), A.P. Crayford (Cardiff University), M. P. Johnson (Rolls-Royce plc) and P. I. Williams (University of Manchester)
IPR OWNER:	European Union Aviation Safety Agency
DISTRIBUTION:	Public

APPROVED BY:	AUTHOR	REVIEWER	MANAGING DEPARTMENT

DATE: March 2025

EXECUTIVE SUMMARY

Towards real-world reductions of emitted non-volatile Particulate Matter (nvPM), after years of extensive development and large-scale engine testing[1], the first nvPM certification requirement and emissions standard for aero-engines with thrust greater than 26.7 kN was introduced into ICAO Annex 16 Volume II during CAEP/10 (February 2016). The certification requirement established a standardised sampling and measurement system facilitating LTO and maximum reported Emission Indices (EIs) of nvPM mass and number and set a standard for nvPM mass. These measures required compliance for in-production engines on or before January 2020 and thereafter.

As part of ICAO CAEP/11, a new regulatory LTO metric system limiting both nvPM mass and number emissions was implemented, with applicability to new engine types (> 26.7 kN) starting in January 2023. However, significant uncertainties remain within the nvPM standard, with the representativeness of reported EIs to nvPM concentrations witnessed at the engine exhaust currently not fully characterised.

This report aims to quantify some of the uncertainties related to instrument calibration and drift, improve current methodologies for calculating the size-dependent loss of nvPM within the standardised sampling system, and additionally, explore some recent technical advancements which offer potential improvements to the sampling and measurement system, specifically in terms of simplifying measurements and reducing particle loss.

Uncertainty in calibrated VPR penetration efficiency was observed across different calibration laboratories, with particle pre-conditioning methods appearing to significantly impact the reported penetration efficiencies. Also, it was observed that two different commercially available compliant VPRs exhibited significantly different penetration performances, circa 15-20% across GMDs representative of nvPM, highlighting potential benefits in further standardising VPR calibration protocols and applying empirically derived correction factors for the known loss of particles. However, incorporating extra calibration points for particles smaller than 15 nm did not meaningfully improve VPR penetration efficiency curve fitting.

The type of particle used in calibration was found to affect CPC counting efficiency. To minimise calibration material dependency on counting efficiency, it is recommended to either use a CPC with a D_{90} or D_{50} well below 15 or 10 nm respectively (e.g., ≤7 nm), given particle type does not affect CPC counting accuracy (i.e., linearity), or to calibrate using appropriately pre-conditioned combustion nvPM. No statistically significant drift in nvPM number instruments was observed within the 12-month calibration period. Therefore, mandating the application of the CPC counting accuracy factor (k-factor), derived during calibration, within aviation nvPM standards (similar to current automotive regulations), would reduce CPC uncertainty from the stated ±10% to less than ±5%.

The current regulatory values of nvPM EI number do not account for size-dependent VPR particle loss and CPC counting efficiency, leading to under-predictions of engine exit number concentration by up to 83% and 5% respectively, for the smallest emitted particle size distributions (PSDs). Applying these values within a full size-dependent system particle loss correction (k_{SL_num}) would address these biases, thus improving airport inventories and likely reducing regulatory reporting uncertainty.

[1] See SAMPLE IV Deliverable 1 report

Calibration aerosol sources are known to impact nvPM mass uncertainty, significantly influencing the uncertainty in reported EIs. Potential surrogate nvPM mass calibration sources were therefore explored to better understand the particle morphology properties affecting nvPM mass instruments and to develop methods for in-field checks prior to engine testing. Various commercially available carbonaceous nanoparticle powders and 'real' aircraft-engine soot, collected from the exhaust system of a certification test-cell, were made into aqueous colloids that were shown to remain stable for several months. Nebulisation and drying of the colloid resulted in carbonaceous aerosols at concentrations representative of aircraft exhaust. The aerosols were characterised in terms of nvPM number, mass, size, and morphology, highlighting their viability as an in-field check for mass, number and sizing instruments. This study also indicates these colloids exhibit the potential to act as mass calibration sources in the future.

An assessment of measured PSD based system loss correction methods was undertaken using novel data, demonstrating a reduction in uncertainty in the reported penetration fraction (k_{SL}), compared to the current N/M-based ICAO regulatory method. It was observed that measured-PSD-based methods are particularly beneficial at low nvPM mass concentrations usually at small particle sizes, where diffusion losses in the sampling system are most pronounced. Towards future adoption of measured-PSD-based system loss correction standards, recommendations concerning best sampling and measurement practices and uncertainties of sizing instruments (DMS500, EEPS, ELPI+, and SMPS) are presented, which guided the development and drafting of SAE Aerospace information reports AIR6504A "Procedure for the Calculation of non-volatile Particulate Matter Sampling and Measurement System Penetration Functions and System Loss Correction Factors " and AIR7382 "Procedures for the Sampling and Measurement of Particle Size Distributions from Aircraft Turbine Engines".

"Novel" nvPM measurement techniques were developed and demonstrated, highlighting the potential to reduce sampling and measurement complexity and cost. Diffusion-based counters were successfully deployed at the probe exit during engine testing, exhibiting good agreement with reference nvPM number instruments and number concentrations derived from PSDs. Additionally, commercially available dilution systems, which offer controllable dilution factors, were shown to function across the full range of powers (dynamic probe pressures) of the engine (circa 30 kN) tested. This offers the potential to reduce uncertainties associated with low particle counts, whilst removing the requirement for a pressure dump line, minimising loss or bias in Splitter 1 and potentially providing greater operational flexibility for engine manufacturers to obtain gas and nvPM measurements in parallel. This work highlights that future optimal nvPM sampling and measurement systems may employ a single analyser with proven knowledge/ assumptions to determine nvPM size, number and mass[2].

[2] Further discussed in SAMPLE IV Deliverable Report 2

TABLE OF CONTENTS

LIST OF FIGURES

LIST OF TABLES

LIST OF ABBREVIATIONS

APC – AVL Particle Counter

APG – AVL Particle Generator

BC – Black Carbon

CAPS – Cavity Attenuated Phase Shift

CAST (miniCAST) – Combustion Aerosol Standard (Jing Ltd.)

CERMS - CPMA Electrometer Reference Mass Standard

CPC – Condensation Particle Counter

CS – Catalytic Stripper

CU – Cardiff University

D_0, D_{50}, D_{90} – Diameter at which 0, 50 or 90% of particles are counted

DEED – Dekati Engine Exhaust Diluter

DEHS – Di-Ethyl-Hexyl-Sebacat

DF2 – Dilution Factor 2

DMA – Differential Mobility Analyser

DMS – Differential Mobility Spectrometer

EEPS – Engine Exhaust Particle Sizer (TSI)

GMD – Geometric Mean Diameter

GSD – Geometric Standard Deviation

GTL – Gas to Liquid (SAF fuel)

ICAO – International Civil Aviation Organization

INTA – Instituto Nacional De Técnica Aeroespacial “Esteban Terradas”

k_{SL_mass} – nvPM mass size-dependent system loss correction factor

k_{SL_num} – nvPM number size-dependent system loss correction factor

LDSA – Lung-Deposited Surface Area

LII – Laser Induced Incandescence

MA – Micro Aethalometer

MPEC – Multipoint Electrostatic Precipitator Charger

MSS – Micro Soot Sensor (AVL)

NAS – Nebulised Aircraft Soot

$NAS_{RRTrent}$ – Nebulised Aircraft Soot from Rolls-Royce Trent engines

$NAS_{HSR\_RRTrent}$ – Nebulised Aircraft Soot from Rolls-Royce Trent engines Hexane solvent rinsed

NCB – Nebulised Carbon Black

NCP – Nebulised Carbon Powder

NCP_{meso} – Nebulised mesoporous Carbon Powder

NCP_{ng} – Nebulised non-graphitic Carbon Powder

NPL – National Physical Laboratory (UK)

nvPM – Non-Volatile Particulate Matter

PCRF – Particle Counting Reduction Factor

PM – Particulate Matter

PMP - Particle Measurement Programme

PSD – Particle Size Distribution

RR – Rolls-Royce

SAG - Spark-Ablated Graphite

SAF – Sustainable Aviation Fuel

SMPS – Scanning Mobility Particle Sizer

SPG – Silver Particle Generator (Catalytic Instruments)

STP – Standard Temperature and Pressure

TC – Thermocouple

UoM – University of Manchester

VPR – Volatile Particle Remover

ZHAW – Zurich University of Applied Sciences

1. Uncertainty and Potential Improvements in Regulatory nvPM Number Measurement

To ensure the robustness and traceability of aviation regulatory non-volatile Particulate Matter (nvPM) measurements, numerous specifications must be adhered to regarding the preconditioning and transfer of exhaust samples, instrument performance, and annual instrument calibration. As part of the calibration protocols of a regulatory nvPM number instrument, Volatile Particle Remover (VPR) penetration efficiencies at 15, 30, 50 and 100 nm, and the Condensation Particle Counter (CPC) counting efficiencies at 10 and 15 nm are measured. This provides a measure of how effectively particles, of different sizes, physically transfer within the instrument and are subsequently counted. Currently, regulatory nvPM number doesn't prescribe VPR and/or CPC particle loss correction, which potentially introduces significant uncertainties if trying to accurately compare reported nvPM number concentrations across different engine technologies and/or engine power conditions. However, the empirically derived VPR penetration and CPC counting efficiencies, reported as part of the calibration, can be used to assess uncertainty in the regulatory reported nvPM number emission indices (EI). Additionally, the empirically derived penetration and counting efficiencies can be applied to calculate the size-dependent system loss correction for nvPM number (i.e., k_{SL_num} as outlined in ICAO Annex 16, vol II, Appendix 8 [1]), thereby reducing engine-exit nvPM number EI uncertainty used for inventory purposes.

Section 1, therefore aims to quantify the various sources of uncertainty in regulatory nvPM number (e.g., drift, calibration, system loss correction) towards better quantification of the existing uncertainties whilst proposing improvements to mitigate them.

To quantify and attribute each source of uncertainty, the variation in k_{SL_num} was assessed using two nominal Particle Size Distributions (PSDs). These were chosen to be representative of the upper and lower range of nvPM PSDs typically measured for the current aircraft fleet. Both the low thrust (small) and high thrust (large) PSDs being selected from real-world data reported by Durdina et al. [2], which compiled data from 42 engines (across 19 turbofan types) covering both unregulated small business jets and regulated large commercial aircraft. The chosen 'representative' PSDs and their corresponding geometric mean diameters (GMDs) are shown in Figure 1, with their engine-exit equivalent GMDs being 13.8 and 41.8 nm, respectively, when corrected for the size-dependent system losses. Consequently, all uncertainties calculated in this section pertain to these two PSDs.

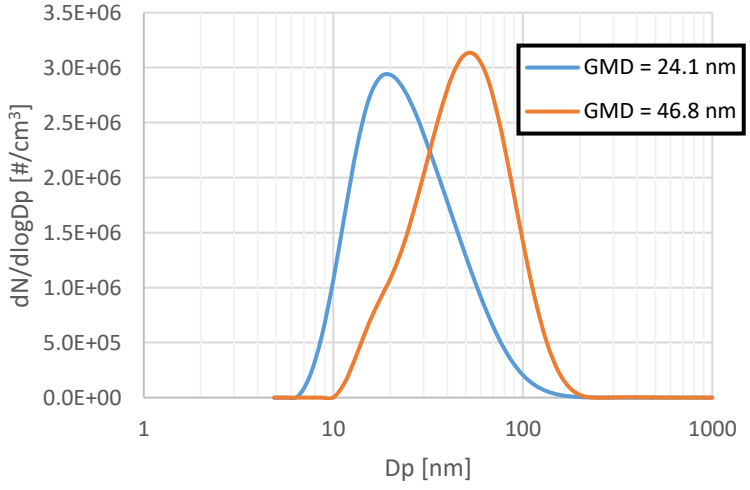

Figure 1: Example low thrust (small (blue curve)) and high thrust (large (orange curve)) PSDs measured in parallel to regulatory nvPM number and mass during aircraft engine emission certification testing

1.1. Quantification of CPC uncertainty

1.1.1. Quantification of CPC Drift from "As Found"

CPC calibration data from the European (EUR) and Swiss reference nvPM sampling and measurement systems which both employ AVL Particle Counters (APC) along with data from a Rolls-Royce owned CPC (Grimm), with details of the specific CPC's in each system detailed in Table 1. For this analysis 'as-found' data from these CPC's were compared with corresponding calibration values measured at least 12 months prior. Using the available data, the 'as-found' CPC counting accuracy, also referred as linearity or k-factor, and the 'as-found' CPC counting efficiency at 10 nm, which is prescribed to be D_{50} (>50% counting efficiency) in the relevant standards, were investigated.

Table 1: Details of the CPCs used in this analysis

Label	**Make – model**	**Serial Number**
EUR CPC	TSI – 3790E	3790132002
Swiss CPC	TSI – 3790E	3790123606
RR CPC (A)	Grimm – 5421	N/A
RR CPC (B)	Grimm – 5421	N/A

This comparison was conducted following considerable instrument usage and transport for both the Swiss and EUR nvPM reference systems, with the results presented in Figure 2 and discussed below.

The 'as-found' CPC counting accuracy (Figure 2a) typically increased over time by up to 2.8%, indicative of a reduced response when compared to the previous calibration. This is well below AVL's quoted CPC counting accuracy of 5.6-7.9% (concentration dependent). Although the differences are relatively low, it is hypothesised that as CPCs are used, the wick becomes contaminated and less efficient, causing the calibration gradient slope to become shallower over time [3]. The CPC counting accuracy allowance for aviation regulatory nvPM number is 10%, however these results, based on limited data, suggest that this allowance could potentially be reduced to a lower value e.g., 5%, if application of k-factor was to be mandated, as has been recently updated in the UNECE automotive regulations, specified in PMP [4].

The 'as-found' CPC counting efficiency at 10 nm (Figure 2b) varied between -1.7 and +1.9% (<1.5% absolute difference), indicating that no significant annual drift was observed. Again, this is significantly lower than the CPC counting efficiency uncertainty of 10.7% stated by AVL. However, both the calibration and 'as-found' experiments were performed by the same calibration laboratory using the same aerosol sources and operating procedures so do not include systematic bias, as would be witnessed if using two different calibration laboratories.

It can be concluded that no significant drift was observed for any of the CPCs investigated over the 12-month period, based on the limited data points available and presented here. This finding further supports the results of the H2020 RAPTOR program [5], which reported good agreement (<2%) between the Swiss and European AVL APCs when sampling RQL rig soot both immediately after in-parallel calibration and then following a 12-month period prior to re-calibration. It is noted that over the 12-month period, the two systems were operated at different test campaigns and hence experienced different transportation and operational times. However, CPCs within aviation regulatory nvPM systems generally have significantly lower usage compared to those used in automotive regulation or atmospheric research, where high usage, continuous operation and relatively higher levels of volatile particles may lead to more significant drift.

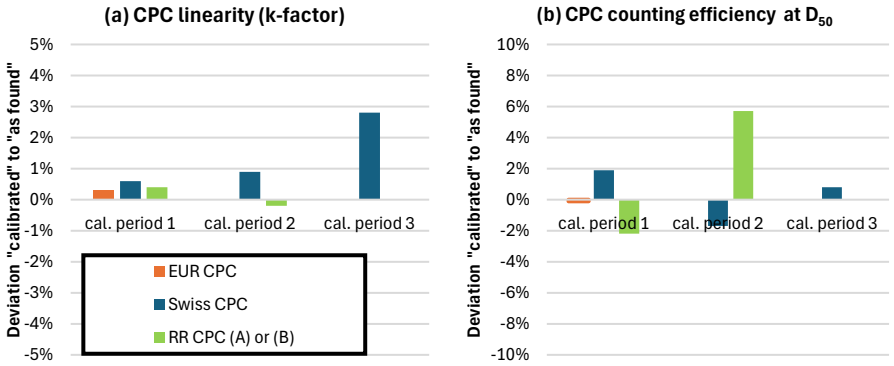

Figure 2: Difference between 'as-found' and previously calibrated values for the Swiss, EUR and RR CPCs over a 12-month period for regulatory nvPM number CPC counting accuracy (a) and CPC counting efficiency at the CPC D_{50}, 10 nm for the EUR and Swiss CPCs and at 7 nm for the Rolls-Royce CPCs (b) for the 2018-2024 period

1.1.2. CPC Year-To-Year Calibration Variability

1.1.2.1. CPC Counting Accuracy

The variability in the calibrated CPC counting accuracy (i.e., linearity or k-factor) was analysed using calibration data for Swiss, EUR and RR CPCs. The analysis approach used was based on a statistical method, developed by the SAE E31P calibration team, for determining the nvPM mass-based instruments year-to-year change after a routine service (not 'as-found'). The change in the annual response from successive calibrations were calculated and plotted as a histogram, with the results shown in Figure 3.

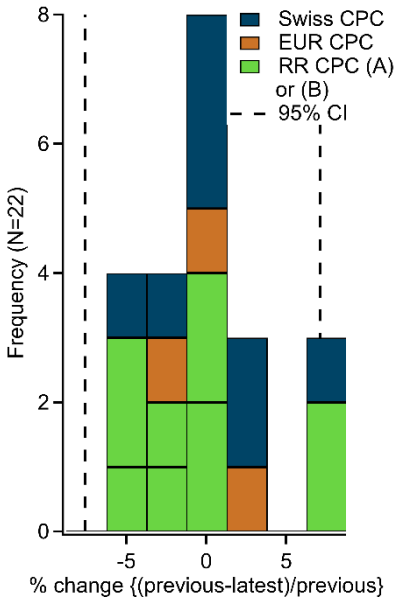

Figure 3: Histogram of year-to-year change (after service, not as found) in the calibrated counting accuracy of the Swiss, EUR & RR CPCs

The year-to-year change in calibrated CPC counting accuracy brought about by maintenance activities, were found to be 5.4% which is higher than what was observed for annual drift. Maintenance activities before calibration, such as wick replacement, optics adjustments and saturation temperature adjustments are known to change the response of any given CPC.

Currently, counting accuracy correction is not mandatory as long as "*The counting accuracy shall be of ±10 percent from 2000 particles/cm^3 to the upper threshold of the single particle count mode against a traceable standard (ISO 27891)*" [1]. Therefore, applying the counting accuracy from calibration (i.e., k-factor), as done by default in AVL number counters (EUR & Swiss), could significantly reduce the uncertainty in nvPM number.

Reducing the counting accuracy requirements from ±10% to ±5% against a traceable standard, and applying a mandatory k-factor correction, in line with new PMP guidelines [4], would reduce nvPM number uncertainty to ±5%.

The dataset presented in Figure 3 shows a 2-sigma value of 7.3%, which is in close agreement with the SAE E31P uncertainty team Task 0[3] year-to-year change for a single type of CPC of 7.1% showing consistency and therefore adding confidence of the uncertainty associated with CPC Counting Efficiency.

Year-to-year variability in CPC response shape was assessed at the 10 and 15 nm CPC calibration counting efficiencies. Data was again assessed for the Swiss, EUR and RR CPCs listed in Table 1. Figure 4 provides a summary of the results, including the calculated CPC counting efficiency (i.e., transfer function). The analysis revealed a large variability on the year-on-year D_0 and D_{50}, with some values physically implausible ($D_0 < 0$ nm). This variability is primarily driven by the large spread in 10 nm penetration values (Figure 4, left), especially when penetration exceeds 0.8, meaning there isn't sufficient data to accurately resolve the shape of the CPC counting efficiency.

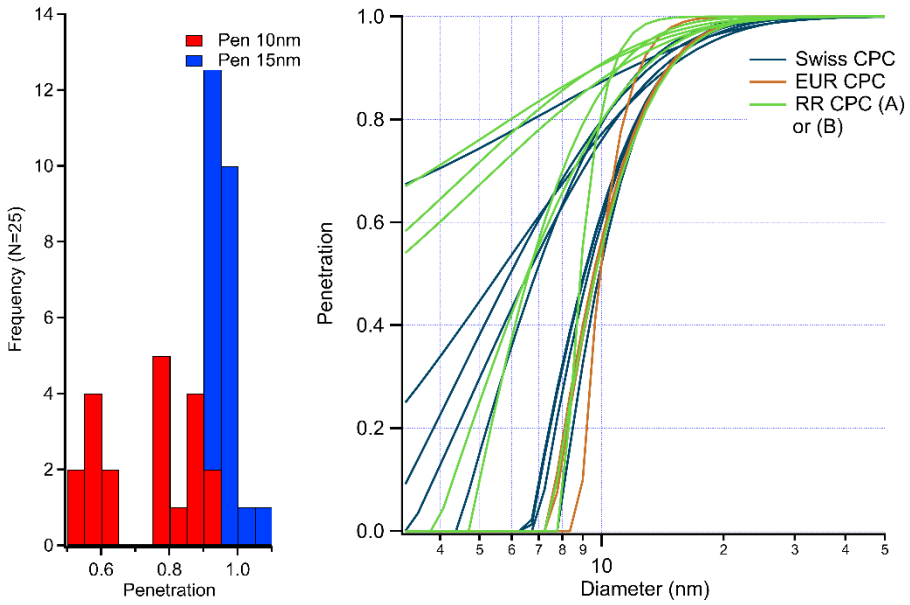

Figure 4: histogram of the combined penetrations at 10 nm and 15 nm of the Swiss, EUR & RR CPCs over the last decade (a) and, calculated transfer functions (b)

The impact of year-on-year variability in CPC counting efficiency on nvPM number correction was assessed by considering the lowest (D_{50}= 0.52 & D_{90}=0.90) and highest (D_{50}= 0.91 & D_{90}=1) counting efficiencies reported during calibration. CPC counting efficiency curves corresponding to these bounds were applied to two the example PSDs (Figure 1) that had been corrected for VPR penetration (average APC VPR values) to represent the PSD entering the CPC. This correction resulted in a 5% change in k_{SL_num} for the smaller PSD and a 1% change for the larger PSD.

However, as novel techniques are developed to reduce the diffusional losses in the sampling systems, and as fuels with lower aromatic (higher hydrogen) content associated with lower GMDs are used more widely, GMDs below 10 nm may occur. This large variability in the CPC transfer function, based on a simple model using two penetration points, may need to be reassessed. It is recommended to look at either improving the repeatability of the counting efficiency at 10 nm or conduct a more rigorous transfer function calibration of the CPCs, to more effectively quantify the D_{50}.

It is noted that CPC calibration at 7 nm is a common capability at CPC calibration laboratories since in CEN/TS 16976:2016 (Determination of particle number concentration in Ambient air), the lower limit of the measured

[3] Task 0: Variability in repeating two engine tests using the same measurement system and identical nvPM emissions source

particle size range is 7 nm. In this calibration method[4], the counting efficiency is measured at 7, 9, 10, 11, 14, 20, 30 and 40 nm using silver particles from a tube furnace, at a low number range (1,000 – 3,000 /cm^3 typically) to reduce the coincidence errors. The measured counting efficiencies are then used to determine the D_{50} and D_{90}, which are then applied to the same CPC transmission efficiency function used in the regulatory system loss tool. The counting accuracy is also determined at 40 nm at 1,000, 2,000, 4,000, 8,000, 12,000, 25,000 and 50,000 /cm^3.

1.2. Quantification of VPR Uncertainty

The ICAO regulation (Annex 16 Vol. II) for nvPM number emissions measurement specifies minimum allowable penetration fractions for a VPR of 30% at 15 nm, 55% at 30 nm, 65% at 50 nm, and 70% at 100 nm, with VPR penetration being validated annually through calibration. Ongoing considerations within SAE E31P regarding VPR calibration uncertainty include whether a) the number and range of calibration test points impact the curve fit of the VPR penetration, b) if the choice of particle calibration material results in variations in observed VPR penetrations, and c) the VPR calibration methodology approach used, which under current specifications could be performed in several ways including alternating upstream and downstream measurements with a single CPC or performing simultaneous measurements with two CPCs. These considerations are focussed on use of VPR penetration curves for system loss correction calculation, for understanding particle loss variation between different VPR technologies and to determine whether drift in VPR penetration efficiency occurs during the calibration period.

The purpose of this section is to evaluate uncertainty associated with different regulatory-compliant VPR technologies, which are known to exhibit significantly different penetration efficiencies [6], and to quantify the resulting uncertainty in current regulated nvPM number EI's (non-system loss corrected) and those that would be reported should system loss-correction be applied. This study also investigates VPR drift uncertainty and whether empirically characterising VPR loss for particles smaller than 15 nm could improve the accuracy of VPR loss prediction used for k_{SL_num} calculation.

1.2.1. Quantification of VPR Drift

In this section VPR 'as-found' calibration data, for the Swiss and EUR and reference nvPM sampling and measurement systems (APC) were compared with corresponding calibration values measured at least 12 months prior. Drift from the Particle Counting Reduction Factor (PCRF), which represents dilution and particle loss in the VPR, was assessed. Again, this comparison was conducted following considerable instrument usage and transport for both the Swiss and EUR nvPM reference systems, with the results presented in Figure 5 and discussed below.

As can be seen the 'as-found' PCRF, which includes upstream and downstream CPC and dilution factor measurement uncertainties, varied by up to 5.6% when compared to the previously calibrated value. In the case of the EUR & Swiss nvPM systems, AVL have reported their PCRF calibration uncertainty to be 8.7% at 30, 50 and 100 nm[5] (k=2, representing 95% confidence interval). Therefore, no measurable drift (outside of stated PCRF measurement uncertainty) was observed on either APC instrument over a typical calibration period of 12-months. Note that the APC is serviced and calibrated after 'as-found' checks. In the case of the RR system a Dekati® Engine Exhaust Diluter (DEED), with an incorporated CS, is employed. It is noted that all calibration data for this DEED may be considered 'as-found' since no specific servicing, beyond standard cleaning, is typically required due to the units low usage (compared to automotive). Details of the DEED calibrations are reported in Section 1.2.2.

[4] https://www.actris-ecac.eu/pnc-greater-10nm.html.
[5] Email communication with AVL

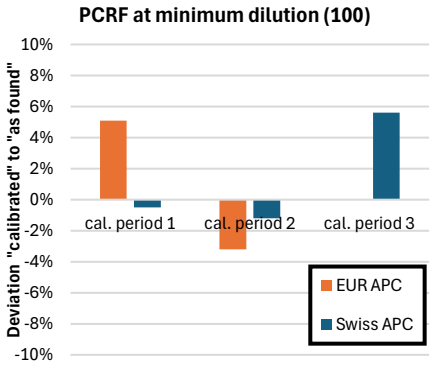

Figure 5: Difference between 'as-found' and previously calibrated values over 12-month period for Swiss and EUR regulatory nvPM number APC PCRF for the 2018-2024 period

1.2.2. Quantification Of Uncertainty Between Different VPR Technologies

The uncertainty arising from different VPR technologies was evaluated by comparing measured penetration efficiencies of two primary technologies used in known nvPM certification systems namely: the DEED (RR System) and APC (Swiss and EUR systems). These VPR technologies differ in design, with most notably the DEED utilising a two-stage ejector dilution system, while the APC uses rotary and axial dilution [7]. This analysis compares VPR penetration calibration values, for the RR DEED and Swiss & EUR APCs over the period 2013-2024. Note that other commercially available VPR technologies which may comply with ICAO Annex 16 Vol.II are available, but to the authors knowledge these are not currently used by any OEM's for certified nvPM measurement.

The APC VPR calibration data (Swiss: 11 & EUR: 6 calibration points) was performed by AVL using propane burner emissions which were thermally-treated CAST soot using a 350°C Evaporation Tube (ET) (pre-2019) and thermally-treated APG soot using a 370°C catalytic stripper (CS) (post-2018). Data of these calibrations are shown in Figure 6 at PCRFs of 100 (a) and 250 (b). Only these PCRFs were investigated, given these are the only two dilution settings typically used during regulatory aircraft nvPM measurements.

It is observed that VPR penetration efficiencies are approximately 5% lower in the pre-2019 data compared to post-2018 data, this difference is thought likely due to particle shrinkage from volatile coatings on the unstripped CAST exhaust. As discussed, during 2018, AVL introduced a 370°C CS replacing the ET, with the soot source also changing from a CAST to an APG burner to ensure that only nvPM was present in the test sections. This change highlights the importance of ensuring that the test aerosol consists solely of nvPM, as the presence of volatiles can lead to underprediction of VPR penetration efficiencies, resulting from particle shrinkage and nucleated particle removal, as discussed in the literature [8].

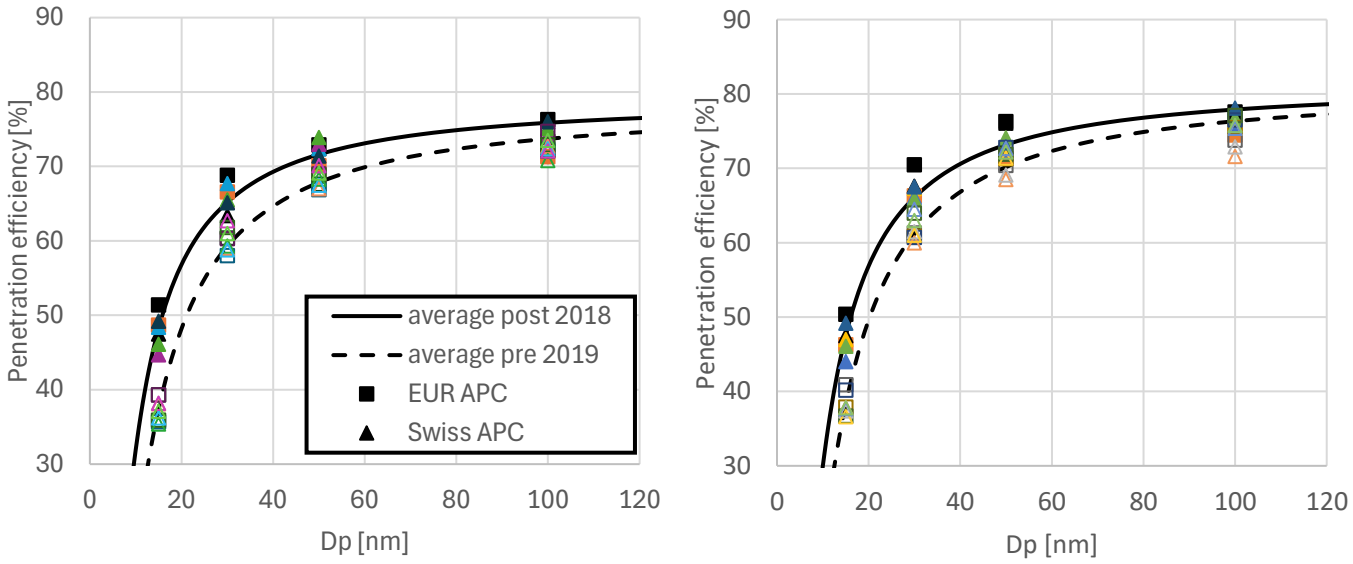

Figure 6: European (squares) and Swiss (triangles) APC VPR calibration data at PCRF 100 (a) and 250 (b) – hollow symbols represent pre 2018 data and full symbols represent post 2018 data

The year-to-year scatter for the post-2018 data is represented in Figure 7 as the difference between the highest and lowest VPR penetration values at a given particle size. Year-to-year differences ranging between ~4% at 50 and 100 nm up to ~7% at 15 nm are observed, resulting in k_{SL_num} differences ranging between 7 and 10% when considering the two example PSDs from Figure 1. Given the actual VPR penetration is not expected to change year-to-year due to its fixed geometry and calibrated flow and temperature, and because the reported uncertainty for PCRF (8.7% for 30, 50 and 100 nm and 14.9 % for 15 nm) is higher than the observed year-to-year difference, it can be concluded that the year-to-year variability is likely driven by the measurement uncertainty rather than instrument drift.

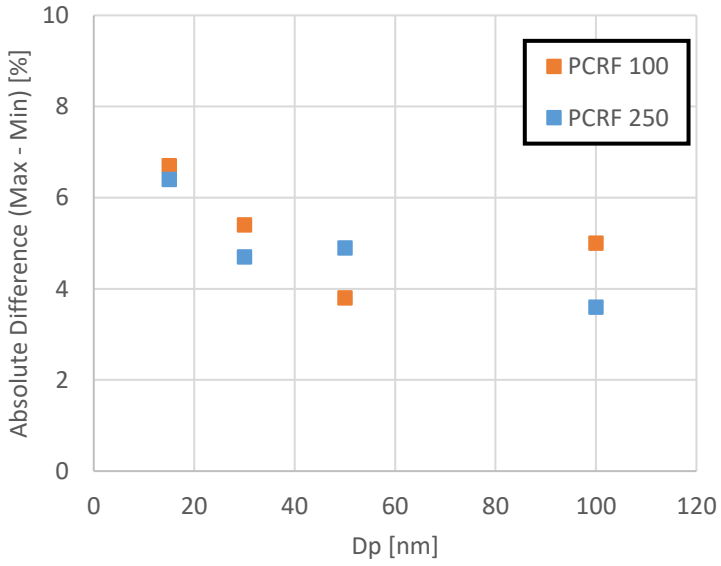

Figure 7: Difference between minimum and maximum APC VPR penetration efficiency between 2019-2024 (5 Swiss APC + 2 EUR calibrations)

DEED VPR calibration data measured by the UK's national metrology institute National Physical Laboratory (NPL) between 2014 and 2024 is shown in Figure 8, with different colour groups representing different particle types used. An additional initial calibration done by Dekati, the DEED manufacturer in 2013 using silver is also

shown. Similarly to the APC, year-to-year scatter is observed, however overall, the differences are larger across all sizes (see Figure 9) and reach a maximum of 30% at 100 nm. Also, no particle type dependence was witnessed between silver, gold and miniCAST soot (noting that the miniCAST exhaust was thermally pre-treated). As can be seen the year-to-year scatter is significantly higher than the measurement uncertainty reported by NPL (~8%[6]). It is thought this discrepancy likely originates from a change in operating procedure, however, physical a physical penetration drift in the DEED could also result in the results presented in Figure 8. On discussing this matter with NPL it was highlighted that in 2023, the tube furnace (400°C) and catalytic stripper (350°C) were replaced with a silica gel dryer downstream of their nebulised gold source. Since this change in aerosol pretreatment, it is observed that the two annual penetration calibrations appear to report efficiencies which are 5-15% lower at sizes of 30 nm and above. When only considering the data between 2014 and 2021 (gold particles with original drying procedure) , a smaller year-to-year difference is observed across the different size ranges, resulting in k_{SL_num} differences ranging between 18 and 30% when considering the two example PSDs from Figure 1.

It is noted that up to 2016, NPL performed the VPR calibration at ambient inlet pressure. However, since this date, in order to replicate 'real-world' testing conditions, calibrations have been performed with an inlet pressure of -60 mbar compared to the VPR outlet pressure. However, sample inlet pressure is not expected to affect the VPR penetration, although it is known to affect DF_2 and therefore the PCRF.

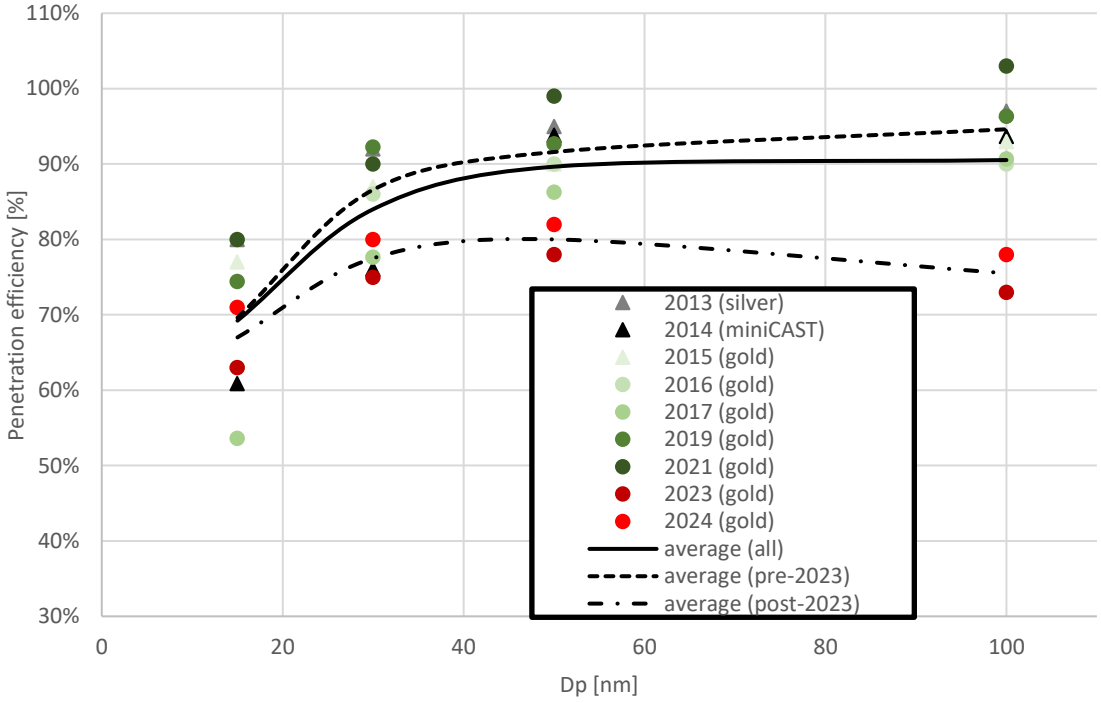

Figure 8: RR DEED VPR calibration data between 2013 and 2024 (triangle represent calibration performed at an ambient inlet pressure while circle represent an inlet pressure of -60 mbar)

[6] Email communication with NPL

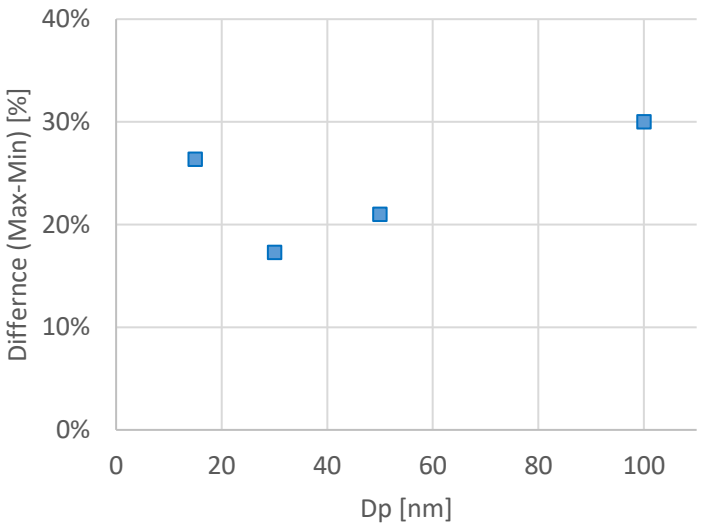

Figure 9: Difference between minimum and maximum DEED VPR penetration efficiency between 2013-2024 (9 calibrations)

The difference between average VPR penetration efficiency from the APC and the DEED taken from Figure 6 and Figure 8 is presented in Figure 10. As can be seen the DEED displays significantly lower losses than the APC on average, between 21% lower at 15 nm and 16% lower at 100 nm. This difference is thought to originate from the difference in design and dilution, with the DEED witnessing lower thermophoretic loss when diluting the hot aerosol post catalytic stripper with an ejector diluter, while the APC uses a mass-flow-controlled axial dilution system, forcibly cooling the sample prior to the mixing plane, as supported by the constant offset witnessed across particle sizes. However, some of this bias could also originate from the difference in calibration aerosols and test procedures used by the different calibration laboratories (e.g., single Vs dual CPC, particle type and conditioning), as discussed in detail in section 1.3.

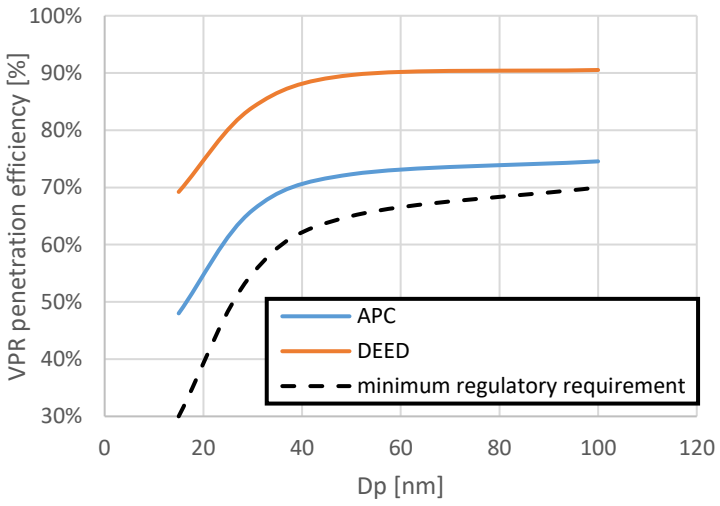

Figure 10: Average VPR penetration efficiency for the AVL APC (7 calibrations post-2018) and the Dekati DEED (9 calibrations)

Overall, the results above highlight that different VPR technologies can have significantly different particle losses. When considering the two 'representative' PSDs (Figure 1), this VPR technology difference results in k_{SL_num} differences (i.e., loss-corrected nvPM number uncertainty) ranging between 20 and 25%. This means that for current nvPM emission regulations, which do not include system loss correction, reported nvPM number EI's can bias data by up to 25% dependent on the VPR instrument type used during the certification.

1.2.3. Impact of Particles <15 nm on VPR Penetration Curve Fitting

VPR losses are currently only quantified down to 15 nm; however, modern aircraft engines do emit particles below 15 nm, as seen in the low power 'representative' PSD (Figure 1). Therefore, work was undertaken to verify if the VPR loss, as currently modelled for $k_{SL\_num,}$ is valid for particles <15 nm. This was achieved by experimentally measuring the VPR loss of the EUR APC down to 6 nm at VPR inlet concentration > 5,000 particles/cm^3 using a commercially available Silver Particle Generator (SPG - Catalytic Instruments). The measured particle loss was then compared to the predicted VPR loss derived from the VPR calibration data. The effect of particle type on VPR loss and CPC counting efficiency is also discussed.

Building on previous experience from this programme[7] and those reported elsewhere ([5] & [9]), a test campaign was performed at the University of Manchester in which the VPR penetration efficiency of the EUR APC was experimentally characterized with silver nanoparticles (SPG generator) that were DMA-classified between 6 - 30 nm with a nvPM number instrument inlet concentration >5000 particles/cm^3, as ICAO regulation prescribes. While reaching inlet concentrations >5000 particles/cm^3 at a GMD <15 nm with nvPM particles is challenging, the SPG can produce significant particle concentrations down to ~5 nm as highlighted by example PSDs, measured in the exhaust of the SPG and presented in Figure 11.

However, the SPG could only achieve the minimum concentration threshold up to 30 nm when DMA-classified. The VPR penetration was estimated using two CPCs (TSI 3756) simultaneously sampling upstream and downstream of the VPR, with the downstream CPC corrected for dilution using the calibrated DF_2. To reduce the measurement uncertainty, the two CPCs were first intercompared to derive a correction factor. Diagrams of the experimental setups can be found in Figure 12 ((a) CPC intercomparison and (b) VPR penetration experiment).

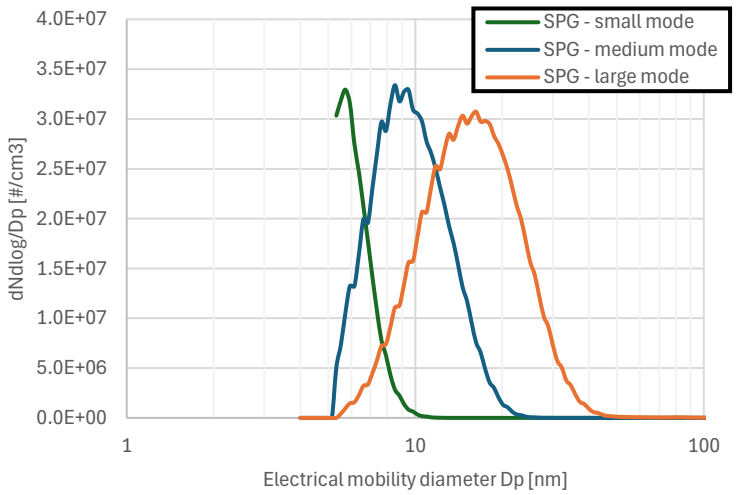

Figure 11: Example silver Particle size distributions used for the EUR APC VPR experiment measured by the CU Grimm SMPS

[7] See SAMPLE IV Deliverable 1 report

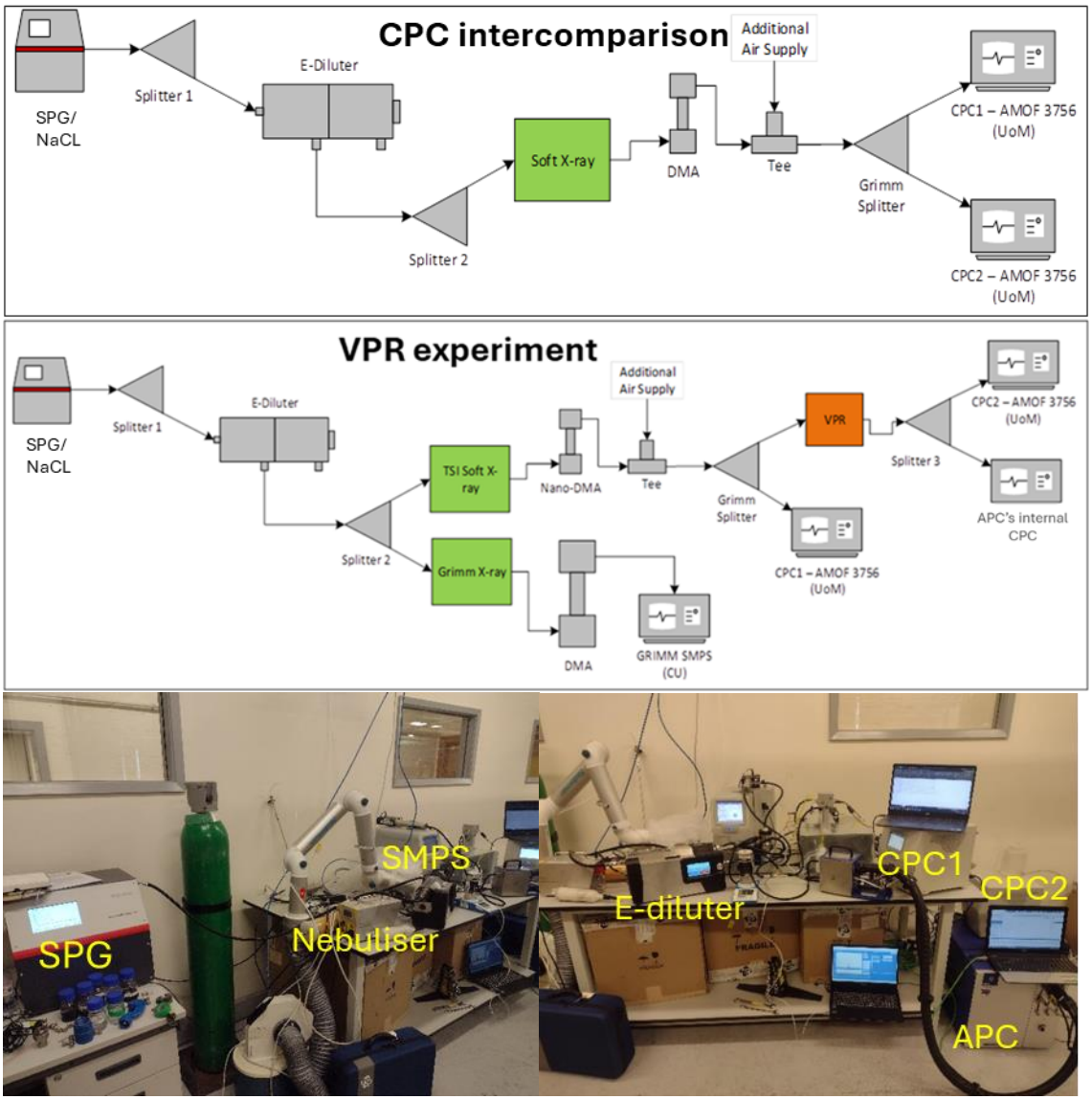

Figure 12: Diagram of the UoM CPC intercomparison (a) and EUR APC VPR penetration (b) & photograph of experimental set-up (c)

The CPC intercomparison was performed at particle sizes ranging from ~10 - 150 nm using NaCl salt at high and low concentrations, as well as SPG aerosol, with the results shown in Figure 13. As seen, the CPC ratio fluctuated between 0.8 and 1 corresponding to an uncertainty of up to 20%, further highlighting the importance of calibrating the CPCs when using a dual-CPC setup. The CPC position was alternated to ensure no splitter bias was occurring. Since CPC counting efficiency is expected to be material-dependent (see Figure 14), only the SPG data was used to derive the CPC correction equation, used to calculate the penetration efficiencies.

A logistic Model fit ($y = a/(1 + e^{-b(x-c)})$) was found to best correlate with the SPG data while ensuring that the CPC ratio remained > 0 at 2.5 nm corresponding to the CPCs D_{50}. Although the CPCs were intercompared only down to 10 nm, this range is believed to be sufficient to capture the shape of the CPC ratio. However, for future studies and certified calibrations, it is recommended to intercompare the CPCs at the same particle sizes as used in the VPR penetration experiments.

Considering the error bars, no meaningful difference was observed in CPC ratio between salt and SPG aerosol at this size range (Figure 13), where the counting efficiency is expected to be 100%, suggesting that particle material does not significantly impact CPC counting accuracy. It is noted that “salt low” typically exhibits larger error bars compared to “salt high” and “silver” primarily due to the lower CPC counts associated with "salt low".

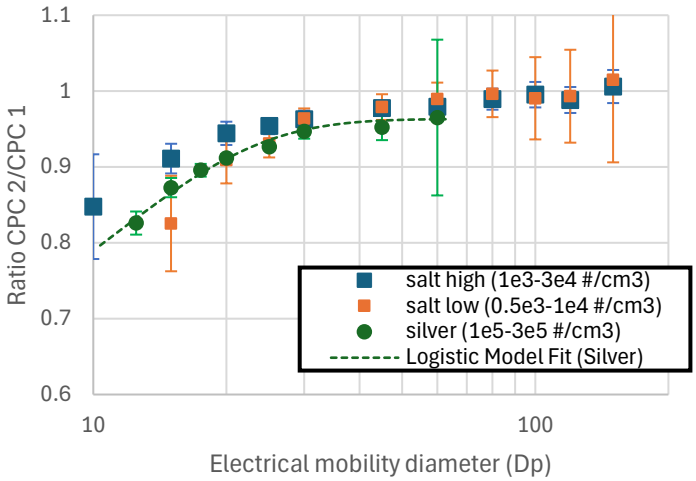

Figure 13: CPC intercomparison on DMA-classified silver and salt at different concentrations (error bars represent the propagated CPC measurement uncertainty at k=1)

However, the particle type used is expected to affect the CPC counting efficiency. To demonstrate this, the internal CPC of the EUR APC (TSI 3790E) was compared to other CPCs (TSI 3752 and 3756) during VPR calibration experiments, with the results shown in Figure 14. The EUR CPC agrees with the two other reference CPCs within 10% (ratio between 0.9 and 1.1) for particles >20 nm but underreports for particles <20 nm, consistent with its lower counting efficiency. According to regulations, the EUR CPC should have a counting efficiency >50% at 10 nm and >90% at 15 nm. However, agreement with the other CPCs at 15 nm fluctuates between 0.71 and 0.85, while the other CPCs are expected to have a near 100% counting efficiency at this size due to their lower D_{50} (2.5 and 4 nm). At this time, it is not known why such a difference in particle morphology should impact only one of the compliant CPCs at particle sizes ~D_{90}, hence factors such as DMA classification uncertainty and sampling and measurement uncertainty of the two laboratories likely contributed to these findings.

It is noted that CPC counting efficiency is typically calibrated using emery oil and may vary when measuring different particles (e.g., gold, silver, soot) due to differences in particle composition, shape, and surface chemistry [10], [11], [12]. For example, emery oil particles are spherical and organic, allowing the working fluid (such as butanol) to condense uniformly, resulting in efficient particle growth and detection. In contrast, gold and silver nanoparticles are metallic and may exhibit different surface properties, which can impact how the CPC's working fluid condenses onto the particles. This is particularly relevant for fractal-like aggregates such as aircraft soot, which have complex, irregular structures and larger surface areas relative to their mass.

These structural differences can reduce the effectiveness of condensation, as the vapor may not fully coat the soot particles, resulting in lower counting efficiency compared to spherical particles. A solution for reducing this uncertainty would be to calibrate the CPC counting efficiency using particles with similar morphologies/properties to aircraft soot as discussed in the literature [8], or prescribe a D_{50}/D_{90} well below the particle size you expect to measure at the end of the particle sampling system (e.g., D_{90} or D_{50} <7 nm for regulatory nvPM number).

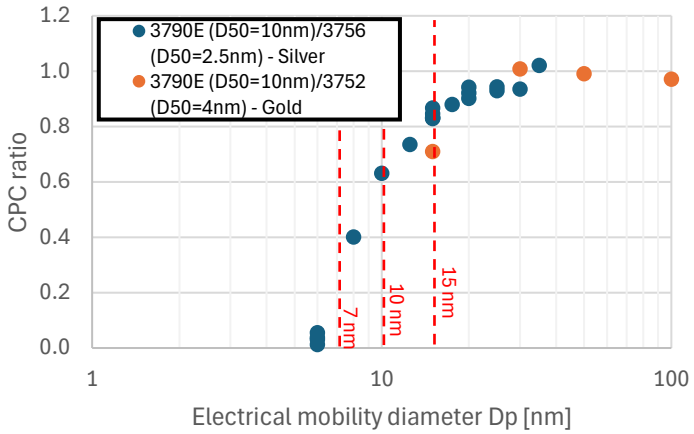

Figure 14: EUR reference system APC internal CPC compared to NPL (3752) and AVL (3792) CPCs during VPR calibration

The EUR APC VPR penetration efficiency measurement, corrected for CPC differences and DF_2, was compared to the latest (2023) AVL Calibration at 15, 30, 50 and 100 nm, as shown in Figure 15. The red line represents the VPR penetration curve fit from the prescribed k_{SL_num} calculation using the calibration data and is seen to agree, within the measurement uncertainty, with SPG aerosol down to 6 nm. This data suggests that the current VPR fit within the k_{SL_num} calculation works well for particles as small as 6 nm. However, it is noted that the 15 nm data point significantly influences the shape of the fit at smaller sizes, thus given higher uncertainties are typically attributed with smaller particle sizes; then adding an additional point at 10 nm, for example, may introduce more uncertainty to the fit rather than improving it.

Additionally, although AVL uses a single CPC approach and APG nvPM to calibrate the VPR losses (discussed in more detail in section 1.2), the penetrations at 15 and 30 nm - where the majority of aircraft nvPM number concentration typically resides - are consistent with those measured using SPG aerosol. This suggests that VPR losses at particle sizes up to 30 nm do not significantly depend on particle type, if there is confidence that the particles are indeed non-volatile in nature.

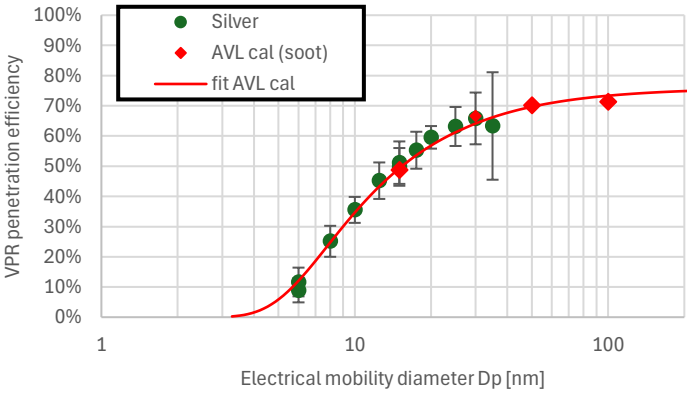

Figure 15: EUR APC VPR penetration measured with silver particles compared to AVL calibration data (error bars represent the propagated CPC measurement uncertainty at k=1)

As there are other commercially available VPR technologies, that meet the ICAO performance specification, it was attempted to repeat the above experiment using a 'loaned' DEED to better quantify the difference in particle loss between the two technologies <15 nm. Unfortunately, numerous technical issues associated with cleanliness and electrical continuity were encountered which prevented data with sufficient quality assurance being generated. However, it is noted that DEEDs have been used extensively in aviation regulatory systems, and typically meet the system cleanliness/leak check, with no reported in-service electrical problems noted by OEMs which employ them.

1.2.4. VPR Year-To-Year Calibration Variability

The analysis of the VPR penetration efficiencies at 15 nm, 30 nm, 50 nm, and 100 nm provides a statistical representation of the data shown in section 1.2.2 and is presented in Table 2.

Firstly, for both the APC and the DEED variability in the penetration efficiency is highest at the smallest sizes. This is consistent with the findings of the CPC work, which showed the variability in those data was driven by the variability in the penetration at 10 nm measurement, and that improvements at small size penetrations are required. Secondly, the DEED variability is much higher than the APC i.e. to year-to-year change of the reported values is higher for the DEED.

Table 2: Details of Uncertainty determined from VPR calibrations from the same laboratory

Year-to-year relative difference in VPR penetration (estimated at coverage factor k=2, C.I. of 95%)	**15nm**	**30nm**	**50nm**	**100nm**	**Number of points**
APC (All data including change of procedure)	35.9%	10.2%	7.7%	5.2%	16
APC (Post 2019 same procedure)	12.0%	8.4%	4.8%	6.6%	5
DEED (All data)	47.7%	27.0%	18.5%	23.6%	8
DEED (2014 – 2021)	50.0%	24.2%	11.3%	8.8%	6

1.3. Improvements In Regulatory nvPM Number Calibration Protocols

This section aims to identify the main uncertainties in nvPM number calibration and proposes protocol improvements to reduce overall uncertainty. To evaluate calibration uncertainties for regulatory nvPM number, the penetration efficiency of the EUR VPR (APC) was experimentally measured by two calibration laboratories (AVL and NPL – see certificates in the A) and in-house at UoM. Each experiment utilised a different setup and methodology, as detailed in Table 3 and Figure 16, with the results and implications discussed below.

Table 3: List of the main differences between different setups used by different VPR calibration laboratories for EUR APC

Laboratory	**Particle type used**	**Conditioning**	**Size-classification**	**Inlet pressure**	**Measurement type**
AVL	nvPM (APG diffusion flame burner)	Thermal pre-treatment (CS at 370°C) & dilution	DMA: 10/1 ratio	-10 to -40 mbar	Single CPC (with monitor CPC): TSI 3792 (D_{50}=10 nm)
NPL	Gold (nebulised BBI solutions suspension)	Post 2023 - Silica get dryer	DMA: 5/1 ratio	-60 mbar	Dual CPC: 2x TSI 3752 (D_{50}=4 nm) Each CPC's response was corrected with a calibration factor determined according to ISO 27891
UoM/CU	Silver (Catalytic Instrument SPG)	Drier & dilution	DMA: 5-15/1 ratio	-10 mbar	Dual CPC: 2x TSI 3756 (D_{50}=2.5 nm) Compared between 10 and 100 nm and corrected on Silver

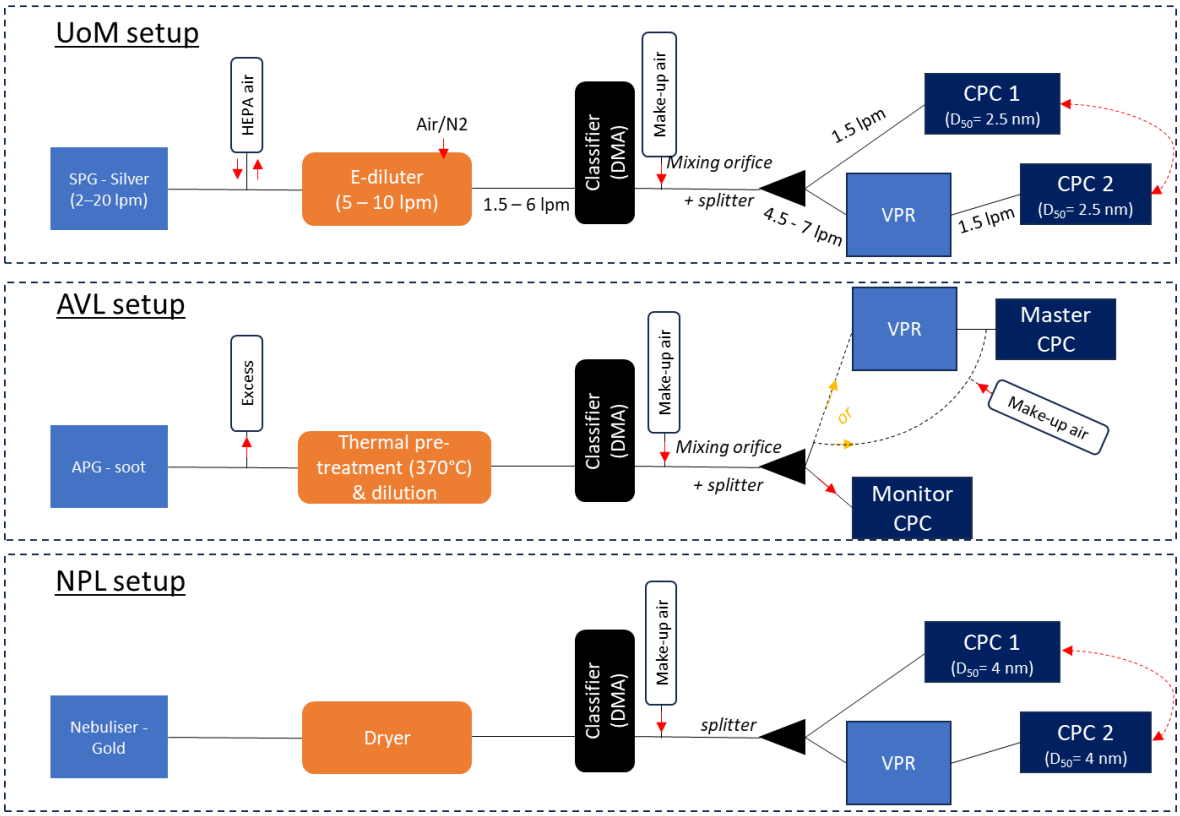

Figure 16: Diagram of the VPR penetration calibration setup from different laboratories

The EUR VPR (APC) penetration efficiency measured by the different laboratories at 15, 30, 50 & 100 nm is reported in Figure 17, with it seen that general agreement was within the measurement uncertainty. At 15 nm, a scatter of 6.2% is observed with NPL reporting a penetration of 45% while AVL measuring 48.7% and UoM 51.2%. At 30 nm, the agreement is significantly better (within 1.6%) with NPL reporting a penetration of 65% while AVL measuring 66.6% and UoM 65.8%. At 50 and 100 nm, NPL reported higher penetration efficiencies than AVL of 3.9% and 7.7% respectively. Considering the relevant set-ups, this observation might be due to the broader classification by the DMA in NPL experiments (5/1 ratio) vs AVL and UoM (10/1 ratio), where larger particles selected by the DMA may shift the penetration to slightly higher values (the effect of DMA resolution will be less noticeable for smaller particles (e.g. 15 or 30 nm) since the cut by the DMA is still quite narrow at 5/1 ratio).

When applying the relative VPR calibration data for the EUR APC, with the two example aircraft nvPM PSDs (Figure 1), a k_{SL_num} difference of 4% for the smaller PSD and 2% for the larger PSD is observed. A standardised measurement approach to VPR calibration - such as intercomparing and correcting CPCs on the same source when using a dual CPC approach - could help reduce these discrepancies. Utilising a single CPC might offer more repeatable results with lower measurement uncertainty but would rely on a highly stable particle source.

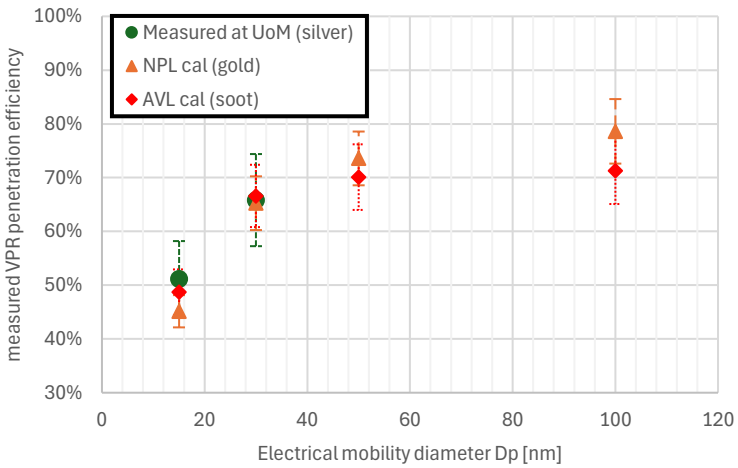

Figure 17: EUR VPR (APC) penetration efficiency measured by different calibration laboratories, using different procedures, at the particle sizes prescribed by regulation (error bars represent the measurement uncertainty at k=2)

To further compare the results from the different laboratories, the fits using the calibration data from NPL and AVL were compared to the measured VPR penetration from UoM using SPG silver particles between 6 and 30 nm, with the results shown in Figure 18. The AVL fit agrees within ±5% at all the silver sizes, while the NPL fit is lower than AVL and UoM penetrations by more than 10% < 15 nm and is higher by more than 5% from 50 nm up. These results along with discussions regarding the sources of uncertainty and their implications are further detailed below.

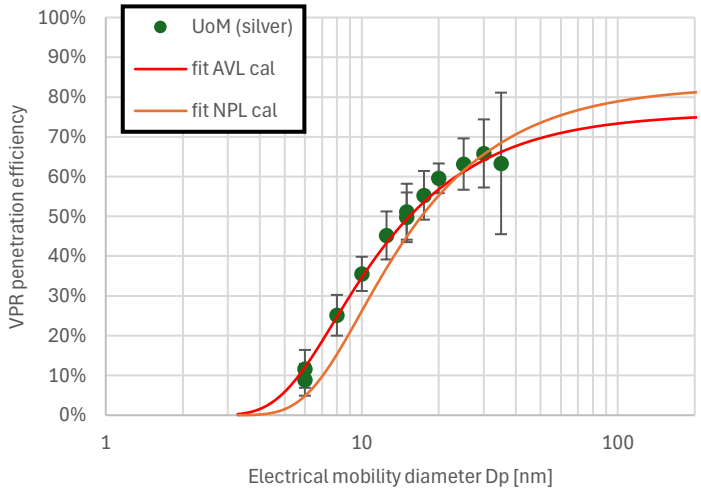

Figure 18: EUR VPR (APC) measured and fitted penetration efficiencies between 5 and 200 nm from different calibration laboratories (error bars represent the propagated CPC measurement uncertainty at k=1)

1.3.1. Impact of Penetration Determination on VPR Calibration Uncertainty

One possible explanation for the reported differences in VPR penetration efficiencies across calibration laboratories is the variation in particle measurement techniques used (Figure 16). As discussed previously, AVL used a single CPC which made alternate upstream and downstream measurements. NPL used two CPCs of the same model, calibrated against a reference electrometer according to the ISO27891 standard, using the same operating procedure, and took measurements simultaneously (without direct intercomparison and correction for observed differences). The two CPCs were also swapped and any bias due to CPC position was corrected for. Finally, UoM used two CPCs simultaneously which were previously intercompared on the same source and corrected for witnessed offsets prior to determination of the VPR penetration.

AVL[8] has indicated that they chose a single-CPC measurement approach because they found it provided more stable results with lower measurement uncertainty. This is because there is no need for intercomparison/correction when using a single reference CPC, with different CPCs known to display slightly different linearities and counting efficiencies. However, this method relies on particle source stability. To monitor stability, AVL uses a 'monitor CPC' which corrects for source drift between the pre- and post-VPR measurements. If the correction is >±5%, the measurement is repeated.

The dilution factor DF_2, needed for the calculation of penetration, is also a source of uncertainty, with the upstream and downstream CO_2 measurement expected to contribute to approximately 0.5% of the overall uncertainty.

It is noted that the APC VPR inlet pressure used by the different laboratories was not the same (see Table 3). However, this is not expected to impact the results given the APC uses a rotating disk diluter for its 1st stage dilution which compensates automatically in real-time for pressure and temperature changes at PND1 by adjusting the disk rotation frequency within ±200 mbar relative to ambient. When investigating different VPR technologies such as the Dekati DEED, this would not be the case. The DEED uses a DI-1000 ejector diluter as its 1st stage dilution, which is known to be pressure dependent, and therefore in this case the inlet pressure during dilution factor calibration should represent the inlet pressure experienced when conducting certification measurements (i.e., NPL choosing -60 mbar).

1.3.2. Impact of Particle Conditioning on VPR Calibration Uncertainty

Aerosol conditioning is essential when measuring VPR penetration efficiency [8]. Another ISO17025 calibration laboratory, METAS in Switzerland, performed a comparison between the Swiss APC and a reference electrometer using combustion exhaust PM from a CAST generator, which was DMA-classified at 10 and 55 nm (see report in A). However, they conditioned the aerosol using a PMP-compliant PALAS PMPD 100 which dilutes at temperatures of up to 200°C, rather than catalytically stripping it at >350 °C as is now done by AVL (post-2018). Using this experimental set-up, METAS reported a VPR penetration efficiency of 10.2% at 10 nm and 77.2% at 55 nm. While the penetration at 55 nm aligns with previously calibrated values around this size (see Section 1.2.2), the 10.2% penetration at 10 nm is significantly lower than expected (~30%). This discrepancy highlights that there was likely still volatile material either nucleated or present as coatings, which were not removed by the PMP dilution strategy. This volatile material is then either lost or shrunk in the VPR, leading to losses, which are brought about by volatile removal and are seen in addition to the diffusion, inertial and thermophoretic loss being quantifying. Similar trends have been observed for pre-2019 AVL calibrations when the CAST was thermally treated at 350°C using an evaporation tube (rather than CS), which also led to lower penetration efficiencies reported at 15 nm (35-45% vs. 45-55% post-2018 see Figure 6).

Another potential conditioning uncertainty is the flow splitter bias between the upstream/downstream CPC and the VPR being tested. However, both AVL and METAS have reported no measurable splitter bias. AVL noted an uncertainty <1%, in accordance with ISO27891:2015 Annex G.3, while METAS reported an expanded measurement uncertainty of <4% (k=2) for splitter bias. It is noted that AVL uses a mixing chamber upstream of the splitter to ensure the aerosol is well-mixed.

1.3.3. Impact of Particle Type Used on VPR Calibration Uncertainty

Another uncertainty which could explain the results from Figure 17 and Figure 18 is the particle morphology used. As discussed, AVL now use an APG combustion PM source which is thermally treated at 370°C using a CS (i.e., nvPM), UoM used SPG non-sintered silver particles, and NPL used a nebulised gold colloid suspension from BBI solutions. Given the results in Figure 13, which showed that the CPC ratio starts drifting <20 nm despite the D_{50} for the CPCs being 2.5 nm, it is possible that the slightly lower-reporting of NPL compared to AVL and UoM at 15 nm was caused by a difference in the counting efficiency between the two CPC used. Another hypothesis could be there is a volatile coating present on the gold colloid at this size, which is removed resulting in smaller particles. At 50 and 100 nm, NPL reported a higher penetration efficiency with gold when

[8] Email communication with AVL

compared to AVL with nvPM, possibly due to the lower DMA resolution used by NPL when compared to AVL as previously discussed.

Using a similar setup and correction method as applied to the UoM data discussed here, the RAPTOR project reported that VPR losses for the EUR APC, using RQL combustion nvPM, matched those from the AVL calibrations (within measurement uncertainty) [5]. However, the project noted a material dependency for nvPM number, between the EUR and Swiss APCs, reporting larger differences in reported nvPM number when sampling exhaust containing metallic particles at around 10 nm. This discrepancy likely arose from slightly different losses, of the smallest particles, in the Swiss and EUR sampling systems. However, it could have also originated from differing CPC counting efficiencies for small metallic particles, although it is noted that CPC models are nominally identical (TSI 3790E) and were serviced and calibrated in parallel at the same laboratory. This disagreement at <15 nm was also witnessed, during a separate dedicated intercomparison test[9].

1.3.4. Impact of Downstream CPC Count on VPR Calibration Uncertainty

Downstream of the VPR, the measuring CPC will experience high dilution ratios combined with VPR loss, resulting is relatively low counting statistics. During the VPR penetration measurement of the EUR APC, NPL reported number counts of 35-70 particles/cm^3 for their downstream CPC, while AVL and UoM reported ranges of 2-70 and 5-230 particles/cm^3 respectively, with the upstream concentration being >5000 particles/cm^3 in all cases. In the UoM experiment, the particle concentration was specifically varied at a given size to assess the impact of the downstream CPC concentration on the uncertainty, with the results shown in Figure 19 (a). Similarly, given that NPL and AVL use different DMA aerosol to sheath ratios (see Table 3**Error! Reference source not found.**), the effect of this ratio on the uncertainty was specifically assessed at 6 and 15 nm (Figure 19 (b)). No clear trend could be established, suggesting that low downstream CPC counts and DMA ratios between 5 and 10 did not impact the VPR penetration efficiency within the measurement uncertainty.

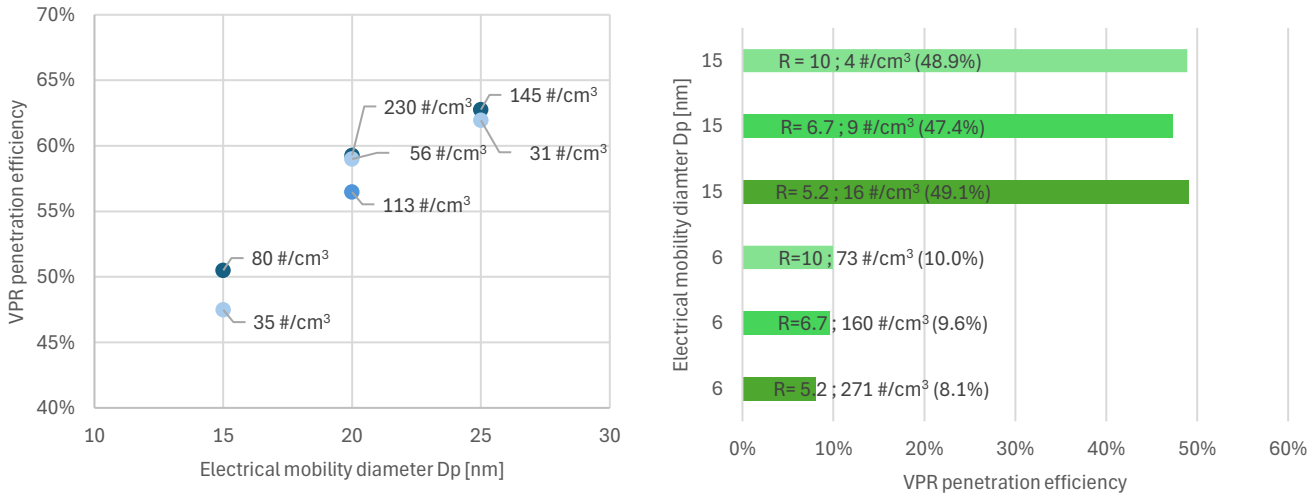

Figure 19: Impact of downstream CPC concentration (a) and DMA resolution (R=sheath/sample flow) (b) on measured VPR penetration efficiencies

[9] See Figure 30 in SAMPLE IV Deliverable 1 report

1.3.5. Impact of DF2 on VPR Calibration Uncertainty

While not specifically investigated in this analysis, internal dilution within the nvPM number instrument (i.e., DF_2) has been seen to contribute significantly to the overall uncertainty, particularly for PCRF ≥500[10]. For some VPR technologies such as the DEED, the inlet pressure affects the dilution (DF_2) and therefore both DF_2 and VPR calibration should be performed at the same inlet pressure as when measuring nvPM number within a regulatory system (i.e., -60 to -80 mbar). The DF_2 calibration measurement itself has uncertainties associated with it, with NPL reporting a DF_2 of 67.6 (rounded to 68) for the EUR APC while AVL measured 69, corresponding to a 2% difference, which is well within the expected CO_2 measurement uncertainty stemming from instrument drift, stability, linearity and span gas accuracies, when deriving DF in two different laboratories. Furthermore, given that nvPM number instruments may experience slight blockage (e.g., diluter inlet) and that DF_2 verification is required, using the measured DF_2 rather than the calibrated one may slightly reduce the nvPM number uncertainty. However, further work would be required to validate this hypothesis.

1.4. Summary and Future Work of Number Measurement Uncertainty

This chapter assessed the uncertainties associated with the calibration and drift of VPRs and CPCs which are specified in nvPM number measurements, focusing on factors such as VPR technology, particle measurement techniques, particle conditioning, particle type, and downstream CPC counts. The variability in VPR penetration efficiency across different calibration and research laboratories (AVL, NPL, and UoM) was examined to identify sources of uncertainty and suggest protocol improvements to enhance measurement accuracy. The findings highlight the importance of standardising VPR calibration protocols to reduce uncertainty in reported nvPM number. While VPR loss is not expected to vary over time due to its fixed geometry and stable temperature requirements, the complexity of accurately quantifying VPR loss introduces significant measurement uncertainties, which are reflected in the annual variations observed in VPR penetration calibration data. By potentially adopting a more stringent specification of the sources of variability, such as experimental set-up required to derive penetration (e.g. intercomparing & corrected 2x CPC's), particle type, and conditioning practices, as detailed below, it should be possible to improve the reproducibility of nvPM number instrument calibrations, ultimately contributing to more effective monitoring and regulation of nvPM emissions.

1.4.1. Summary of quantified nvPM number uncertainties

Based on assessment of the two hypothetical PSDs representing low- and high-power aviation nvPM (Figure 1), the following uncertainties have been determined:

- Not correcting for VPR particle loss, as is currently the regulatory method, in reported EI nvPM may result in up to an 83% under prediction in engine exit number concentration (at the smallest PSDs).
- Different compliant and commercially available VPR technologies (APC Vs DEED) have significantly different penetration efficiencies, resulting in an added uncertainty between 20 and 25% for reported EI nvPM number when derived as currently specified in ICAO Annex 16 Vol. II.
- Year-to-year variability for VPR penetration is currently 7-10% for an APC calibrated by AVL and 18-30% for a DEED calibrated by NPL and has been seen to be significantly impacted (causing a bias) by a change in the preconditioning of the aerosol used to determine the penetration. This has no impact on current nvPM emissions regulatory reporting but does have an impact on airport inventory system loss reporting.
- Laboratory-to-laboratory VPR penetration measurement variability for the same APC VPR resulted in an uncertainty ranging between 2 and 4% in reported EI nvPM number.

1.4.2. Summary of findings and recommendations

[10] See Figure 31 in SAMPLE IV Deliverable 1 report

- Drift observed within the 12-month calibration period for the nvPM number instruments investigated (including counting accuracy, counting efficiency, VPR penetration & DF_2) was well within expectations with observed results within the measurement uncertainty.
- Year-to-year CPC variability observed after a 12-month calibration period, for the Swiss, EUR and RR CPCs, matched well with E31P calculated variability.
- Mandating application of the CPC accuracy factor (i.e., k-factor), derived during calibration, within the aviation nvPM standards (as is already done for automotive regulation) would reduce the CPC uncertainty from ±10% to ±5%.
- There is currently no perceived benefit in calibrating VPR penetration at sizes below 15 nm, given the increased penetration measurement uncertainty at small sizes (low counts, CPC counting efficiency, etc).
- No evidence was found that VPR loss are particle type dependent (to within the measurement uncertainty), as long as the particles are correctly preconditioned to ensure they are non-volatile at temperatures witnessed in the VPR.
- Calibration aerosol pre-conditioning can significantly impact VPR calibration. Inadequate conditioning, such as not sufficiently removing volatile material, can result in lower-than-expected penetration efficiencies, particularly at smaller sizes (e.g., 15 nm), as these volatile particles are shrunk and/or destroyed by the VPR as per its design. Implementing rigorous conditioning protocols that include thermal treatment at appropriate temperatures is warranted if combustion sources are used (i.e., 350°C as stated in A16V2 [1]).
- The type of particle used in calibration (e.g., emery oil, combustion nvPM, silver, or gold) impacts the CPC counting efficiency. Using representative nvPM particle type during CPC and VPR calibrations could reduce uncertainty in system loss corrected nvPM number emissions reporting. It is therefore recommended to either use a CPC with a D_{90} or D_{50} well below 15 or 10 nm respectively (e.g., ≤ 7 nm) as particle type isn't expected to affect CPC counting accuracy, or to calibrate on appropriately conditioned combustion nvPM, to minimise the calibration material dependency on counting efficiency.
- A standardised measurement approach to VPR calibration could reduce nvPM number uncertainty. Using a single CPC with a suitably low D_{90} (<<10nm) to measure before and after the VPR is perceived to offer lowest uncertainty, in the case of a perfectly stable calibration source. If two CPCs are employed, it is recommended to intercompare them using the same particle type as that used for the VPR penetration calibration to ensure consistency. Additionally, due to the particle-type dependency of CPC counting efficiency, it is advisable to first calibrate the CPC using the same particle type that will be used for the VPR penetration calibration.
- During VPR calibration, neither low downstream CPC counts, nor differing DMA aerosol-to-sheath ratio (between 5 and 10) significantly contributed to measurement uncertainty for particles < 30nm. Further validation is required at 50 and 100 nm. Also, maintaining higher particle concentration downstream of the VPR can only help improve the measurement accuracy. Given (some types of) CPC counting accuracy are only currently calibrated down to 2500 particles/cm^3, further work would be needed to verify CPC counting accuracy down to 10's of particles/cm^3.

2. Novel nvPM Mass Calibration Sources

Currently, nvPM mass instrument calibration must be conducted using either a diffusion flame combustion aerosol source (DFCAS) or gas turbine engine exhaust nvPM [1]. Calibration requires collecting source concentrations from as low as 50 µg/m³ up to 500 µg/m³ on quartz filters, often resulting in lengthy and costly calibration campaigns. Furthermore, no affordable, commercially available method currently exists to verify nvPM mass instrument operation in-field before a test campaign.

Nebulised aqueous colloids composed of either fresh aircraft soot or a proxy carbon nanopowder are considered a promising alternative for the calibration and in-field check of aircraft nvPM mass instruments. A preliminary study[11], demonstrated that commercially available carbon-black nanopowder and small quantities of 'scraped' aircraft soot (1 µg/mL) could be successfully suspended in water, nebulised, and measured in the aerosol phase as Nebulised Carbon Black (NCB) and Nebulised Aircraft Soot (NAS). As such, further work was undertaken to explore the potential of nebulised carbonaceous colloids to act as a calibration source for nvPM mass instruments and for in-field checks.

In this study, the procedure for suspending carbonaceous nanopowders in water was further developed. Four new powders were investigated namely: a commercially available non-graphitic carbon nanopowder[12] , a commercially available mesoporous graphitic carbon nanopowder[13], and two aircraft soot powders 'scraped' from a de-tuner wall within a Rolls-Royce Trent engine testing facility. Given the aircraft powders were likely contaminated with lubrication oil, a fraction of the collected powder was 'rinsed' with hexane to remove the potential oil residues. Briefly, the powders were placed onto a Millipore filter, with hexane being continuously passed through it allowing oily deposits to be transferred from the powder to the filter paper. The powder was then dried using an external vacuum. The process was repeated until the powder did not look visibly contaminated with oil.

Following ultrasonic dispersion of the powders in water and subsequent nebulisation, the aerosols were measured by the instruments as Nebulised non graphitic Carbon Powder (NCP_{ng}), as Nebulised mesoporous graphitic Carbon Powder (NCP_{meso}), nebulised aircraft soot from Rolls Royce Trent engines ($NAS_{RRTrent}$) and nebulised aircraft soot from Rolls Royce Trent engines, which was treated with a Hexane Solvent Rinse ($NAS_{HSR\_RRTrent}$).

Figure 20: Photographs of the different carbonaceous powders tested (left: vials containing aircraft soot 'scraped' in different sections of a de-tuner, right: commercially available carbonaceous nanopowders)

Several parameters, including the mass of powder in suspension, vial type, diluent type, and sonication duration, were evaluated. The nebulised aerosol was then characterised in terms of particle number (using APC, DMS500, and SMPS), mass (using LII-300 and MSS), and size (using DMS500 and SMPS). Additional analyses were conducted on selected colloids to further quantify the aerosol properties, including

[11] See SAMPLE IV Deliverable 1 report
[12] https://www.scientificlabs.co.uk/product/metal-and-ceramic-other/633100-25G
[13] https://www.scientificlabs.co.uk/product/metal-and-ceramic-other/699624-25G

transmission electron microscopy (TEM), particle effective density, fluence measurements, and thermogravimetric analysis.

2.1. Nebulised Carbonaceous Powder Colloid Properties

2.1.1. Main Aerosol Properties

The aerosol output of four nebulised carbonaceous powders (NCP_{ng}, NCP_{meso}, and $NAS_{RRTrent}$ and $NAS_{HSR\_RRTrent}$), manufactured as part of this study, were characterised for PM mass, number and size, with the experimental setup depicted in Figure 21.

Each colloid was nebulised using a Topas ATM226 which produces nanodroplets (see Figure 25), which were mixed with HEPA filtered air to afford sufficient flowrate for the diluter inlet. The diluted aerosol was then further diluted and heated using a Dekati eDiluter pro to ensure evaporation of water and good mixing before measurement. It is noted that an x-ray neutraliser (Grimm 5524-X) was always used in line with DMS500 measurement, as all colloids were previously found to exhibit highly charged particles shown to affect this instrument (see section 2.3.2).

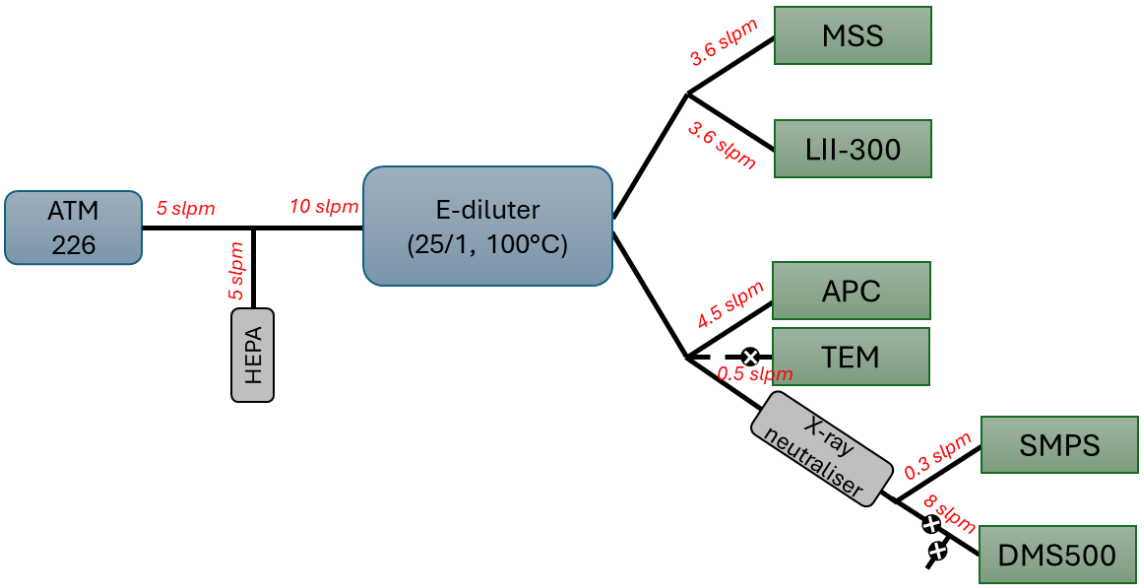

Figure 21: Diagram of the experimental setup used to characterise the particle number, mass and size produced by the carbonaceous colloids

Example particle size distributions of the four nebulised carbonaceous powders mixed at concentrations of approximately 0.2 g per 150 mL of water are shown in Figure 22, with the corresponding dilution-corrected number, mass and GMD outputs given in Table 4. Consistent with the conserved mass loading per unit volume, it is seen that NCP_{meso} and NCP_{ng} typically produced a relatively lower number of particles at GMDs of circa 100 nm when compared to the $NAS_{RRTrent}$ and $NAS_{HSR\_RRTrent}$ which produced a higher number of particles with a GMD of circa 25 nm.

A small peak observed around 10 nm for both NCP_{meso} and NCP_{ng} was not consistently observed across similar colloids and is thought to have originated from contamination while fitting the vials to the nebuliser, or when trying to re-mix colloids in an ultrasonic bath. It is noted that significantly higher mixed concentrations were also achieved for the hexane solvent washed aircraft soot and non-graphitic carbon powder colloids, as discussed in section 2.1.2. Also, the NCP PSDs appear noisier when measured with the SMPS (Figure 22 (b)) due to the relatively lower number concentration measured when compared to NAS (y-axis normalised).

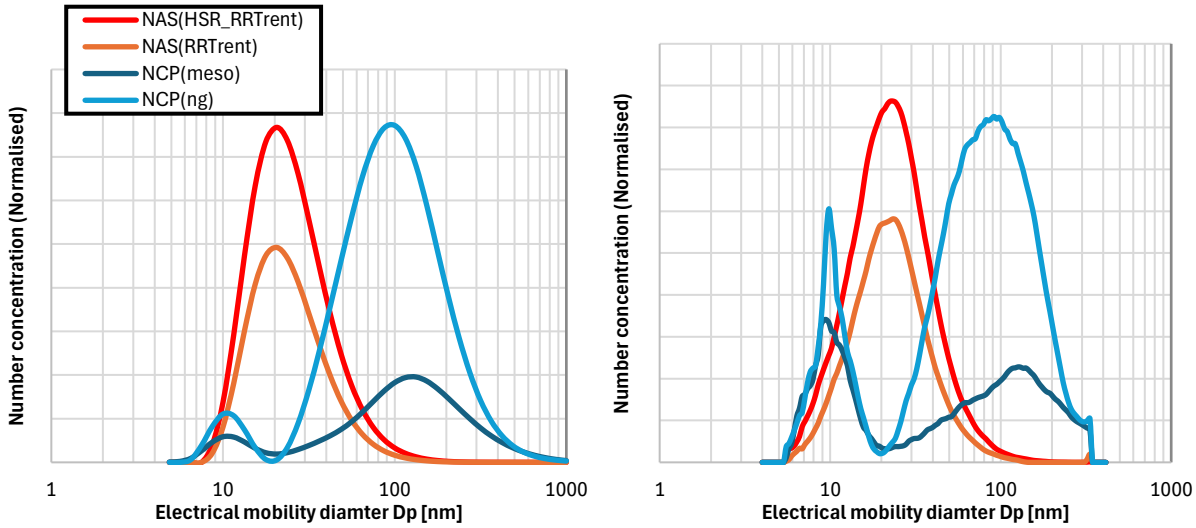

Figure 22: Normalised to the maximum of the NAS distribution, DMS500 particle size distributions (a) and SMPS particle size distributions (b) for different nebulised carbonaceous colloids at mixed concentrations of 0.2g per 150 ml

Table 4: Approximate (average over different instruments) dilution-corrected mass and number concentrations produced when nebulising different carbonaceous colloids at mixed concentration of 0.2g per 150 ml with a Topas ATM226

	mass [mg/m^3]	**number [#/cm^3]**	**GMD [nm]**
NCP_{ng}	Up to 6.4	2.6E+06	100 - 130
NCP_{meso}	Up to 4.7	7.6E+05	100 - 130
$NAS_{RRTrent\_t}$	Up to 0.3	1.4E+07	22 - 28
$NAS_{RRTrent}$	Up to 0.1	1.1E+07	22 - 28

TEM images were taken to assess the morphology of the different nebulised colloid types and were compared to the primary particle size measured by the EUR LII-300. Looking at Figure 23, NCP_{meso} and NCP_{ng} appear as aggregates of several primary particles, with the LII-300 reporting their primary particle size to be ~14-16 nm for NCP_{ng}, and ~ 19 nm for NCP_{meso}. Conversely, the $NAS_{RRTrent}$ shown in Figure 24 appears composed of a single particle, with an LII-300 primary particle size of ~21-24 nm, similar to the GMD of the output PSD. It is hypothesised that the ultrasonication used during the colloid-making process (see section 2.2) separated the component particles of the agglomerates (i.e., weakly bound particles held together by Van der Waals forces) in the powder. Meanwhile, the nebulisation process, during which the particle-containing droplets evaporate, likely exerted stronger surface tension forces on the particles. This may have caused the aircraft soot aggregates (i.e., strongly bonded particles) to collapse and form more spherical aggregates [13].

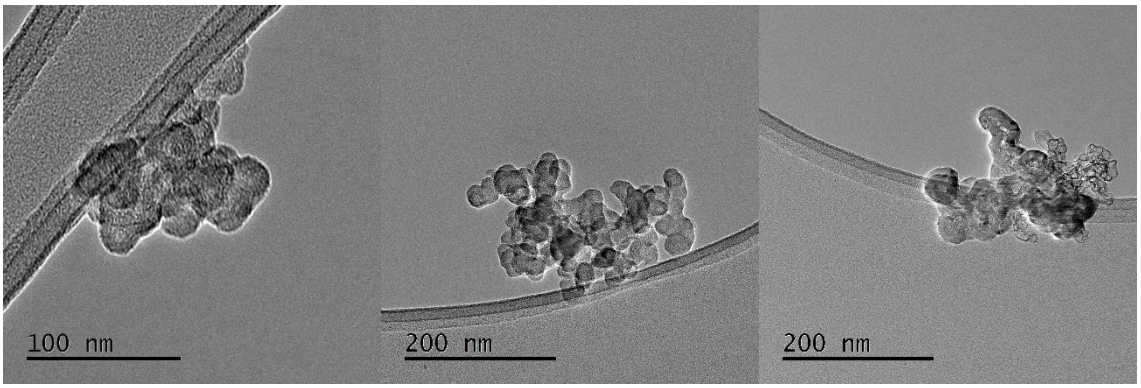

Figure 23: TEM images of NCP_{ng} (left and middle) and NCP_{meso} (right)

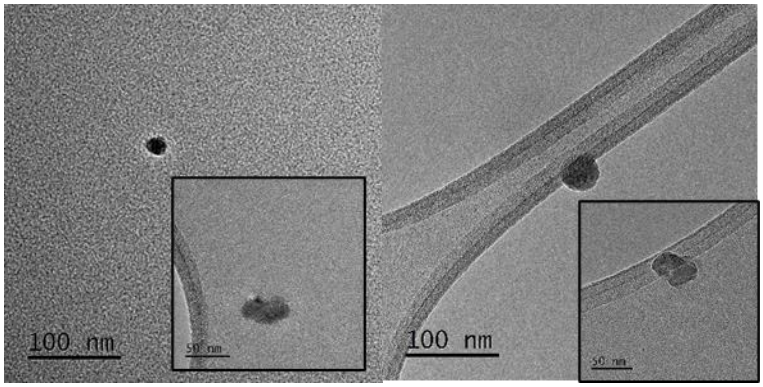

Figure 24: TEM images of $NAS_{RRTrent}$ (left) and $NAS_{RRTrent\_t}$ (right)

Additional particle effective density measurements were performed for each of the colloid types using a DMA-ELPI+ combination[14]. The NCP_{meso} and NCP_{ng} were found to have a density between 0.5 – 1 g/cm^3 while the density for $NAS_{RRTrent}$ and $NAS_{HSR\_RRTrent}$ were around 1.5 g/cm^3.

2.1.2. Maximum Output Achieved from Nebulised Colloids

To facilitate filter-based and CERMS calibration using nebulised carbonaceous colloids, a minimum raw concentration of 1 mg/m³ may be needed (4-12 mg/m³ recommended) to achieve the current calibration requirement of 500 µg/m³ maximum concentration. However, future adoption and improvements to the CERMS charger particle throughput may reduce the raw particle concentration required. Here, the maximum particle number and mass output was examined by varying the amount of carbonaceous powder - up to 4 g – that could be suspended in approximately 150 mL of distilled water.

Initially, experiments were conducted to determine whether the nebuliser produced enough nano-droplets to carry individual particles. This was assessed by comparing the particle size distributions from different nebulised colloids with those of nebulised di-ethyl-hexyl sebacat (DEHS), which closely approximates the water droplet size distribution [9, p. 71], as shown in Figure 25. The total DEHS concentration was typically an order of magnitude higher than any nebulised carbonaceous colloids, suggesting that the nebuliser generated enough droplets to transport individual particles effectively.

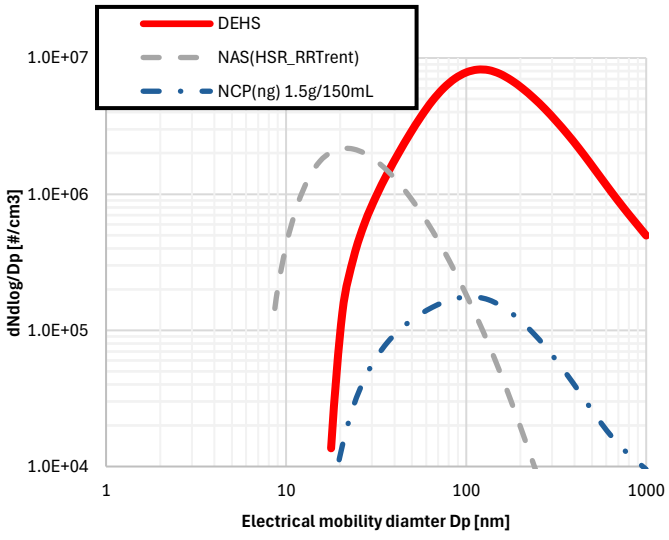

Figure 25: Measured particle size distributions from nebulised DEHS and carbonaceous colloids behind a ~60/1 dilution at maximum nebuliser setting

[14] G. McPherson, 'DP33 SAE E31 Huntsville - "Effective density measurement comparison"', Jun. 2023

Subsequently, additional colloids were prepared using carbon powders and aircraft soot at various concentrations: 0.2g to 1.5g per 150mL for the carbon powders, and 0.2g to 4g per 150mL for the aircraft soot. The resulting nvPM mass concentrations from the nebulised colloids are presented in Figure 26, with maximum dilution-corrected output masses of ~45 mg/m³ for NCP_{ng} and ~3.6 mg/m³ for $NAS_{HSR\_RRTrent}$. It is important to note that the output mass is significantly lower than expected if all the powders were fully transferred into the liquid — approximately 4 times lower for NCP and 200 times lower for NAS. This discrepancy is attributed to a considerable amount of undispersed residue remaining at the bottom of the sample bottle following ultrasonication of the colloid, which was disregarded when the prepared colloid was transferred into the test vials.

The results from Figure 26 suggest that commercially available carbon powders were more efficiently dispersed into the water than aircraft soot, which was also evidenced by the larger amounts of residue remaining at the bottom of the aircraft soot colloid after the ultrasonication process. Potentially commercial carbon blacks may be surface modified (or have surfactants) to be hydrophilic, which would mean that they are more easily suspended in water. Whereas it is known that soot emissions, such as the NAS, are hydrophobic and difficult to disperse in water.

It was observed that $NAS_{HSR\_RRTrent}$ produced significantly higher particle number concentrations than NCP_{ng}, albeit at smaller particle sizes. Furthermore, a linear relationship was observed between the mass of powder mixed in the water and the output mass, indicating that doubling the powder mass in the colloid, roughly leads to a corresponding doubling of the output mass in the generated aerosol.

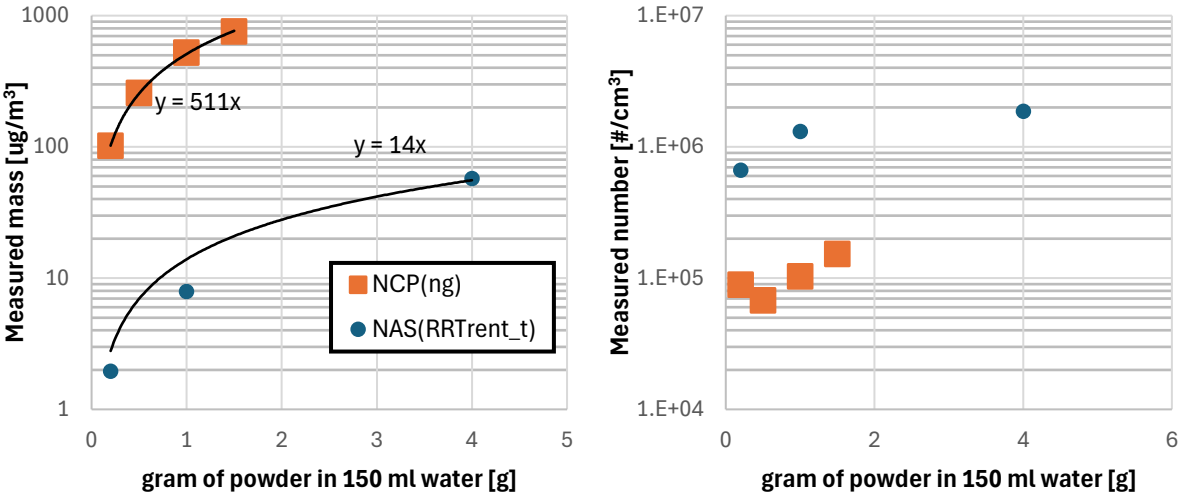

Figure 26: Measured nvPM mass (left) and number (right) concentrations from nebulised carbonaceous colloids behind a ~60/1 dilution

2.2.Carbonaceous Colloid Development

Several experiments were conducted to better understand and optimise the methodology for making colloids from carbonaceous powders in water. Namely, the effect of vial & aqueous medium, nebuliser setting, ultrasonication time, re-mixing and shelf life were investigated.

2.2.1. Colloid-Making Process

Briefly, the carbonaceous powders were weighed and mixed in distilled water. The mixture was then dispersed using ultrasonic bursts from a probe for up to 5 hours. The resulting colloid was carefully decanted into a 150 ml vial compatible with the nebuliser, leaving behind any residues, which had gravitated to the bottom of the sample bottle used to prepare the colloid.

2.2.2. Ultrasonication Time and Aqueous Medium

The ultrasonication time was varied between 1 and 5 hours when preparing non-graphitic carbon powder colloids to assess its effect on the output NCP_{ng}. Simultaneously, two types of aqueous mediums were tested: reagent-grade distilled water and ultrapure water (Type 1). As shown in Figure 27, and as expected, nebulised distilled water generated a larger residual particle mode, indicative of a higher concentration of impurities.

However, Figure 28 demonstrates that the choice of aqueous medium had no significant impact on the ultrasonicated nebulised carbonaceous colloids, with the nebulised carbonaceous powder colloids in either water type showing similar particle size distributions. Notably, the residual peak seen in nebulised water alone was minimised in the nebulised carbon colloids. It is believed that the ultrasonication process, along with the transfer of the colloid from the beaker to the vial, caused most the impurities to settle at the bottom and be excluded from the final colloid. Additionally, the carbon nanoparticles in the colloid will scavenge the smaller residuals, causing that residual fraction to nearly disappear [14]. When comparing 1-hour and 5-hour sonication times, no significant difference was observed in the main peak. However, the smaller residual peak was reduced after 5 hours, supporting the above hypothesis.

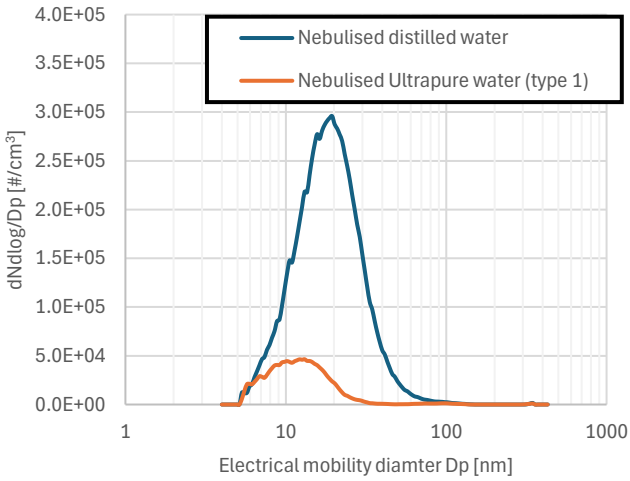

Figure 27: Measured particle size distribution from different nebulised aqueous mediums (after ~60/1 dilution), illustrating the residual impurities

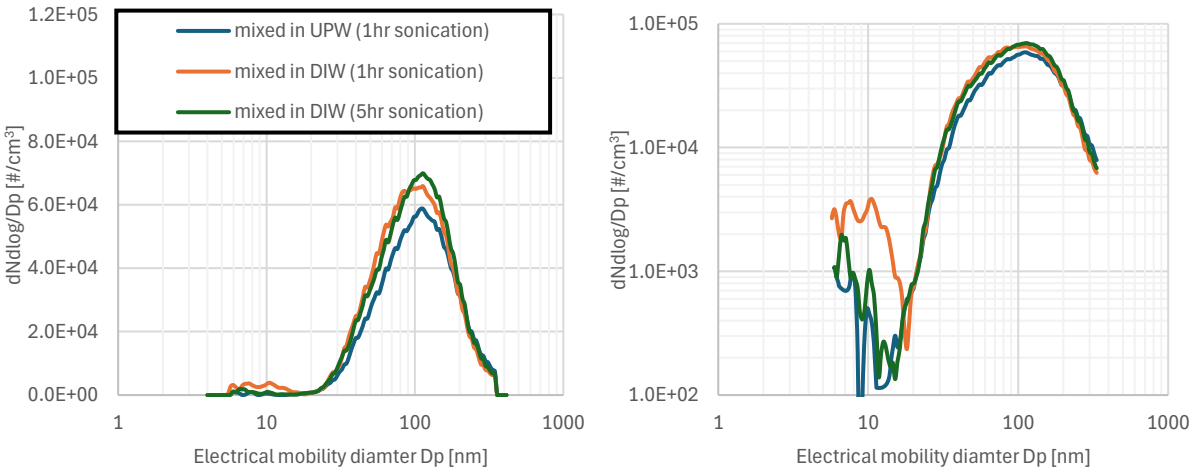

Figure 28: Measured particle size distribution for NCP_{ng} with different aqueous mediums (UPW= ultrapure water type 1, DIW=Distilled water) and probe sonication times (left linear y-scale, right log y-scale)

2.2.3. Colloid Vial Material

The nebulised output was compared when the same colloid was stored in both a 150 ml Glass (high-purity, clear, USP/EP Type I borosilicate glass 3.3) and Plastic (polystyrene) laboratory bottles. No measurable difference was observed, in line with previous work [9]. However, it is known that plastic bottles can leach overtime, potentially contaminating the colloid, but is unlikely to happen before months.

2.2.4. Shelf-life and repeatability

The PSDs from prepared NCP_{ng} and $NAS_{HSR\_RRTrent}$ samples were measured repeatedly over a period of up to 7-weeks using a nominally identical measurement setup, with the results shown in Figure 29. The PSDs showed no significant change within the bounds of measurement and sampling uncertainty, indicating that the colloids can be considered stable for at least several weeks/ months, in glass bottles, when stored appropriately.

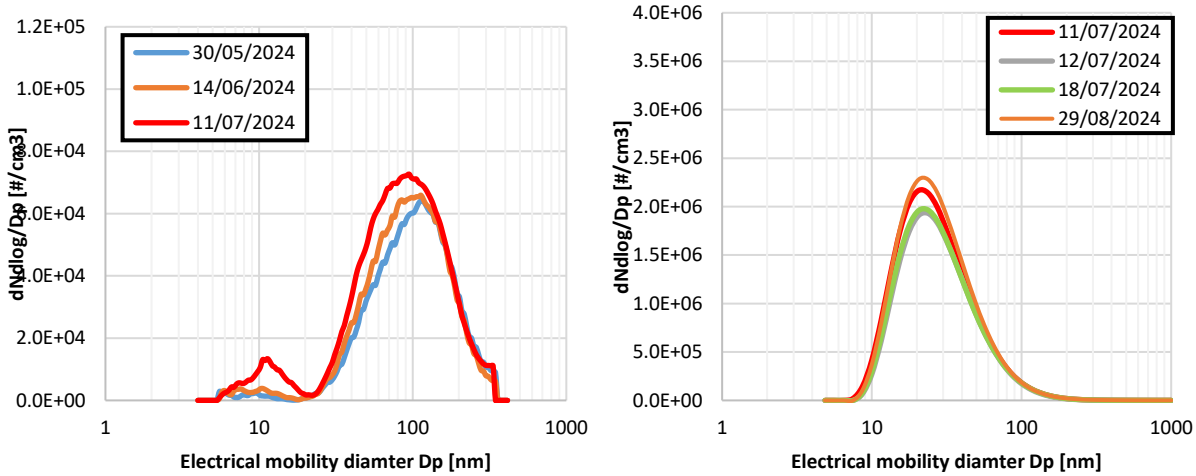

Figure 29: Impact of colloid storage/ageing on output particle size distribution for 0.2 g/150mL NCP_{ng} measured by an SMPS (left) and 1g/150mL $NAS_{HSR\_RRTrent}$ measured by a DMS500 (right)

2.2.5. Re-mixing of Stored colloids

Slight reductions in particle concentrations were observed in the case of NAS (Figure 30) so it was assessed whether putting the vial of colloid into a 100W ultrasonic bath filled with water, helped with re-suspending any settled particles, hypothetically resulting in a higher particle output, with results shown in Figure 30. For the NCP_{ng}, while the sonic bath slightly increased the main mode around 100 nm, it also significantly increased the residual/contamination mode around ~10 nm. For the $NAS_{HSR\_RRTrent}$, 30-minutes of sonic bath has slightly increased the output size distribution magnitude. Overall, using an ultrasonic bath didn't appear to make significant impact over shaking the colloids by hand prior to usage, and may have introduced some contamination from the bottle walls, and therefore isn't recommended. It is noted that during bath sonification process there was an observed rise in the colloid temperature to approximately 50 °C, which may have impacted the colloids composition.

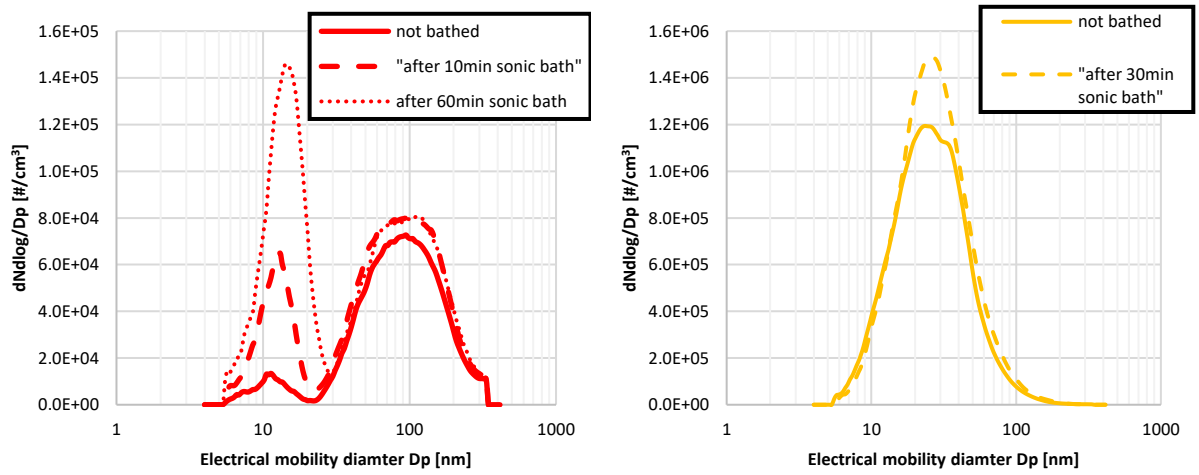

Figure 30: Impact of colloid re-mixing (ultrasonic bath) on output particle size distribution for 0.2 g/150 mL NCP_{ng} (a) and 1g/150 mL $NAS_{RRTrent\_t}$ (b) measured by an SMPS

2.2.6. Topas ATM-226 Nebuliser Operation

The nebuliser flow rate was varied from low to high setting to assess its impact on the observed PSDs from the nebulised carbon colloids, with the results shown in Figure 31. As the flow rate increased, both the particle number and mass concentrations were seen to rise, consistent with a higher droplet count. However, some issues were encountered, including suspected nozzle blockages when nebulising certain carbonaceous colloids using this specific nebuliser (Topas ATM-226), despite regular cleaning in an ultrasonic bath. Bypassing the internal pump and using compressed HEPA-filtered air instead resolved these issues and resulted in a more stable output.

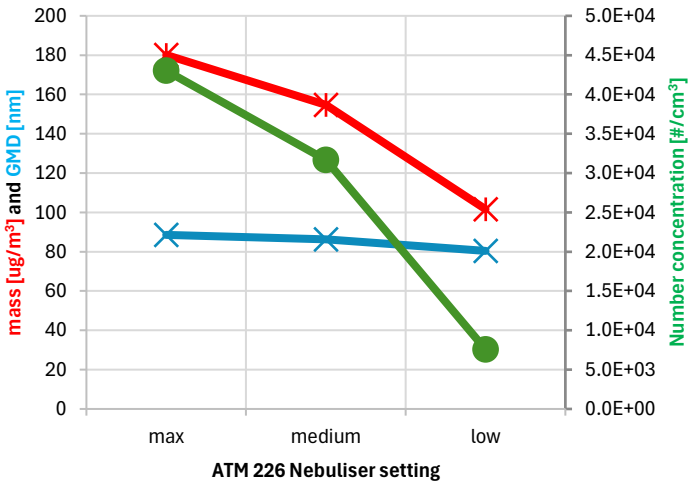

Figure 31: Impact of nebuliser setting on the measured number, mass and size for 0.2 g/150 mL NCP_{ng}

2.3. Nebulised Carbonaceous Colloid Properties

The morphology and suitability of different carbonaceous colloids for in-field checks and calibration of regulatory nvPM mass were further explored through additional measurements. An additional carbonaceous colloid[15&16] described and used in the AVIATOR project[17], labelled nebulised carbon black (NCB) was also included in this comparison.

2.3.1. Differences Between LII-300 and MSS nvPM Mass Measurements

While both the Artium LII-300 and AVL MSS meet the regulatory specification for aircraft nvPM mass measurement, the LII-300 measures refractory black carbon (rBC) through absorption and then incandescence, the MSS measures equivalent black carbon (eBC) through absorption and then acoustic waves due to thermal expansion. A change in the mass ratio between the LII-300 and the MSS could indicate differences in the particle morphology or composition (e.g., elemental composition), where one instrument might be more sensitive to certain types of particles than the other.

Therefore, this ratio was compared for various NCP's and NAS's in addition to fresh aircraft exhaust as a measure for assessing changes in particle morphology, with the results presented in Figure 32 and Figure 33. Generally, the ratio between the LII-300 and MSS ranged from 1 to 1.5 for both NCP_{ng} and NCP_{meso}, whereas it fluctuated between 0.7 and 0.8 for $NAS_{RRTrent}$.

To determine whether this impact was mass-dependent, the mass concentration of the same nebulised colloid was measured at different dilutions (black triangles in Figure 32 and blue circles in Figure 33). For both NCP_{ng} and $NAS_{RRTrent}$, it is seen the relative agreement of the LII-300/MSS ratio changes across the mass concentration, it is however noted this may well not be a mass concentration effect as particle size, soot morphology etc. are all known to change across the engine power curve, which also correlates with mass concentration. For the NCP_{ng}, the ratio is consistent, with a slight decrease as mass increases between 100 and 600 µg/m³. In the case of $NAS_{RRTrent}$, the ratio is even more consistent, with a very slight decrease as the mass increases between 40 and 100 µg/m³, and a slight decrease when the mass fell below 40 µg/m³.

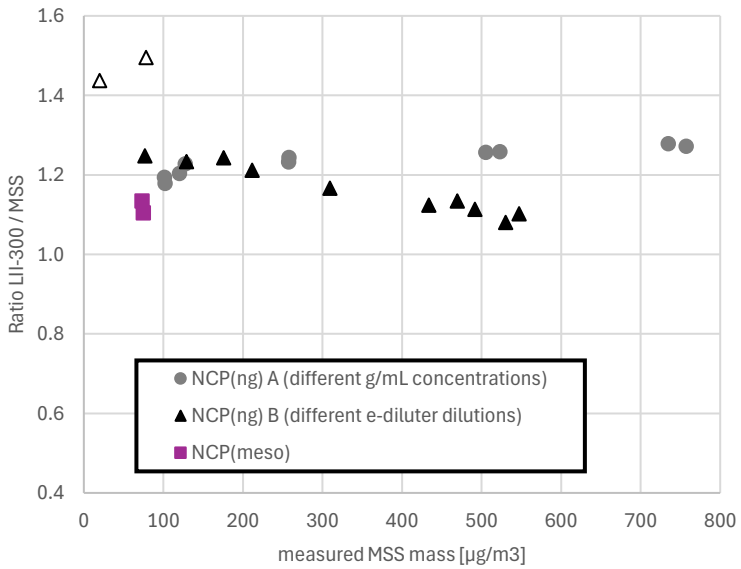

Figure 32: mass ratio between the LII-300 and the MSS when sampling different nebulised carbon powder colloids

[15] Described in more detail in SAMPLE IV Deliverable Report 1
[16] https://www.nanoshel.com/product/carbon-black-nanopowder
[17] A. Crayford, M. Johnson, and E. Durand, 'AVIATOR WP2 & 3 Emissions Engine Testing Deliverables Report', 2023

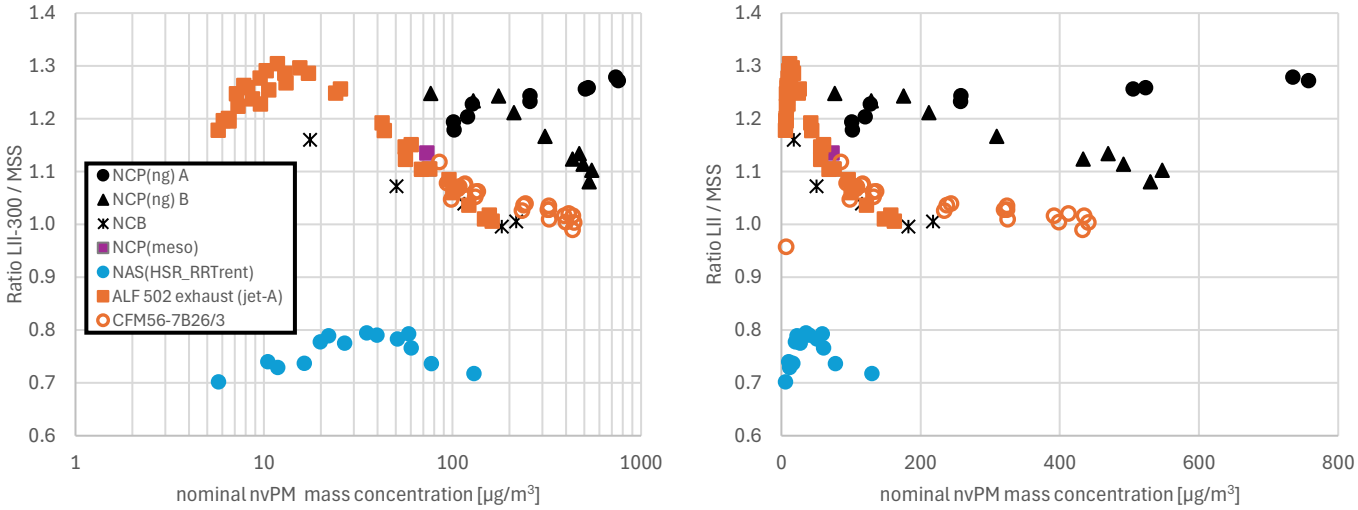

Figure 33: mass ratio between the LII-300 and the MSS when sampling different carbonaceous sources (CFM56-7B26/3 from Lobo et al. 2020 [15]) - log-x axis (left) and linear-x axis (right)

Additionally, a comparison of full and hollow triangles in Figure 32 — representing similar dilutions with different nebuliser settings — shows that the droplet size distribution produced by the nebuliser exhibits a different trend comparing the LII-300/MSS ratio. This suggests that droplet size may influence the morphology of the nebulised carbonaceous particles, with more carbon particles being forced together when a relatively larger droplet evaporates, resulting in a relatively larger compact particle as seen in the slightly larger GMD observed for the high flow rate case in Figure 34.

The LII-300/MSS ratio for the different colloids was also compared to that measured on an ALF 507 and CFM56 [15] engine exhaust using the EUR nvPM system, with the data shown in Figure 33. For these engines, the ratio fluctuated between 1 and 1.3, varying with engine thrust, aligning with the range observed for some of carbon powder colloids but not aircraft soot colloids, although the shape is similar.

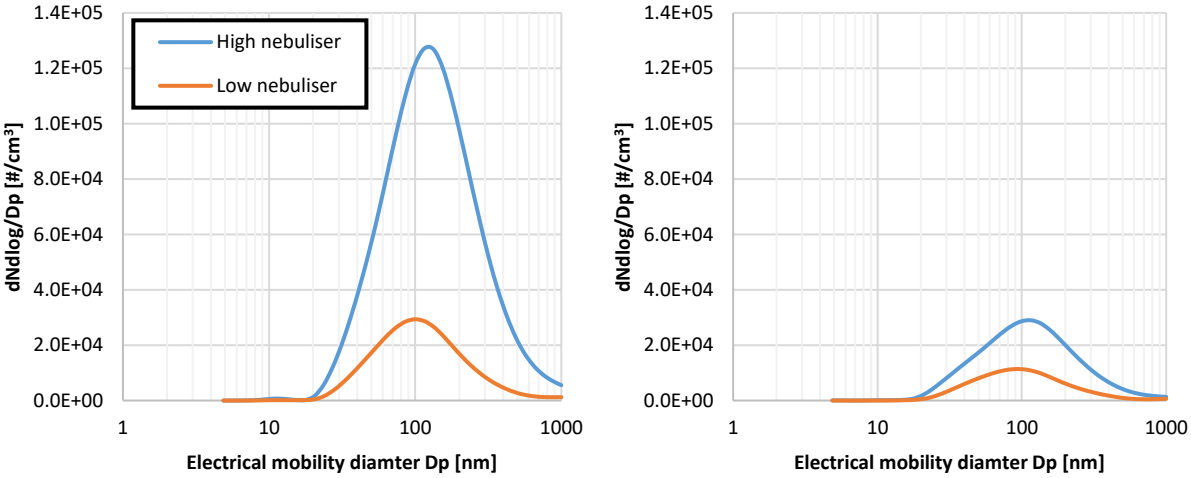

Figure 34: Particle size distribution of nebulised NCP_{ng} at same dilution but with different nebuliser setting (left – 25/1 dilution; right – 225/1 dilution)

2.3.1. LII-300 Fluence Measurements of Novel Mass Sources

The LII-300 measures nvPM mass by heating particles to near sublimation temperatures (~4000 K) with a laser pulse, then measuring the emitted incandescence to determine mass concentration. Laser fluence (energy per unit area of the laser beam) affects the signal; high fluences can cause sublimation, while low fluences may not heat particles sufficiently. A plateau region of moderate fluences yields consistent mass concentrations regardless of fluence, known as the optimum range [16], [17]. To establish the optimum fluence, fluence sweeps—gradually increasing fluence and observing responses—are performed. For aircraft engines, where varying thrust levels affect particle properties, the LII-300's fluence is optimised within a range suitable for diverse particle types.

To gain further insight into the factors driving the differences between the LII-300 and MSS measurements, fluence sweeps were performed on various sources using both the EUR LII-300 and a RR LII-300, with the results shown in Figure 35.

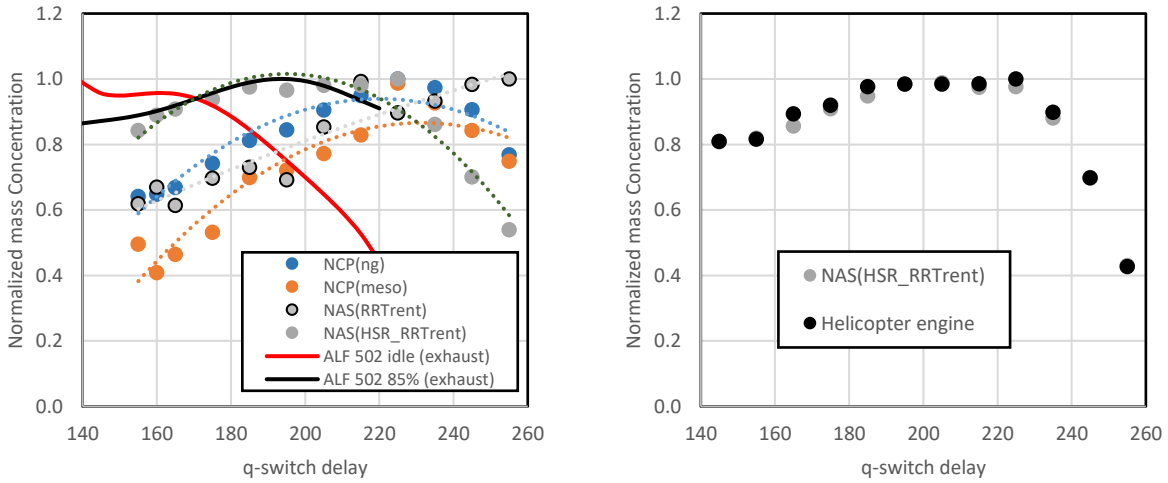

Figure 35: Fluence sweeps performed on various sources by the EUR LII-300 (a) and RR LII-300 (b)

Among the tested sources, only the $NAS_{HSR\_RRTrent}$ exhibited a fluence profile similar to that of direct exhaust from the ALF 502 at high power (EUR LII-300) and the Rolls Royce Gnome (helicopter) engine (RR LII-300). NCP_{ng} and NCP_{meso}, displayed comparable mass concentrations to the engine nvPM emissions only at Q-switch settings in a range near 220 µs. It is important to note that the EUR LII-300 is currently set to operate at a Q-switch of 160 µs, with further data of q-switch impact presented below (Figure 69).

Moreover, while the fluence sweeps appear similar for both ALF 502 exhaust and $NAS_{RRTrent}$, the LII-300/MSS ratio was shown to differ significantly between these two sources (see Figure 33) when experiments were undertaken with a Q-switch delay of 160 µs. This suggests that in this case, the MSS might be responding differently to these sources. It is also worth noting that all colloid data was collected at a relative humidity of approximately 20% and a temperature between 20 and 25°C.

2.3.2. Charge State of the Nebulised Carbonaceous Colloids

Charged particles smaller than 30 nm can significantly impact sizing accuracy of a Cambustion DMS500, which is why the use of an in-line neutraliser is recommended when sampling aerosols suspected to carry a significant charge [18]. This issue was previously encountered[18], where the DMS500 reported markedly different PSDs when measuring NCB with and without the use of an in-line neutraliser, and here when sampling nebulised PSL spheres as shown in Figure 36.

[18] Further discussion is found in SAMPLE IV Deliverable Report 1

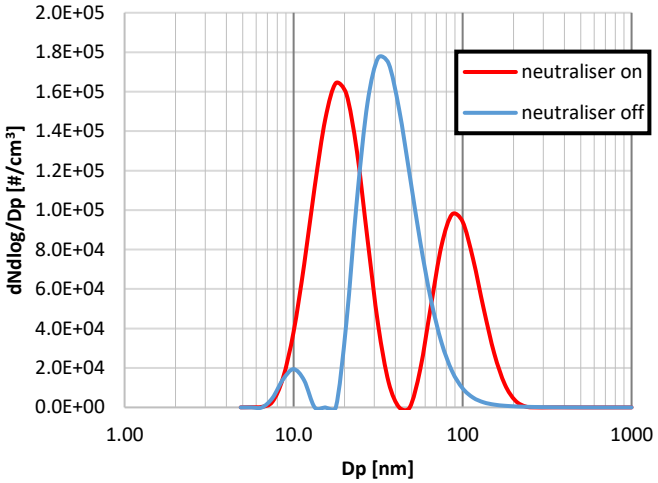

Figure 36: Measured DMS500 particle size distribution when sampling nebulised 92 nm PSL spheres with and without a soft X-ray neutraliser. The peak at ~18 nm with the neutraliser on is likely due to the presence of surfactants and residuals in the PSL colloid

In this study, the charge state of the nebulised carbonaceous colloids was preliminarily assessed by comparing DMS500 measurements with the in-line neutraliser switched on and off, with the results shown in Figure 37. For the NCP_{ng}, turning off the neutraliser led to the measurement of smaller particles at a higher number concentration, indicating the particles likely carried a positive charge, as the DMS500's corona discharge imparts a positive charge. In contrast, the NCP_{meso} and $NAS_{RRTrent}$ showed a reduction in particle number, suggesting these particles carried a negative charge. For comparison, no significant differences were observed for the DEHS aerosol, which is not expected to hold a significant charge. This approach can therefore provide a first indication of the charge state and polarity of any given challenge aerosol.

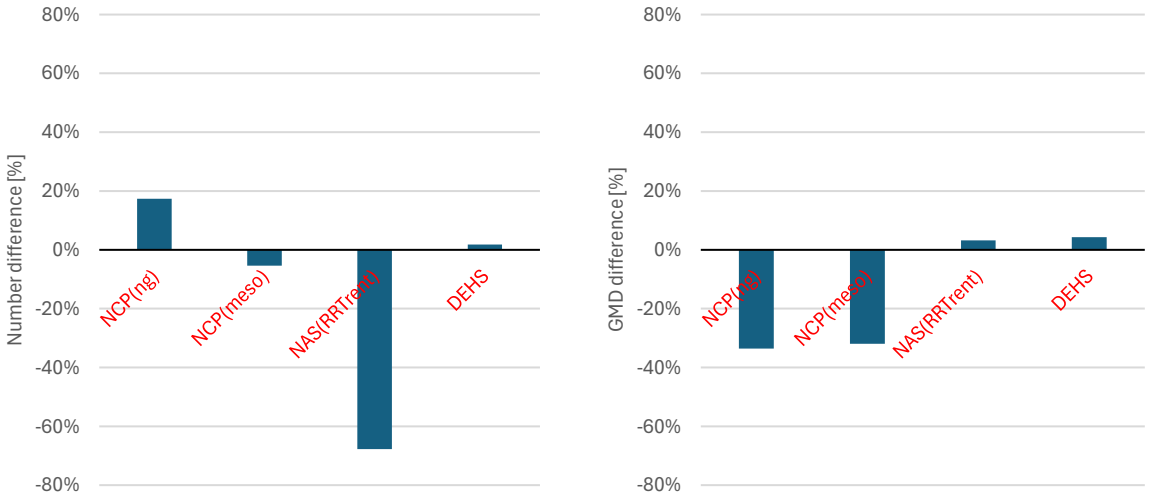

Figure 37: Difference in DMS500 measured particle Number (left) and Geometric Mean Diameter (right) between the in-line neutraliser being switched off relative to that when the neutraliser was switched on when sampling different nebulised colloids

2.3.3. Thermogravimetric Analysis of Powders

To try to better understand the differences observed in nvPM mass measurements between the various nebulised colloids, the carbonaceous powders (Figure 20), before they were mixed with the aqueous solution, were further analysed using Thermogravimetric Analysis (TGA), heating from ambient temperature to 900°C in both nitrogen and nitrogen/air environments, following the TOA temperature profile prescribed in ICAO regulation (A16 V2A7 [1]). The results, shown in Figure 38, highlight that the commercially produced carbon powders exhibit minimal mass loss until air is introduced at 550°C, indicating that they are primarily composed

of elemental carbon (EC/OC ratio > 0.9). In contrast, the Rolls-Royce 'scraped' detuner soot sample powders (without hexane solvent rinse treatment) begin to lose mass at around 300°C even without oxygen, suggesting that a significant portion (30-50%) is organic carbon. After oxygen is introduced, there is a minimal additional mass loss (5%) observed, implying that the remaining material is not predominantly composed of carbonaceous material, but could be other elements, which have been collected along with the nvPM, on/or as part of the detuner surface (e.g. metals, ceramics or sand/dust), given these material types would likely have a significantly higher density, only a relatively few of these particles would dominate the total mass of the deposit sample. The difference between the blue and green line (~20%) highlights the effectiveness of the hexane solvent treatment at removing volatile (i.e., oils & organic carbon) residues. Further preliminary analysis of the 'scraped' detuner samples was performed using an Innov-X Systems Olympus x-5000 X-ray fluorescence, which indicated a significant fraction of metallic elements including Iron, Nickle, Chromium, etc.

It should be noted that although the 'scraped' detuner soot powder may include a significant metallic fraction (potentially contamination from detuner metal surface and/or ambient dust), this fraction is mostly expected to be removed during the ultrasonication and sedimentation conditioning process and therefore may not be present in the NAS measured by the nvPM instruments. Chemical composition analysis of all nebulised sample types (after ultrasonification) should be performed in the future to understand potential differences when using prepared particle sources.

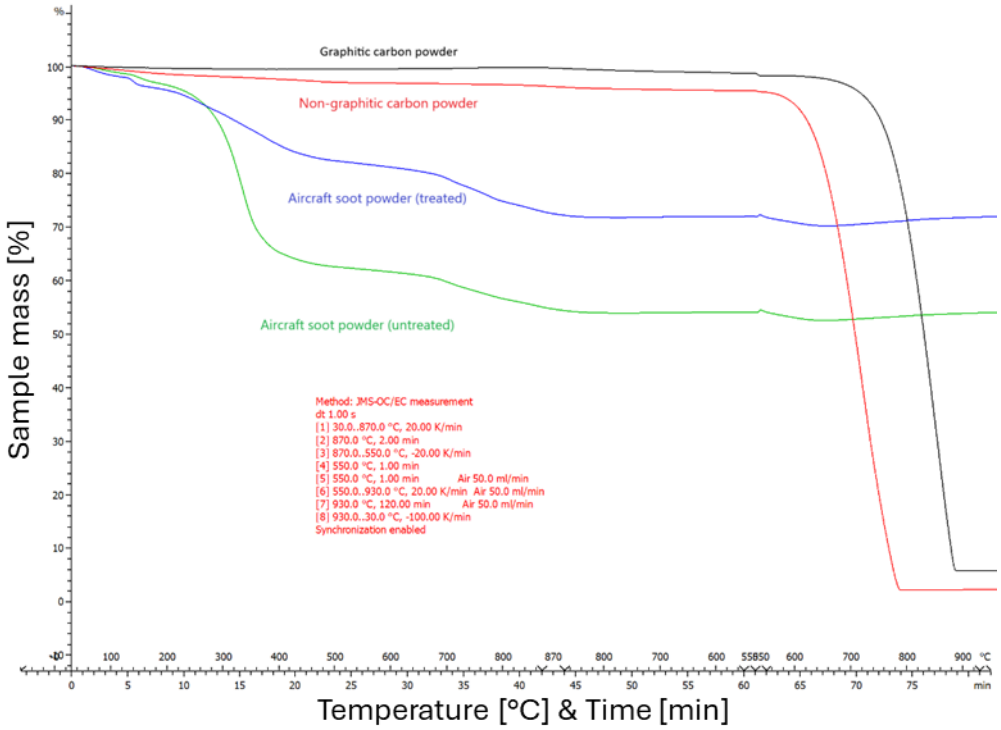

Figure 38: Thermogravimetric Analysis results for the different sample powders before sonification process

Given the potential usefulness of NAS sources, further consideration should also be given as to how best soot from aircraft engines could in the future be collected, in order to maximise the nvPM fraction and hence reduce the amount of pre-processing required prior to making the colloid.

2.4.Summary and Future Work of Nebulised Carbon Powders

This chapter has presented and discussed an optimised procedure for creating carbonaceous particle colloids from commercially available powders and 'scraped' aircraft soot. Once nebulised, these colloids can produce a range of particle sizes (~20–100 nm GMD), masses (up to 64 mg/m³), and concentrations (up to 1.4×10^7 particles/cm³). The aerosol properties largely depend on the carbonaceous powder used to form the colloid, the nebuliser's droplet size distribution, and the colloid preparation process.

Given the observed stability of the colloids and generated nebulised aerosols, it has been demonstrated that they could in theory be used in-field and in laboratory to check the performance of any given nvPM mass instrument prior to a test (e.g. with a proven dilution bridge to check linearity, to assess relative response of different instruments and to check fluence response for the LII-300, etc.). However, more work is needed to characterise the nebulised aerosols and assess their suitability as a calibration source for a specific instrument type. Since different nebulised carbon powder colloids were found to produce particles of different morphologies which resulted in different LII-300 fluences and responses between the LII-300 and MSS then particular care will be required to assess that repeatable particle morphologies can be created across different batches/ years and that the specific particle properties for any given instrument is matched so as the instrument responds in a similar fashion as it would on nvPM from a real gas turbine engine.

Current regulation specifies that an nvPM mass instrument shall be calibrated using a diffusion flame combustion aerosol source (DFCAS) (including gas turbine engine exhaust nvPM source). However, these have known significant uncertainties [5], [19]. Potentially, with additional work, it may be possible to demonstrate that nebulised aircraft gas turbine (DFCAS) soot colloids meet all the requirements for a valid calibration source. Additionally, developing improved collection protocols for aircraft nvPM powder that minimise background interference and volatile contamination could further enhance the reliability of these measurements as has been demonstrated in Certified Reference Material (CRM) Diesel particles which are now commercially available and utilised for traceable health studies and could, in theory, also meet the specification of a suitable calibration source (DFCAS).

3. Advancement of Particle Size Measurement for system loss correction

3.1. Rationale

Current regulation for nvPM emissions from aircraft engines accounts only for thermophoretic losses (i.e., k_{thermo}) within the collection section of the prescribed sampling system. However, other significant particle losses occur within the sampling and measurement system, such as diffusional and VPR losses, which are not currently corrected.

Durand et al. (2023) [20] reported size-dependent system loss correction values ranging from 1.6 to 7.8 for k_{SL_num}, and between 1.06 and 2.5 for k_{SL_mass}, based on data from thirty-two civil turbofan engines representative of the current fleet. These variations are equivalent to a bias of 60 to 680 % (i.e., (7.8-1)/1 x 100) for k_{SL_num} and 6 to 150% for k_{SL_mass}, for engine-exit nvPM emissions.

As a result, under current regulations, two engines emitting the same nvPM number concentration at different particle sizes would appear to have different emission profiles. Specifically, the engine producing smaller particles would report significantly lower EI number concentrations and hence appear cleaner, even though both engines actually emitted the same number of particles. Figure 39 illustrates this problem, showing that the green PSD appears approximately three times cleaner than the orange PSD, despite both emitting the same nvPM number at engine-exit.

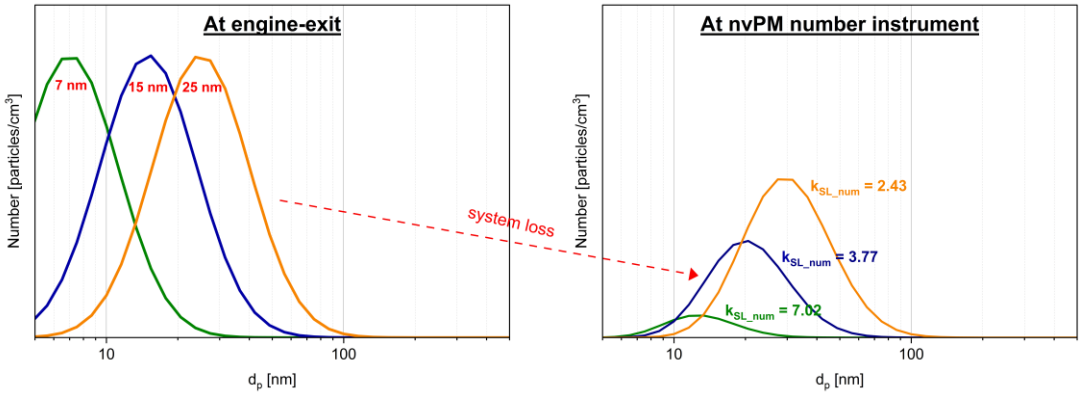

Figure 39: Example engine-exit (left) and at instrument (right) aircraft exhaust nvPM size distributions when measured in parallel with nvPM number and mass instrument (number-weighted)

The impact of particle size and size-dependent losses on regulatory nvPM number and mass is becoming increasingly important with the introduction of SAF and novel engine combustion technologies, both of which tend to produce smaller particles [2], [21], [22], [23], [24]. For instance, in an RQL combustor, the reduction in nvPM emissions due to SAF usage was overestimated by 6% when size-dependent losses were not corrected, for particles with GMD >25 nm. This bias is expected to be much larger for particles with GMDs <25 nm. Additional factors, such as variations in ambient temperature and humidity during aircraft engine certification testing, are also likely to affect measured PSD, further contributing to the uncertainty in currently reported aircraft EI nvPM.

To address this uncertainty, a size-dependent system loss correction method was introduced in the ICAO Annex 16 vol II (July 2017 revision, Appendix 8). However, as PSD measurement is not currently prescribed, this method, labelled $R_{N/M}$, uses nvPM number and mass measurements, along with several assumptions (e.g., PSD lognormality, GSD, effective density) to predict an engine exit PSD which is subsequently used to predict the size-dependent losses. This approach reduces systematic bias to a lower but still significant level (up to 67% for k_{SL_num} and up to 49% for k_{SL_mass} [20]), and hence is currently only reported for inventory purposes, rather than the setting of nvPM limits. The uncertainty from the ICAO prescribed system loss correction method, also discussed in ARP6481A [25], is primarily driven by the uncertainties in the input nvPM number and mass measurements, particularly at the lowest concentrations of mass (< 10 µg/m^3) which typically occur

at the smallest sizes <25 nm measured GMD and is further constrained by the assumption of a single lognormal PSD.

With advancements in real-time particle size instruments, over the last two decades, PSDs are regularly measured alongside regulatory nvPM number and mass, to gain a better understanding of combustion and emission processes and to more accurately correct for system losses [2], [20]. Directly measuring the PSD, rather than predicting it from measured nvPM number and mass, has been shown to significantly reduce the uncertainty in k_{SL}, making size-dependent system loss correction more appealing within current nvPM regulation. However, for this advancement to be implemented, PSD measurement would need to be formally defined within a regulatory context.

Three commercially available instruments are commonly used for measuring PSD in aircraft exhaust, namely, the Cambustion DMS500, the TSI EEPS, and SMPS (manufactured by TSI, Grimm, Brechtel, etc.). Each manufacturer employs different operational and calibration procedures, potentially introducing new uncertainties. The SMPS is typically calibrated against NIST-traceable polystyrene latex (PSL) ≥100 nm while the DMS500 and EEPS are calibrated for both spherical/compact aerosols and aggregates (see example calibration certificates in the A). Notably, the DMS500 is calibrated on soot from a Mini-CAST generator against an electrometer while the EEPS is calibrated on soot from a diesel engine against a CPC. Moreover, these instruments measure over different size ranges (DMS500 from 5 to 1000 nm, EEPS from 6 to 560 nm, and SMPS typically from 10 to 300 nm) and have different data acquisition frequencies (e.g., DMS500 and EEPS at 10 Hz, while SMPS scans range from seconds to minutes).

Although only nvPM is expected to be present during parallel sampling with regulatory nvPM number and mass instruments—due to rapid dilution and cooling to 60°C—volatile PM has occasionally been detected within a regulatory sampling system either as a nucleation peak or coating on nvPM. This volatile PM is believed to originate from oil or fuel contamination in the probe or diluter. As a result, there is growing consideration as to whether a catalytic stripper should be installed at the inlet of the particle size measurement system, to ensure accurate measurement of nvPM as defined. However, the use of a catalytic stripper would introduce additional uncertainty, as the significant particle losses within the stripper would need to be quantified and corrected. Additionally, if the primary purpose of the PSD measurement is to correct for system loss, then the measurement should capture the true PSD of aerosol being transported, as the actual PSD rather than a 'stripped' PSD at the measurement location determines the witnessed losses within the system to the point of measurement.

To date, the focus has been on assessing the current uncertainty in particle size measurements between the main commercially available instruments and determining the most suitable particle size measurement-based system loss correction method for regulatory purposes. In this regard, three size-measurement-based methods have been developed and investigated, as detailed in Durand et al. (2023) [20]. The following methods are briefly outlined below, with a visual representation provided in Figure 40:

- **Method PSD_B** (i.e., bin by bin): This method predicts the PSD at the engine exit by directly applying the measured PSD and the system penetration function calculated using the UTRC model. Its accuracy depends primarily on the precision and size range of the PSD measurement.
- **Method PSD_{L1}**: This method minimises the difference between the measured PSD and a single lognormal distribution, scaled by the system penetration function (i.e., at the engine-exit). While it reduces uncertainty at the PSD tails and allows for extrapolation to any size range, it is best suited for PSDs with a single, near-lognormal mode.
- **Method PSD_{L2}**: Like PSD_{L1}, this method uses a minimisation, but with two lognormal distributions at the engine exit. It can handle non-monomodal PSDs and those that significantly deviate from lognormality, while offering the same benefits as PSD_{L1}.

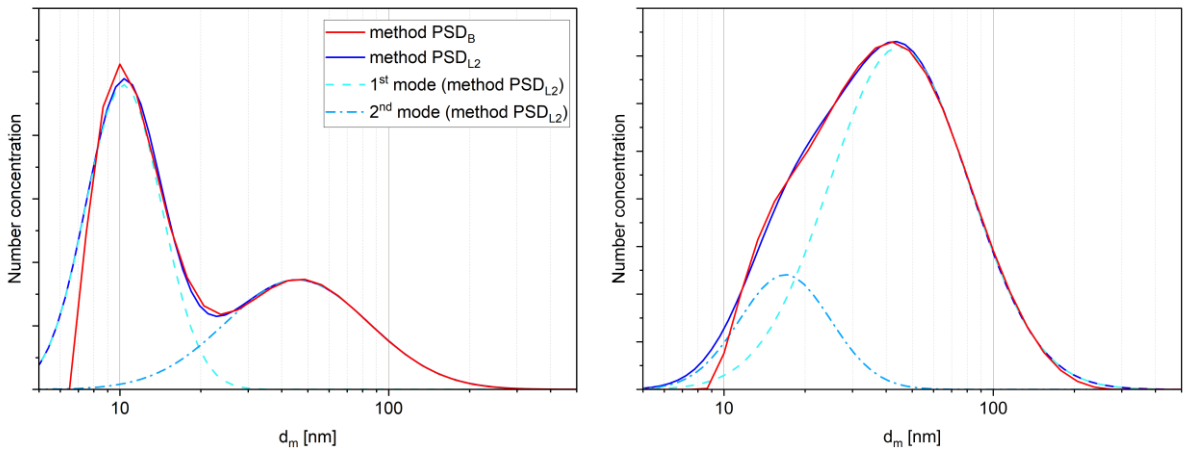

Figure 40: Example engine-exit particle size distributions fitted using different size-measurement-based methods

3.2. Impact of PSD Variability on Size-Based System Loss Correction Uncertainty

Durand et al. [20] demonstrated significant improvements that come with using a measured PSD to correct for system losses in regulatory nvPM number and mass measurements. However, they also reported variabilities of up to 19% for k_{SL_num} and up to 8% for k_{SL_mass}, attributed to differences in particle sizing instruments (SMPS vs DMS500 vs EEPS), measurement locations, and reference nvPM sampling systems, with an agreement of ±2 nm for GMD and ±0.08 for GSD (i.e., ±5%) reported on aircraft-like particles generated from a generic aero representative RQL combustor. To date, this study remains the only analysis that explicitly assesses the uncertainty introduced by particle size measurements in the calculation of measured-size-based k_{SL}.

This uncertainty was further quantified in this project using novel particle size measurement data from multiple laboratory and engine experimental campaigns, with the results presented below. These findings offer additional insight into the factors driving PSD measurement uncertainty and provides a comparative analysis of the three size-measurement-based system loss correction methods introduced above.

3.2.1. Assessing Uncertainty in GMD and GSD Particle Size Measurements

The ALF 502 and 507 engines tests, performed as part of the SAMPLE IV programme of work[19], enabled a comparison between a Cambustion DMS500 and a Grimm SMPS+C (model 5420), with both instruments sampling in parallel alongside the regulatory nvPM number and mass instruments. The instrument's GMD agreed within ±4 nm, with an average difference of 0.6 ± 1.0 nm, while the GSD agreed within ±0.16, with an average difference of 0.01 ± 0.05 nm. Example measured PSDs are provided in Figure 41.

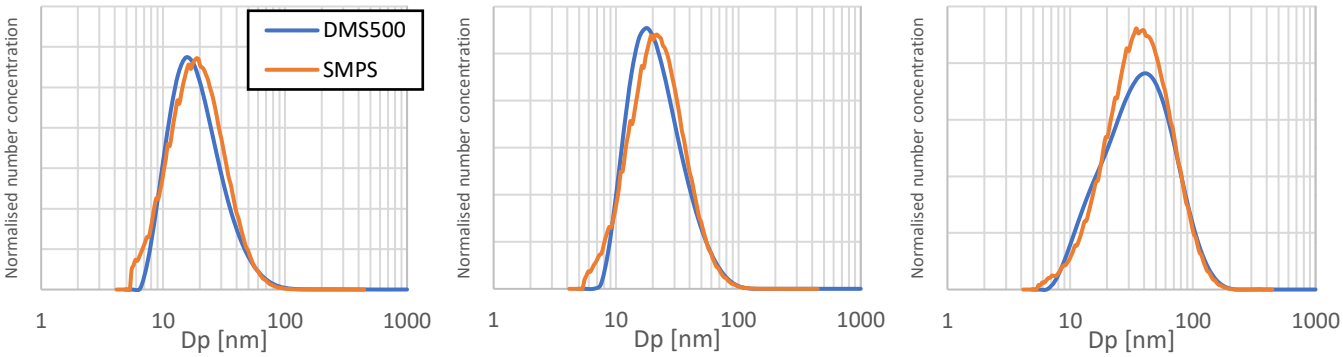

Figure 41: Example measured particle size distributions measured on the ALF 507 at idle (left) approach (middle) and take-off (right) – The number concentration is normalised for each instrument

[19] See SAMPLE IV Deliverable 5 report

Other studies have also compared the performance of particle size instruments when sampling aircraft nvPM or surrogate particles. For instance, Giannelli et al. [26] reported GMD agreements within 12% between a DMS500, an EEPS and high-flow SMPSs when sampling aircraft exhaust. Kittelson et al. [27] found a GMD agreement of ±4 nm across five TSI SMPS when sampling different particle sources (diesel, silver, DOS, PSL). Additionally, Durand et al. [9] reported that the DMS500 GMD was larger than that measured by a TSI SMPS GMD by 3.3±1.7 nm (i.e. 9.6±4%) and observed a GSD difference of 0.04±0.03 when sampling helicopter engine exhaust. Similarly, during the earlier SAMPLE IV particle size instrument comparison[20], a reported agreement of 8.3% for GMD and 3.4% for GSD when considering a TSI SMPS, a TSI EEPS and two Cambustion DMS500s measuring Spark-ablated Graphite (SAG), spark ablated gold and NCB, including the DMS500 and EEPS data processed using both the spherical and soot-like inversion matrices.

These GMD and GSD discrepancies between instruments are typically within the uncertainty limits quoted by manufacturers. Both TSI and Cambustion specify a tolerance of ±10% for GMD accuracy for the EEPS and DMS500 in their calibration certificates respectively. In contrast, the SMPS can in theory achieve a better sizing accuracy (<±3%), with uncertainties influenced by factors such as sheath flow accuracy, charging efficiency, calibration size, and variability in the CPC concentration and sample flowrate [28], [29], [30], [31].

Additional laboratory experiments were conducted, where a Cambustion DMS500, two TSI SMPS systems (Long DMA with CPC 3756 high flow & soft x-ray) and a Dekati ELPI+ were compared while sampling nebulised salt, PSL, Spark Ablated (Palas GFG-1000) graphite, and SPG nanoparticles in parallel downstream of a diluter. The PSD for PSL and salt are presented in Figure 42, and those for silver and graphite in Figure 43. When comparing the DMS500 to the two SMPSs, the GMD agreed within ±5 nm and the GSD within ±0.1 across all particle types.

In Figure 42 (a), all instruments successfully detected the 92 nm PSL peak. However, an in-line x-ray neutraliser was required for the DMS500 to resolve the peak, as discussed in section 2.3.2. This result suggests that nebulised NIST-traceable PSL colloids could be used as in-field check to verify the particle size instrument performance before testing. A key concern with PSL colloids is the significant amount of surfactant needed to stabilise the colloid, which typically results in a surfactant/residue mode dominant <60 nm. However, Corbin et al. [14] demonstrated that carboxylate-modified PSL (CML) can minimise this residue. Alternatively, traceable solid particle colloids such as silica, gold or silver could be used, provided their residue mode does not interfere significantly with the particle mode. The carbonaceous powder colloids discussed in section 2 would also be suited for in-field checks of nvPM mass, number, and particle size instruments, although their size is not currently traceable.

The ELPI+ operates in aerodynamic space (d_a) and has a significantly lower resolution (4 channels per decade) compared to the DMS500 (16 channels per decade) and the SMPS (typically 64 channels per decade), both of which measure in electrical mobility space (d_m). However, the ELPI+ includes a high-resolution algorithm (ELPI+ HR) that increases its output resolution to 32 channels per decade.

To compare ELPI+ HR data with the mobility-based instruments, the data were converted using the equation below and particle effective densities from the literature (Perraud et al. [32] for salt and Charvet et al. [33] for graphite and silver). After conversion, the ELPI+HR showed good agreement for salt nanoparticles, with the GMD only 1.4 nm smaller than those reported by the SMPSs. However, for silver and graphite, the ELPI+HR PSDs deviated significantly from those of the SMPSs and DMS500, likely due to the lower "physical" ELPI+ resolution and the assumptions made regarding particle effective density, which may not be representative. It is noted that without the high-resolution mode, the ELPI+ data were found to be nonsensical.

$$d_m \approx d_a \sqrt{\frac{\rho_0}{\rho_{eff}}} \sqrt{\frac{C_c(d_a)}{C_c(d_m)}} \quad [34]$$

[20] Further information can be found in SAMPLE IV Deliverable Report 1

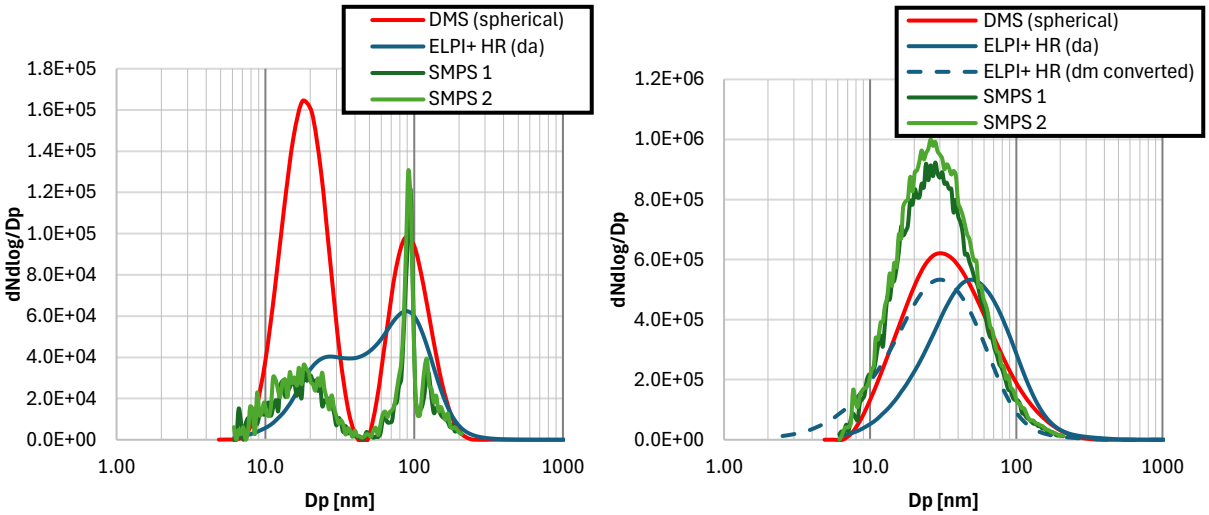

Figure 42: Measured particle size distribution from different instrument when sampling (a) nebulised 92 nm NIST-traceable PSL spheres with in-line neutraliser and, (b) nebulised salt nanoparticles

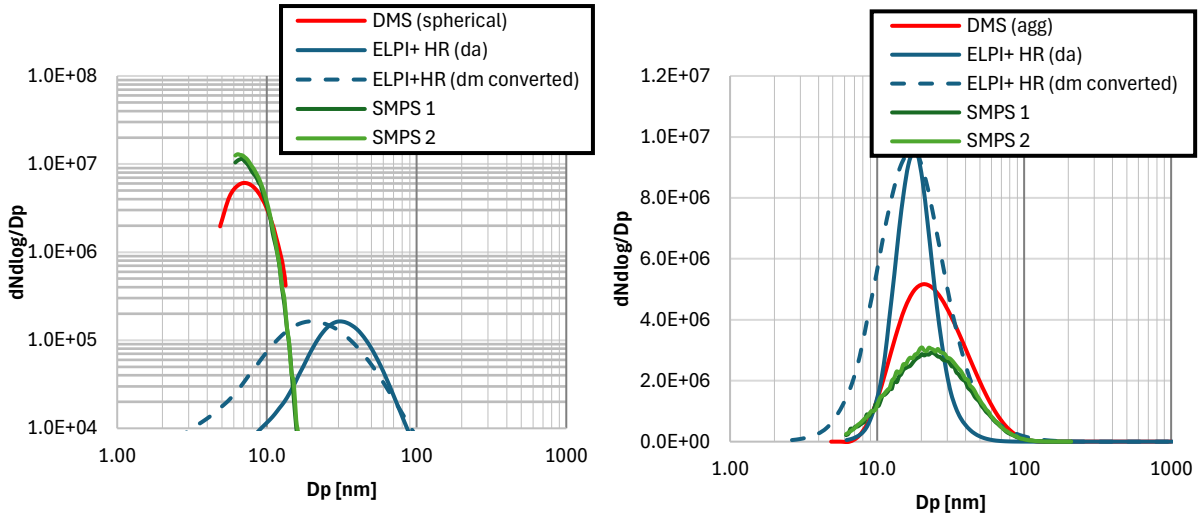

Figure 43: Measured particle size distribution from different instrument when sampling (a) Catalytic instrument SPG silver nanoparticles and, (b) PALAS GFG 1000 graphite nanoparticles

The laboratory experiments and ALF 502 and 507 engines test datasets were also used to evaluate the impact of the DMS500 inversion matrix on the output GMD and GSD. When comparing the spherical and aggregate inversion matrices for laboratory-generated particles, only minor differences were observed, with GMD deviations of up to 1.6 nm and GSD differences of up to 0.06. Similar differences were observed when sampling fractal aircraft exhaust PM, where the spherical matrix yielded GMD differences up to 2.2 nm (0.2±0.7 nm on average) and GSD differences up to 0.13 (0.01±0.03 on average) compared to the aggregate matrix, with deviations increasing with particle size, as shown in Figure 44.

Only minor differences were observed, as particle morphology and the choice of inversion matrix are expected to significantly impact particles with mobility sizes above 80 nm. At these larger sizes, agglomerates can carry a substantially higher mean charge than spherical particles due to their greater relative surface area, which leads to an overestimation of electrical mobility and, consequently, an underestimation of mobility diameter [35].

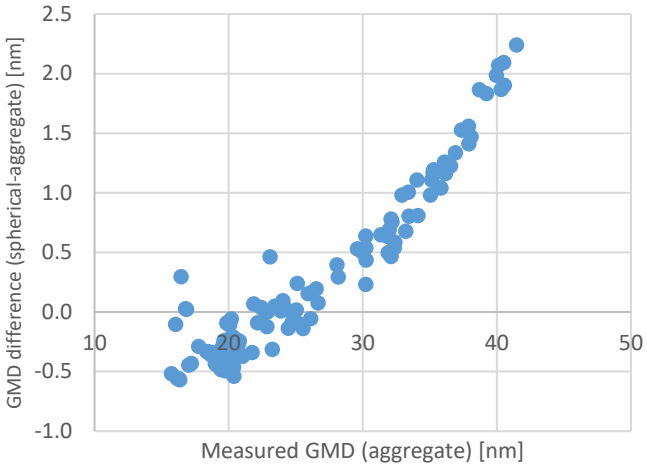

Figure 44: Impact of DMS500 inversion matrix (spherical Vs aggregate) on output GMD when sampling aircraft engine exhausts (ALF 507 and 502) across a range of aviation fuels

However, it has been noted in the literature that failing to apply the appropriate inversion matrix for fast-sizing instruments and neglecting the internal loss and STP corrections can lead to more significant discrepancies. Corbin et al. [23] reported a GMD agreement of ±20% and a GSD agreement of ±5% when comparing a DMS500 processed with a spherical inversion matrix and SMPSs fitted with thermodenuders or catalytic strippers placed at different sampling locations on an aircraft engine burning various fuels. Similarly, Delhaye et al. [36] found a 25% differences in CMD when comparing a Grimm SMPS+C with a DMS500 using a spherical inversion matrix during turbofan engine emissions sampling. Xue et al. [37] also observed significant discrepancies between a TSI, processed with its default inversion matrix, and an SMPS when sampling highly fractal diesel particles.

While number concentration is not required for measured-size-based system loss corrections, it is worth noting that the number uncertainty was significant. The SMPS reported ~40% higher number concentrations compared to the DMS500 and the ELPI+ when sampling salt, ~30% higher than the DMS500 on silver, but ~40% lower on SAG. This variability is suspected to be driven by the DMS500's sensitivity to particle charge state, when particles aren't neutralised. For instance, SAG particles were found to carry a relatively high positive charge while salt exhibited a negative charge on average[21], in-line with the number concentration discrepancies discussed above. Additionally, Figure 45 illustrates the impact of using a neutraliser in-line with the DMS500 during RQL combustor emissions sampling with a regulatory nvPM system, where changes of up to 5% in GMD, 1% in GSD and 22% in number concentration were observed for the EUR DMS500. In contract, the EEPS showed no significant changes due to its design, which includes two unipolar chargers in series.

[21] F. Lidstone-Lane, 'DP27 SAE E31 Albuquerque - "Electrostatic Aerosol Losses for nvPM Sampling Systems"', Jan. 2024 & 'DP33 SAE E31 Cranfield - "Electrostatic loss prediction and routes ahead"', Jan. 2025.

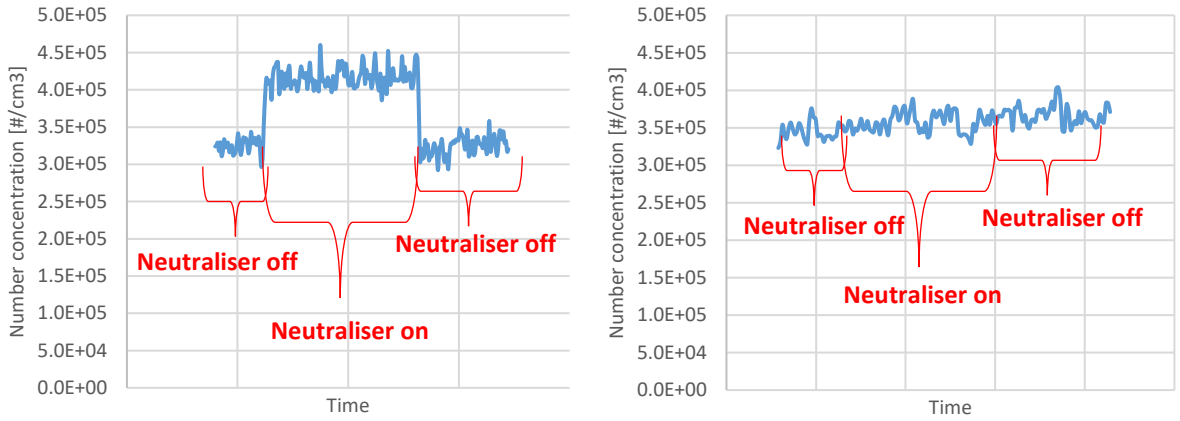

Figure 45: Example timeseries of a DMS500 (left) and an EEPS (right) sampling RQL combustor exhaust using a regulatory nvPM sampling system with an in-line X-ray neutraliser alternatively switched on and off

Compared to fast-sizing instrument like the DMS500 and the EEPS, which use a unipolar charger, SMPS systems operate with a bipolar charger. Recently, Soft X-ray neutralisers have gained popularity over the traditional radioactive neutraliser (e.g., Kr-85, Ni-63, Am-241), largely due to the regulatory handling and transport requirements for radioactive materials. However, soft X-ray charging efficiencies deviate from widely accepted charging theories (e.g., ISO 15900), exhibiting higher fractions of positively charged particles and lower fractions of negatively charged particles than predicted by theory [38]. As a result, when using a soft x-ray neutraliser in an SMPS, it is essential to select a soft X-ray-specific charging model, such as those provided by TSI and Grimm.

Additionally, while radioactive neutralisers have a half-life of several years, soft x-ray neutralisers typically have an operational lifespan of thousands of hours, with the potential for performance degradation over time [39].

The impact of bipolar soft x-ray neutralisers on the output PSD from an SMPS was experimentally assessed comparing measurements from a Grimm soft X-ray neutralizer (5524-X) with relatively low usage and two TSI soft X-ray neutralizers (3088), which had seen significantly more use. The result, shown in Figure 46, indicate that the neutraliser had minimal impact on the GMD (with a change of up to 0.5 nm) and GSD (with a change of up to 0.02). However, the TSI x-rays resulted in a significantly lower total number concentration (~22% lower). This difference is likely due to the greater degradation in the TSI x-rays from longer usage, highlighting the importance of checking charging efficiency against a radioactive reference when using soft X-ray neutralisers.

TSI has reported similar findings, observing differences of less than 5% for GMD and up to 20% for total number concentration when comparing their soft X-ray to a radioactive source [40]. They hypothesised that the differences were likely due to incomplete charge neutralization of the soft X-ray (e.g., due to ion depletion). In contrast, both Wiedensohler et al. [39] and Crayford et al. [5] found no significant differences in performance between radioactive neutralizers and relatively new soft X-ray devices. It is also noted that particle morphology is not expected to significantly influence bipolar charging [41], unlike unipolar chargers.

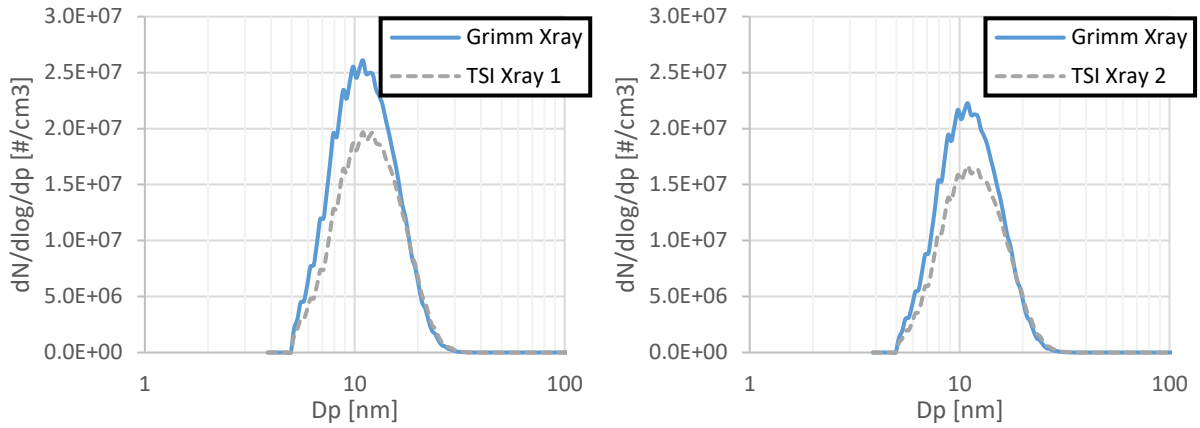

Figure 46: Measured particle size distribution using a Grimm SMPS+C (5420) with different neutralisers when sampling silver nanoparticles produced by Catalytic instrument SPG

3.2.2. Impact of Particle Size Measurement Uncertainty on k_{SL} Calculation

Consistent with the approach by Durand et al. [20], the uncertainty associated with k_{SL} when using different particle size instruments was assessed by comparing values of k_{SL_num} and k_{SL_mass}, calculated with methods PSD_B, PSD_{L1} and PSD_{L2}, using either the CU DMS500 (with aggregate inversion matrix) or SMPS as inputs. First, the data from the ALF502/LF507 test campaign dataset was used, which includes 146 data points.

The results are shown in Figure 47 for k_{SL_num}, and Figure 49 for k_{SL_mass}, with representative PSDs and MSDs displayed in Figure 48 and Figure 50, respectively. The reported k_{SL} differences are calculated as the relative difference between the maximum and minimum k_{SL} values over the average.

When considering only nvPM >10 nm at the EEP (Figure 48 a), as currently prescribed, using the DMS500 or SMPS as input PSDs results in k_{SL_num} difference of up to 15% across the three measured-size-based methods. Methods PSD_B, PSD_{L1} and PSD_{L2} exhibit a similar behaviour, with an average difference of 7±3%, and the difference increasing with decreasing GMD. Expanding the input PSD to include nvPM between 7 and 10 nm (Figure 48 b) raises maximum difference increases to 19%, although the average agreements are reduced to 5±3% for PSD_{L2} and 4±3% for PSD_B. These differences primarily originate from the variation in PSD shapes between the DMS500 and the SMPS, particularly for particles < 10nm, as highlighted in Figure 48.

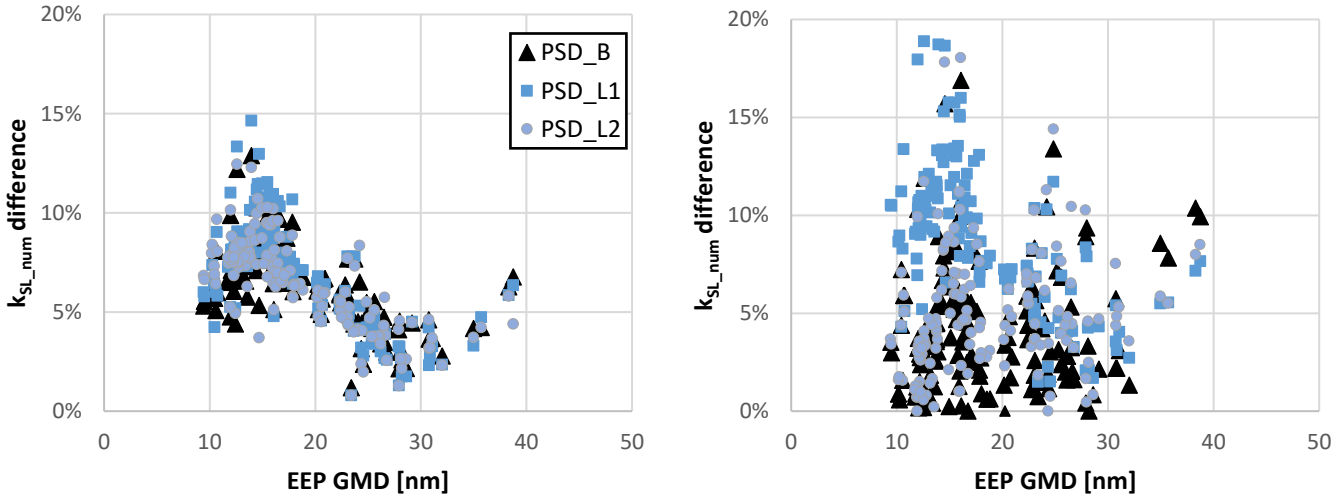

Figure 47: k_{SL_num} difference > 10 nm (left) and >7 nm (right) between using a DMS500 or SMPS particle size distribution as an input plotted against engine-exit-plane GMD for different measured-size-based system loss correction methods

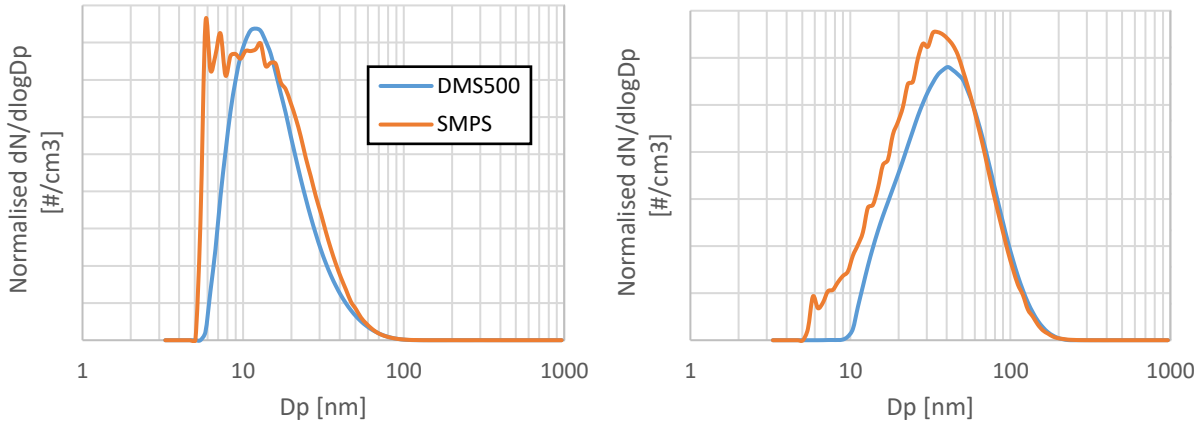

Figure 48: Example engine-exit-plane small (left) and large (right) number-space particle size distribution from different instruments sampling aircraft engine exhaust in parallel

The average k_{SL_mass} was found to be within 2±2% across the three methods when considering particle size bins <240 nm (Figure 49 a), and 3±2% when considering size bins up to 350 nm (Figure 49 b). Similar to the behaviour observed with k_{SL_num}, the difference in k_{SL_mass} increases with decreasing GMD, with maximum differences of 18% <240 nm and 44% <350 nm. The relatively larger maximum differences in k_{SL_mass} at 350 nm are attributed to noise and measurement uncertainty from the DMS500 at sizes above approximately 200 nm, as illustrated in Figure 50 (a).

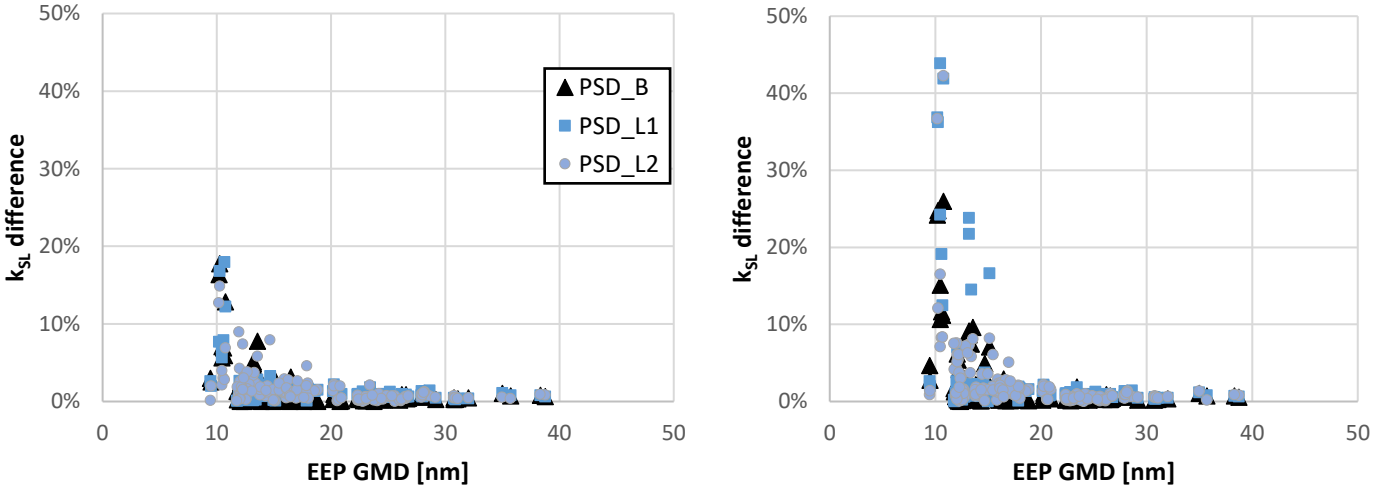

Figure 49: k_{SL_mass} difference <240 nm (left) and <350 nm (right) between using a DMS500 or SMPS particle size distribution as an input plotted against engine-exit-plane GMD for different measured-size-based system loss correction methods

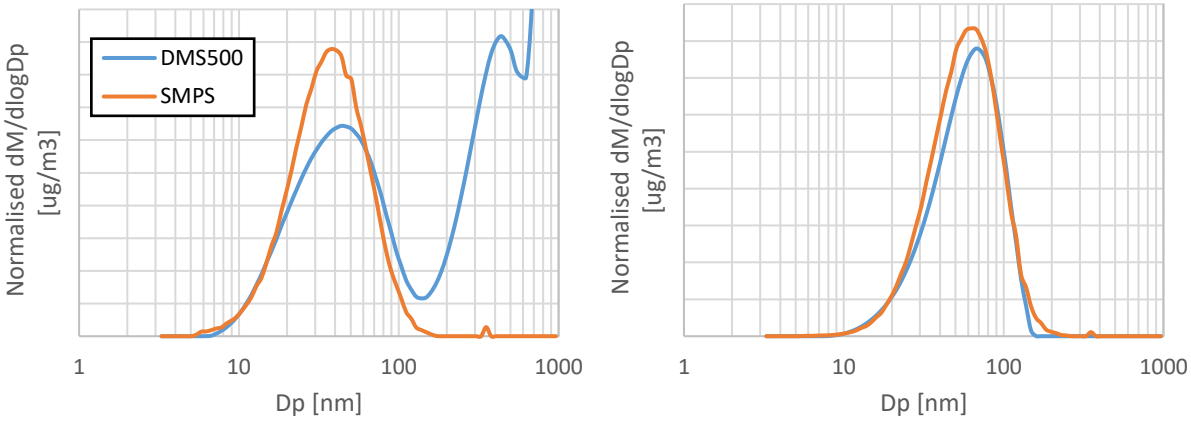

Figure 50: Example engine-exit-plane small (at) and large (b) volume/mass-space particle size distribution from different instruments sampling aircraft engine exhaust in parallel

The differences in k_{SL_num} and k_{SL_mass} reported here closely align with findings from Durand et al. [20], who observed k_{SL_num} differences of up to 19% (9.5% average difference) and k_{SL_mass} differences of up to 7.7% (2.4% average difference) when comparing four size instruments on RQL combustion exhaust. Additionally, the three measured-size-based methods demonstrated consistent behaviour when considering only measured data between 10 and 240 nm.

The impact of PSD variability on measured-size-based system loss correction was further evaluated using laboratory size comparison data[22]. This dataset included a TSI SMPS, two Cambustion DMS500 units, and a TSI EEPS, compared on Spark ablated gold, SPG, and NCB with measured GMDs ranging from 7 to 71 nm. Additional comparison involving two TSI SMPSs, a Cambustion DMS500 and a Dekati ELPI on nebulised salt were also analysed. For this analysis, both k_{SL_num} and k_{SL_mass} were calculated using PSD data between 10 and 240 nm across different instruments and different inversion matrices and assuming typical dimensions of a regulatory nvPM sampling and measurement system.

When considering the size instrument comparison on spark ablated gold and SAG using the most suitable inversion matrices (e.g., spherical for the DMS500 and compact for the EEPS on gold and aggregate for the DMS500 on graphite and nebulised carbonaceous colloids), average agreements within 10±5% for k_{SL_num} (with a maximum of 21%), and within 7±9% for k_{SL_mass} (with a maximum of 29%) were achieved. Similar correlations were observed across methods PSD_B, PSD_{L1} and PSD_{L2}, with uncertainty typically increasing as GMD decreased.

The choice of inversion matrix (spherical vs. aggregate) was found to influence k_{SL_num} by up to 15% and k_{SL_mass} by up to 16% for the DMS500. Comparable results were seen with the EEPS, where differences between the compact and soot inversion matrices resulted in k_{SL_num} deviations of up to 18% and k_{SL_mass} deviations up to 17%.

For the ELPI+, which produced PSDs consistent with those from mobility-based instruments for salt (see Figure 42, b), both k_{SL_num} and k_{SL_mass} agreed within 6% across all three measured-size-based methods.

The differences in k_{SL_num} and k_{SL_mass} observed from the laboratory data for methods PSD_B, PSD_{L1} and PSD_{L2} are consistent with those reported for the ALF502/LF507 dataset and Durand et al. [20]. Overall, k_{SL_num} typically agrees within 10% when using different particle size instruments with appropriate inversion matrices, and k_{SL_mass} shows agreement within 6%, when limiting the PSD input to between 10 and 240 nm. The uncertainty typically increases as GMD decreases, with differences of up to 21% for k_{SL_num} and up to 23% for k_{SL_mass}.

3.3. Summary and future work of PSD based loss correction

[22] Further information in SAMPLE IV Deliverable Report 1

This chapter detailed particle size measurement for aircraft nvPM, assessing the differences, best operating practices and corrections, and uncertainties from different commercially available size instruments. It highlights and emphasises the importance of correcting for size-dependent system losses to ensure accurate reporting and regulation of nvPM number and mass. The experimentally derived uncertainty associated with measured-size-based system loss correction (k_{SL}) is also summarised in Table 5. The variability is reported in two different ways ((1) and (2) in Table 5), highlighting that the method used to quantify variability can also significantly impact the outputs:

(1) The relative difference between the maximum and minimum k_{SL} values over the average $(maximum\ k_{SL} - minimum\ k_{SL})/average\ k_{SL}$, as previously reported in the literature [20].
(2) The relative difference between the furthest k_{SL} from the average and the average over the average $(furthest\ k_{SL} - average\ k_{SL})/average\ k_{SL}$.

Table 5: Uncertainty summary for k_{SL_num} and k_{SL_mass} when using different PSD measurements with method PSD_{L2} (PSD input between 10 – 240 nm)

	Particle type (GMD range)	Instrument used	k_{SL_num} variability				k_{SL_mass} variability				Additional info
			Avg (1)	Avg (2)	Max (1)	Max (2)	Avg (1)	Avg (2)	Max (1)	Max (2)	
Durand et al. [20] (PSD_{L2})	RQL combustor exhaust (24 – 42 nm)	2x DMS500 (M44&125) 1x TSI SMPS 1x TSI EEPS	10%	5%	19%	10%	2%	1%	8%	5%	Multiple sampling locations
Novel engine data	ALF 502 & 507 (14 – 43 nm)	1x DMS500 (M44) 1X Grimm SMPS	7%	3%	15%	6%	2%	1%	15%	7%	Near regulatory nvPM instruments
Novel laboratory data with multiple inversions	Gold, Graphite, salt, carbon colloid (8 – 71 nm)	1x DMS500 (M44) 2x TSI SMPSs 1x Dekati ELPI+HR	10%	7%	21%	10%	6%	4%	23%	16%	Different inversion matrices tested

In terms of measuring PSD to inform system loss correction, several recommendations come out of this work, namely:

- Recommendations for measuring aircraft exhaust particle size distribution:
  - The DMS500 should be processed with the aggregate inversion matrix, with an additional neutraliser used if there are concerns over the exhaust being highly charged.
  - The EEPS should be processed with the compact inversion matrix until a more suitable matrix becomes available.
  - The SMPS should be processed applying all relevant internal correction, including adjustments for neutraliser type, diffusional losses, STP correction, multiple charge correction.
  - If the primary use of the size instrument is for system loss correction, sampling of exhaust should be near the nvPM number and mass instruments without a catalytic stripper.

    - When using a soft x-ray neutraliser, particularly when it has been substantially used, it is recommend verifying it against a radioactive source to check that it is charging particles as expected.

- Recommendations for measured-size-based correction:
    - System loss correction is estimated to reduce uncertainty of emitted nvPM (compared to using reported EI nvPM) by up to 680% for nvPM number and up to 150% for regulated nvPM mass.
    - Measured-size-based correction reduces the maximum variability from 67% to 19% (or 10% using calculation (2)) for k_{SL_num} and from 49% to 15% (or 7% using calculation (2)) for k_{SL_mass} compared to the currently prescribed method ($R_{N/M}$) when only considering engine and RQL data.
    - Methods PSD_B, PSD_{L1} and PSD_{L2} demonstrate similar performance on emissions representing the main aircraft fleet. However, method PSD_{L2} stands out as the most promising method due to its customisable size range, supporting the use of various instruments, and the multiple mode resolution, accommodating deviations from lognormality and capturing nucleation modes.
    - For measured-size-based k_{SL_mass} calculations, only PSD data < 300 nm should be used as noise and artifacts in fast sizers above this size can significantly increase the uncertainty.

Beyond this project, further work is needed to fully establish best practices for particle size measurement, further address its associated uncertainties, and determine which size-measurement-based system loss correction method is most suitable for the implementation of size-dependent system loss correction in aircraft PM emissions regulation. This would require additional data collection and processing, towards the revision of ARP6481 (loss correction) and ARP6320 (sampling and measurement). Additionally, other known uncertainties in the calculation of penetration efficiencies within the regulatory sampling and measurement system—such as Diluter 1 losses, probe electrostatic losses, and Splitter 1 losses would benefit from further quantification.

4. Novel Advanced Measurement Techniques for nvPM Number and Mass

4.1. Novel/scientific optimum experimental work carried out on rich burn combustor rig exhaust

4.1.1. Portable sensors proof of concept for number and mass measurement

In recent years, various portable (low fidelity) aerosol analysers have been developed. Portable instruments have proven useful for periodic inspection of emission sources, dosimetry, and ambient monitoring. Such instruments may prove to be viable, cost-effective additions to the standard nvPM measurement system given their simplicity of use, robustness, relative low cost, and size. This could be particularly advantageous should future measurements closer to the engine source be considered desirable.

However, at this time, there is very limited information on the performance of portable analysers in comparison to regulatory nvPM mass and number instruments. Therefore, a SAMPLE IV campaign using the RQL combustor rig at Cardiff University's GTRC, provided a perfect opportunity to evaluate portable aerosol analysers owned by the Swiss research team including a naneos Partector 2 and Aethlabs MA300. This study was complimentary to other appraisals which have seen recent comparisons of diffusion chargers: Pegasor DT Sensor & Naneos Partector 2; and optical absorption: DST ObservAIR, which were facilitated during the AVIATOR test-cell and On-wing test campaigns.

The Partector 2 utilises induced currents to measure the lung-deposited surface area (LDSA). The Partector signal is proportional to the product of particle number and diameter. According to the manufacturer, the measurement uncertainty is largely determined by the unknown shape and peak of the particle size distribution. Partector 2 is calibrated for lognormal particle size distributions with a geometric standard deviation of 1.9, which is a reasonable assumption for gas turbine engine soot. In addition to LDSA, the instrument displays estimated UFP number concentration, average size, surface area and mass (PM0.3) at 1 Hz.

The microAeth® MA300 is a portable 5-wavelength UV-IR Black Carbon monitor (880 nm, 625 nm, 528 nm, 470 nm, 375 nm). It measures the rate of change of transmitted light due to continuous particle deposition on a filter. The instrument contains a built-in pump, flow control, data storage, onboard GPS, satellite time synchronization, accelerometer, altimeter/barometer, and sensors for relative humidity and temperature. The spectrum measurement should help to distinguish among the different optical signatures of various combustion sources. Measurement at 880 nm is interpreted as Black Carbon (BC). Measurement at 375 nm is interpreted as organic carbon (UV absorbing PM), indicative of woodsmoke, tobacco, and biomass burning. The time base can be set between 1 and 300 seconds. During these experiments, a 30 s sampling period was chosen. The specified limit of detection is 30 ng BC/m^3 at a 300 s time base.

The weak pumps in these specific portable analysers cannot handle the sub-atmospheric pressure, of up to ~-90 mbar, experienced by analysers at the end of a >25 m compliant nvPM sampling system. Therefore, to address this, the portable monitors were positioned to sample directly from the diluter vent, which is at ambient pressure. This sampling strategy also minimises particle loss prior to measurement and offers the potential for other future simplified measurements.

1.1.1.1. Portable Sensor Experimental setup

The Partector 2 and the MA300 sampled from a two-way splitter connected to a tee-fitting downstream of the diluter vent as shown in Figure 51, sampling from a RQL combustor rig. In addition, the MA300 was included in a mass instruments intercomparison, again using diluted sample from the RQL combustor rig soot.

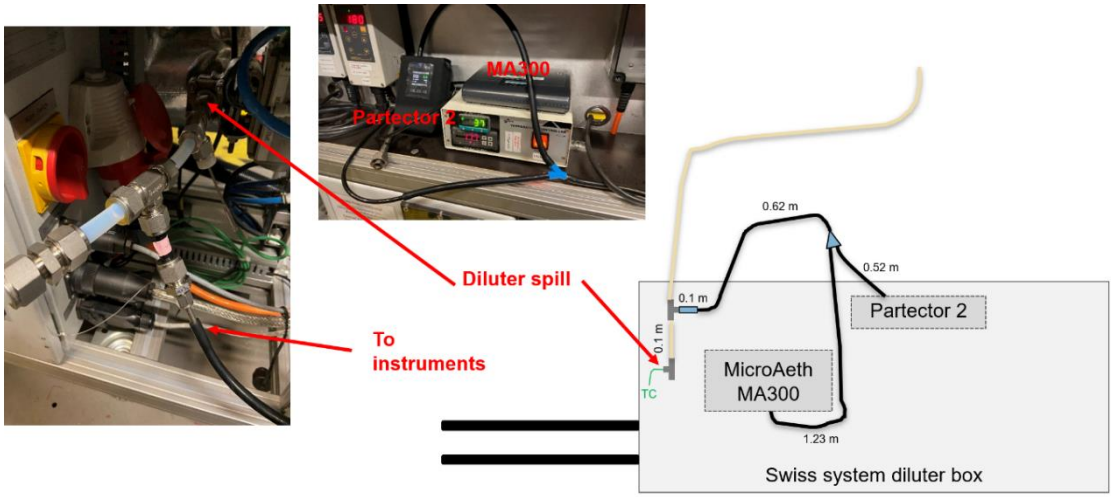

Figure 51: Partector 2 and micro aethalometer MA300 sampling from the diluter vent in the Swiss reference system

1.1.1.2. Portable Sensor Results

MA300: Figure 52 shows an example of a time series with the MA300 running in parallel with the MSS, LII-300 and CAPS during the mass intercomparison study using diluted RQL combustor rig soot. It appears that the MA300-reported mass concentrations correlated well with the other mass instruments, with the output tracking the shape of the time series reported by the 1 Hz instruments. However, from the correlation plot with the MSS, it can be seen that the BC mass concentration reported by the MA300 was over an order of magnitude higher (Figure 53).

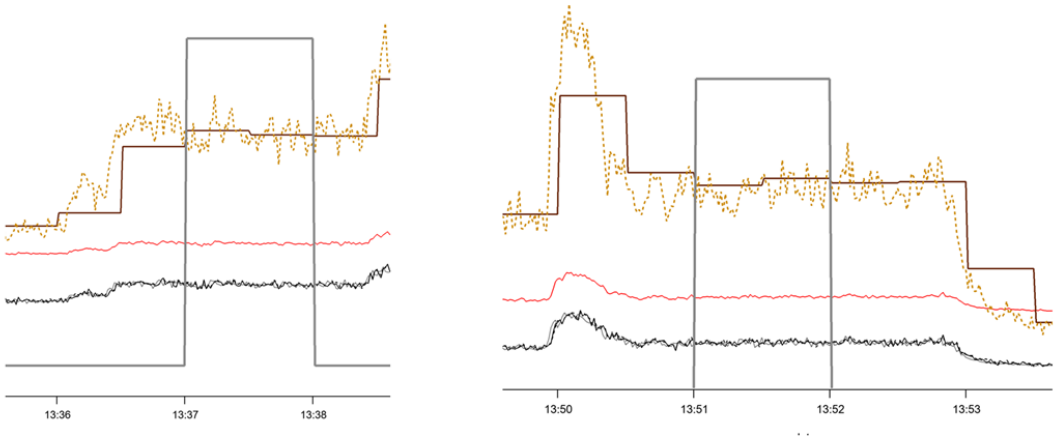

Figure 52: Time series of mass instruments comparison. Red: CAPS extinction coefficient, black: MSS mass concentration; orange: LII-300 mass concentration; and brown: MA300 IR BC mass concentration. The grey line represents the 60s averaging period

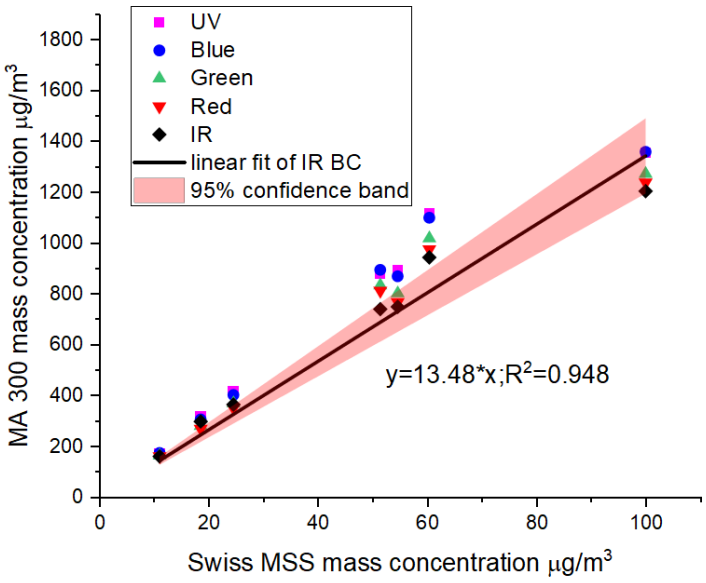

Figure 53: Comparison of the MA300 BC mass concentration and the MSS mass concentration during the mass instruments comparison on 6 December 2021 using the RQL combustor soot

A similar result was obtained from the comparison of the MA300 sampling in the diluter vent and the MSS measuring downstream of the PM line (Figure 54). The difference in the slope in Figure 53 and Figure 54 can be attributed to particle loss in the PM line. The mass-based system loss correction factor for the PM line is expected to be in the range from 1.1 to 1.3, depending on the particle size distribution shape and mean size.

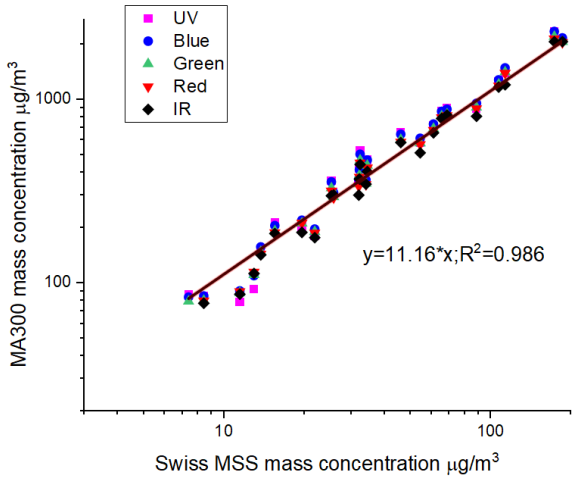

Figure 54: Comparison of the MA300 BC mass concentration measured in the diluter vent and the MSS mass concentration during the RQL rig tests of the complete nvPM systems on 7 December 2021

Given the strong correlation with the MSS over a wide range of combustion conditions, it is plausible that the instrument could be calibrated according to ARP6320. The instrument allows the user to perform an automatic optical calibration, but details on the calibration reference are unknown. Further investigation should also focus on the wavelength-dependent response. Future tests should investigate the instrument performance at 1 Hz time base and establish the limit of detection.

From an operational point of view, a disadvantage of the instrument is the need for 'tape advancement', which happens automatically, once a certain loading is reached on the tape/filter being measured. This advancement means that data can be lost mid-test point, which given the expense of large engine testing would be of significant concern.

Partector 2: Figure 55 shows the comparison for particle mass and number concentrations reported by Partector 2, with the nvPM mass and number measured by the MSS and APC in the Swiss reference system. The portable instrument primarily measures the LDSA, and the number and mass concentrations are derived assuming lognormal distribution with a GSD of 1.9. The assumptions used for the calculation of the mass concentration (e.g. likely a fixed effective density) are not known. The manufacturer quoted typical accuracy for the number measurement is ±30% and ±50% for the mass[23]. As with the MA300, the concentrations reported by the Partector 2 are expected to be higher due to much lower particle loss. In addition to the particle line penetration loss experienced by the sample measured by the MSS and APC, VPR penetration and CPC efficiency are also not included. The concentrations reported by the Partector 2 correlate well with the nvPM instruments, especially for particle number concentrations. The particle mass concentration measurement with the Partector 2 is limited by its upper size limit of 300 nm and it is affected by particle morphology. Further analysis towards a true comparison would require a detailed size dependant system loss correction. The instrument could also be compared directly with nvPM mass and number instruments in parallel in the future to establish the expected accuracy of this portable measurement analyser.

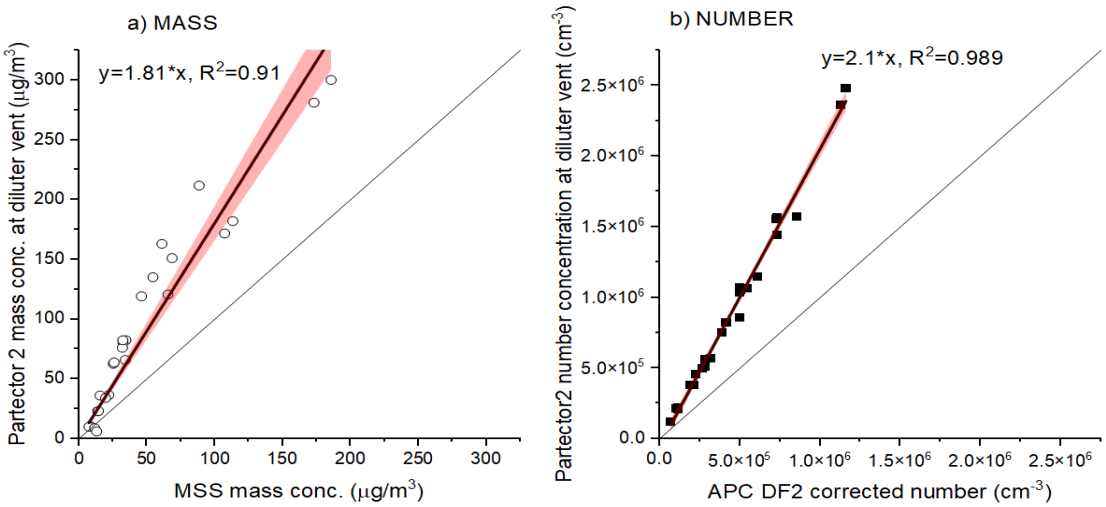

Figure 55: Comparison of the mass (a) and number (c) concentrations reported by the Partector 2 at the diluter vent with the nvPM mass and number (no system loss correction applied)

4.1.2. Near Probe Combustion exhaust particle Size measurement with SMPS

Particle loss correction of sub-10 nm particles is a very challenging task due to high uncertainties in the measurement, with substantial particle losses and uncertainties in the penetration functions applied. There is limited measurement data of nvPM size distributions close to the engine exit plane, which would provide information on the fraction of sub-10 nm particles, whilst demonstrating the feasibility of acquiring particle size data with lower size dependant sampling losses towards simplification of measurements and potential reduction of particle loss.

Specific interest in such measurements is the information provided on the smallest mobility size particles at the engine exit plane. Towards this aim, quantification of the smallest particles was attempted by sampling an SMPS instrument from the diluter vent of the Swiss nvPM system. The particle size distribution at this position was then compared with EEPS data, sampling from the conventional location at the end of the nvPM sampling system after correcting for calculated size dependant particle loss between locations.

1.1.2.1. SMPS Experimental setup

During an RQL combustor rig test, the SMPS was positioned in the diluter vent of the Swiss reference system as shown in Figure 56. The SMPS was operated with the long DMA (TSI Model 3081A) during four test points. The sheath flow was set to 25 lpm with the resulting size range 4.78 – 156.8 nm. Subsequently, the SMPS was

[23] https://www.naneos.ch/pdf/naneos_partector2_operation_manual.pdf

operated with the nano DMA (TSI Model 3085) during three test points. The sheath flow was set to 8 lpm with the resulting size range 2.79 – 88.2 nm. The lower sheath-to-aerosol flow ratio with the nano DMA reduced the sizing accuracy (transfer function broadening) compared to the long DMA setup. These settings were a compromise to maximise the overlap of the size ranges of the two DMAs (reduce the lower size limit of the long DMA and increase the upper size limit of the nano DMA).

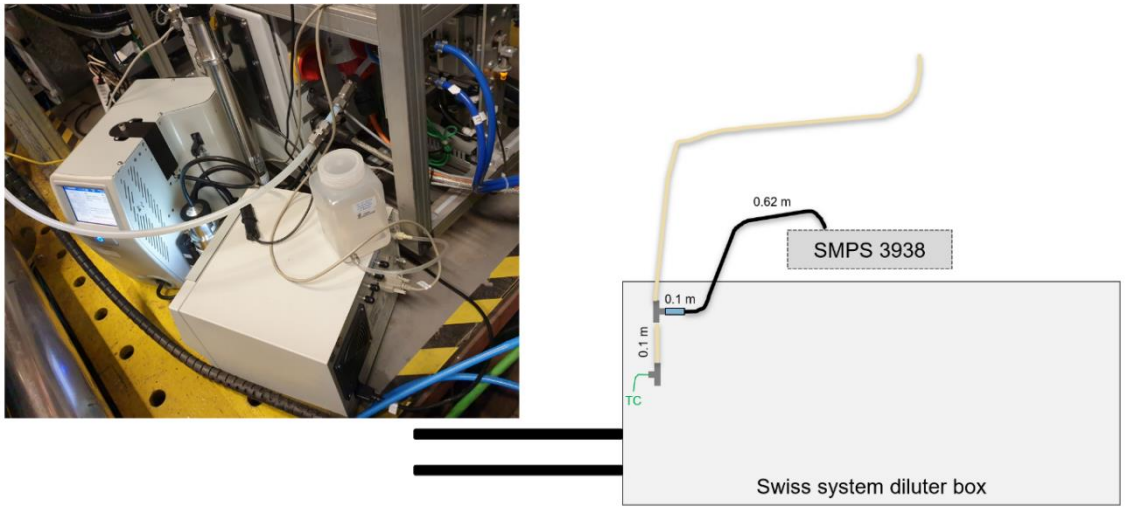

Figure 56: Experimental setup of the SMPS measurement at the diluter vent

1.1.2.2. SMPS Results

The results of the experiments with the long DMA are shown in Figure 57. The smallest mobility size detected using the long DMA was 5.73 nm across the 4 test points. The size distributions for TP27 to TP28 appeared monomodal and agreed well with the EEPS data corrected for system loss to the diluter outlet. The lognormal GMD and GSD, obtained from single peak fits, are summarized in Table 6. After switching to 100% GTL fuel, the soot concentration decreased and the SMPS resolved a nucleation mode at ~7 nm. This mode becomes more visible as the soot concentration decreased between TP29 and TP30. Downstream of the 25m nvPM sampling line, this mode would not be detectable by the EEPS, as the small particles are lost via diffusion to the sample line wall.

Figure 58 shows the results obtained using the nano DMA. The smallest size detected across the 4 test points, was 4.6 nm (i.e., concentration in the size bins from 2.79 to 4.45 nm was zero). It is noted that TP31 was the cleanest test point of the entire campaign (nvPM mass ~ 1 µg/m^3). At this test point, the nano DMA SMPS resolved a nucleation mode at ~7 nm. This mode is too small and too close to the soot mode to be resolved by the EEPS, although the concentration in the smallest size bin is higher for this case, relative to other test points. It seems that this mode was also present at TP32 and TP33 with a similar amplitude. However, it is obscured by the much more dominant soot mode as the rig switched to dirtier nvPM conditions (nvPM mass ~ 4-7 µg/m^3).

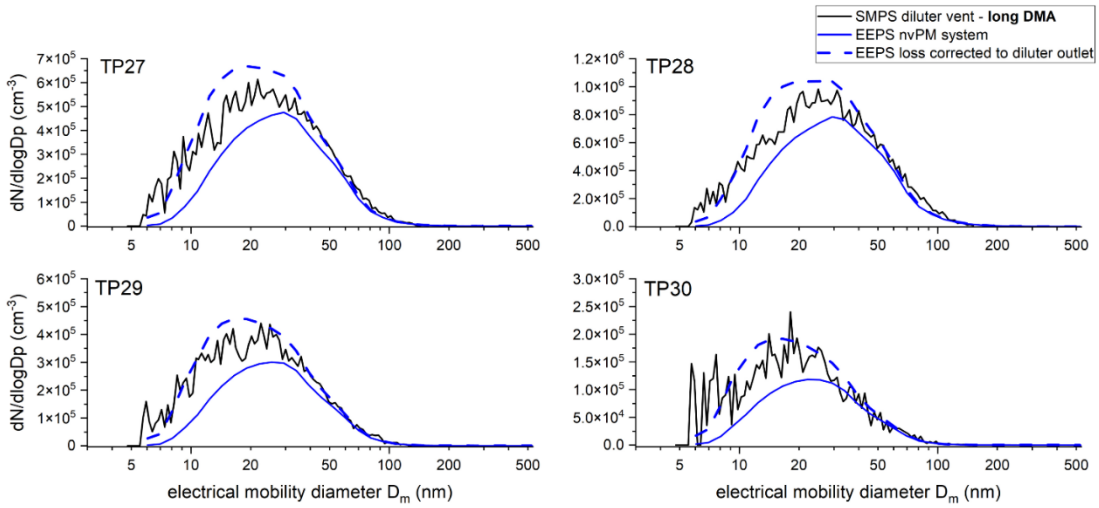

Figure 57: Comparison of SMPS size distributions at the diluter vent using the long DMA (black) with EEPS size distributions measured in the nvPM system (solid blue) and system loss corrected to the diluter outlet (dashed blue). TP27 & TP28 75% GTL JETA Blend and TP29 & T30 100% GTL

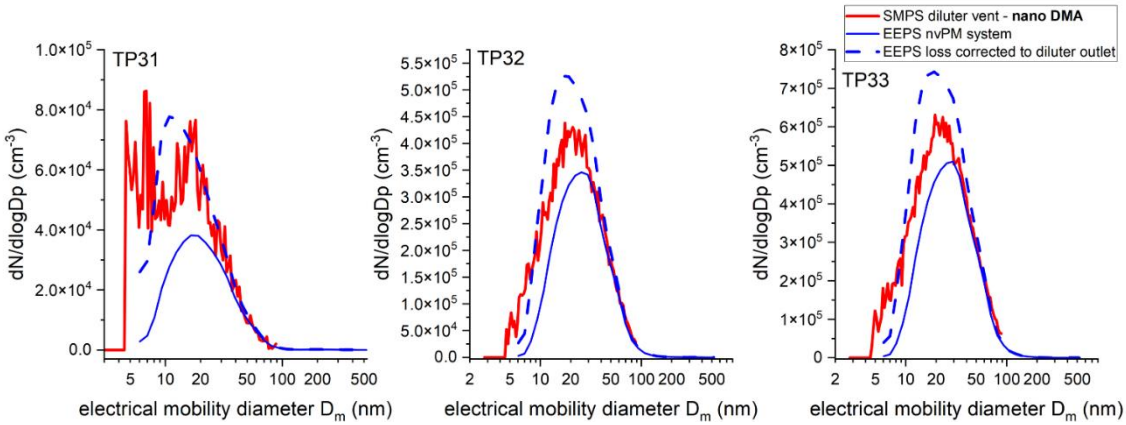

Figure 58: Comparison of SMPS size distributions at the diluter vent using the nano DMA (red) with EEPS size distributions measured in the nvPM system (solid blue) and corrected to the diluter outlet (dashed blue)

Table 6: Results of the lognormal single peak fits to the particle size distributions at the diluter. The SMPS data were used as measured. The EEPS data collected in the nvPM system are corrected for particle loss to the diluter outlet

Test Point	Fuel and rig settings	GMD SMPS	GMD EEPS	GSD SMPS	GSD EEPS	R^2 SMPS	R^2 EEPS
TP27	75% GTL clean 1	22.83	21.78	2.02	1.88	0.95	0.99
TP28	75% GTL clean 1	25.38	23.74	2.01	1.91	0.98	0.99
TP29	100% GTL clean 2	20.40	20.06	1.96	1.84	0.95	0.98
TP30	100% GTL clean 1	17.83	18.18	1.96	1.83	0.80	0.98
TP31	100% GTL clean 3	12.36	13.93	2.18	1.85	0.68	0.98
TP32	100% GTL dirty 1	20.68	20.17	1.96	1.82	0.98	0.99
TP33	100% GTL dirty 2	21.90	21.27	2.00	1.84	0.99	0.99

A nucleation mode is not commonly witnessed during nvPM tests of gas turbine engines when particle size distribution measurements are performed done in parallel with the nvPM mass and number measurement. An interesting exercise is the correction of the particle size distributions measured at the diluter vent with the nano DMA to the nvPM instruments plane. Figure 59 shows the SMPS data corrected to the nvPM instruments

plane (red dashed line) in comparison to the EEPS data (blue line). Here the nucleation mode measured at the diluter vent is indistinguishable. Thus, fitting a single lognormal peak to the SMPS data at the nvPM instruments plane would misrepresent the distributions seen at the diluter vent. The SMPS data corrected to the instrument plane agreed well with the EEPS data.

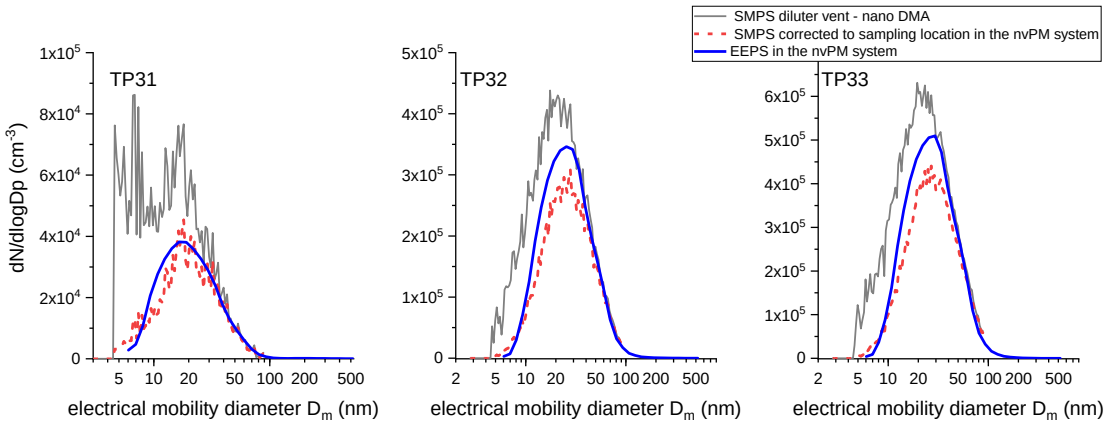

Figure 59: Comparison of SMPS size distributions at the diluter vent using the nano DMA (grey) and the same data corrected to the location in the nvPM system (red dashed) with EEPS size distributions measured in the nvPM system.

This experiment provides valuable information for particle loss correction using size distribution measurement highlighting that further evaluation of loss correction using the bin-by-bin approach and using lognormal fits is required. The limitation of this work is the relatively large GMD produced, even at the cleanest conditions, compared to measurements done on some turbofan engines which produce GMD ~15 nm at the nvPM instrument plane. Similar near engine size experiments are therefore required on engines known to produce very small GMD. The data indicates that a nucleation mode could be present when sampling close to exhaust sampling probe, thus careful sample conditioning is likely required for an nvPM measurement close to the probe.

4.2. Evaluation of Novel Measurement Techniques in Small Engine Testing

By collaborating with a NERC (UK Natural Environment Research Council) ALF 507-1H and an ALF 502R-5 emissions measurement campaign, several additional novel nvPM measurement techniques were tested in parallel to regulatory gaseous and nvPM number and mass measurements as part of the SAMPLE IV research programme. Two Jet-A and two ASTM-approved SAF blends were used, with a dedicated secondary sample line implemented to accommodate nvPM instrumentation sampling near to the probe inlet.

4.2.1. Near-probe Measurements

PM measurement near the engine-exit were facilitated within the “Death-box” an enclosure mounted directly under the engine connected directly to the probe outlet, which was used to house the EUR nvPM reference systems dilutor box and various instruments that sampled either behind or in parallel with a Dekati eDiluter Pro. The eDiluter pro, as illustrated Figure 60, is a dilution and conditioning system designed for particle measurements. It consists of two ejector diluters and allows heating of the dilution air for the first dilution stage up to 400 °C. Compared to the current single-stage ejector diluters used in regulatory nvPM systems, the eDiluter Pro offers significant advantages: an adjustable dilution factor ranging from 5:1 to 225:1, and automatic compensation for sample pressure variations between 960 and 1500 mbar, ensuring stable dilution performance.

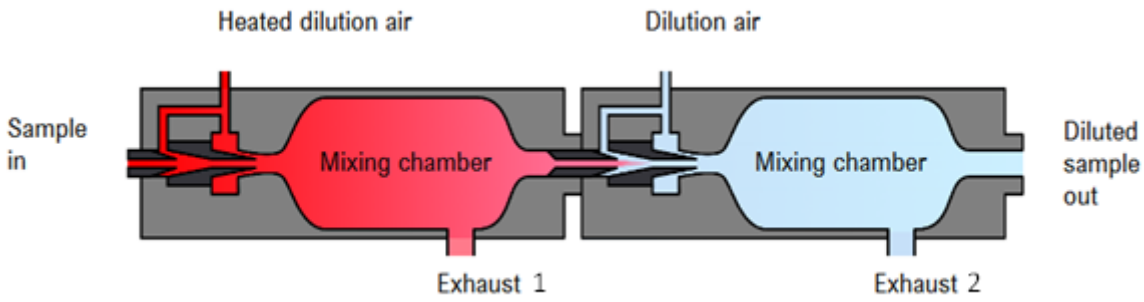

Figure 60: Diagram of the Dekati eDiluter Pro operating principle [36]

Two sampling setups were used during the test campaign. For most of the testing, both a Dekati MPEC+ and a CAP3070 (Pegasor-DT), real-time particle number counters based on diffusion charging, sampled from the 1st diluter stage exhaust of the eDiluter pro within 4 meters of the probe inlet, as shown in Figure 61. Both instruments were equipped with a water trap and a heated evaporation tube to eliminate volatile material, with the MPEC operating at 300 °C and the DT at 250 °C. On the final day of the test campaign, the MPEC+, Pegasor-DT, and ELPI+HT sampled raw exhaust in parallel with the eDiluter Pro, as illustrated in Figure 62. Additionally, the eDiluter Pro enabled continuous measurements of particle effective density from the first dilution exhaust and particle charge state from the second dilution exhaust.

The MPEC+ currently reports only nvPM number, while the DT also provides a GMD by automatically switching its trap voltage, enabling correction for size-dependent counting efficiency (though unverified for particles smaller than 23 nm). Since the Pegasor-DT is nominally set for automotive exhaust, the lower trap voltage was reduced to improve the counting efficiency for smaller particles. The MPEC's trap voltage can be manually adjusted, and its counting efficiency can be corrected using calibration data from monodisperse DMA-classified soot particles, accounting for all components, including the sample line and water separator. The MPEC+ reports measurements at standard temperature and pressure (STP) and was originally calibrated with a trap voltage of 110V, providing a counting efficiency of approximately 50% for 23 nm particles, in line with automotive regulations. In this study, however, the MPEC+ was typically operated at a lower trap voltage of 10 V to improve the counting efficiency for smaller particles.

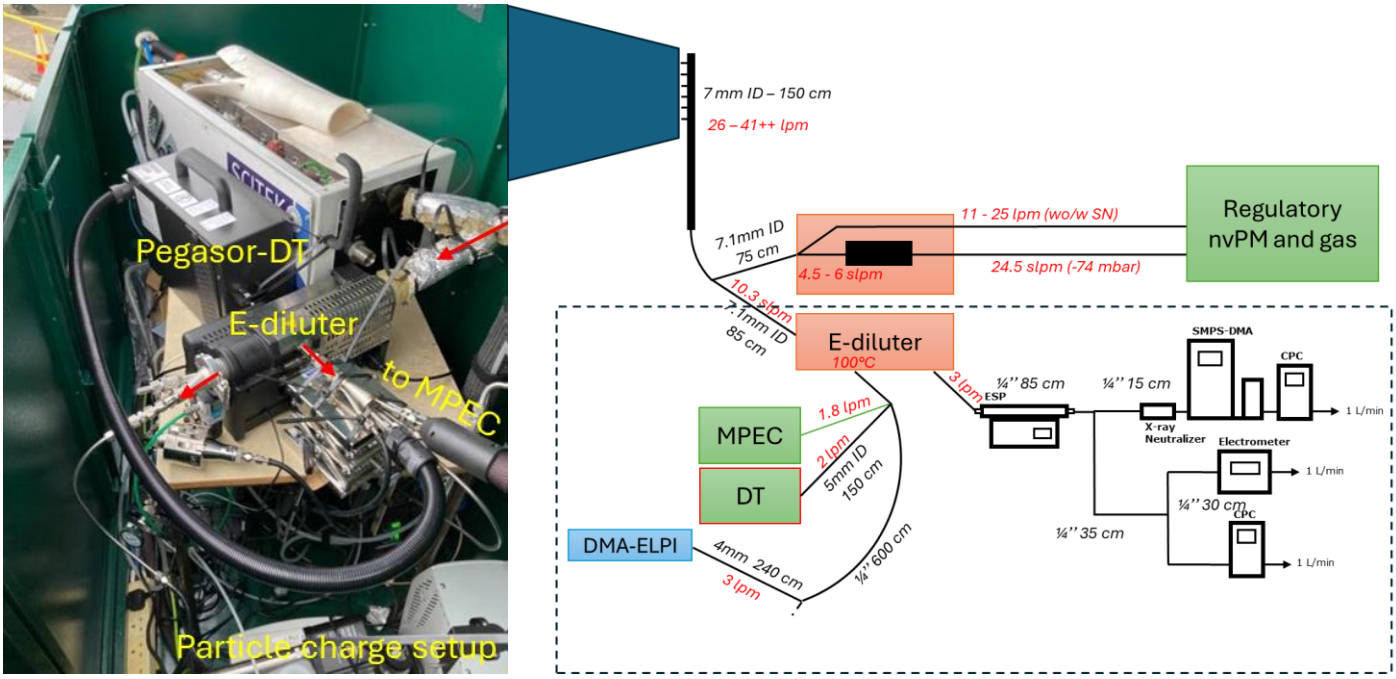

Figure 61: Picture (left) and diagram (right) of the Deathbox and experimental setup used during day 1-4 of the ALF 507 and 502 tests

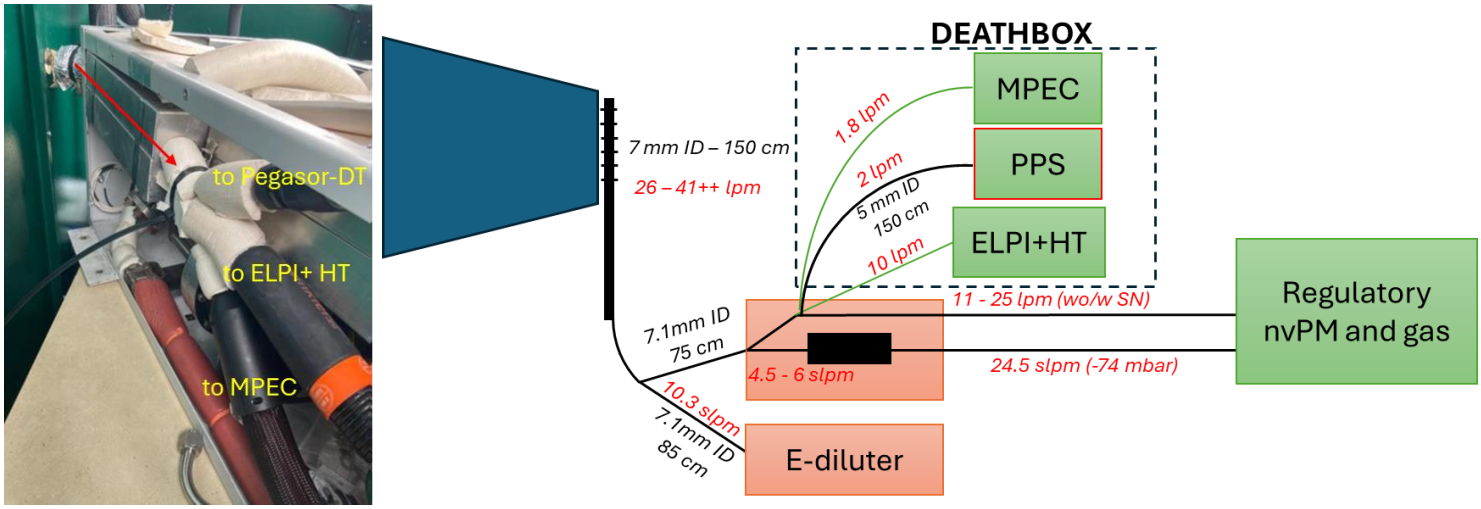

Figure 62: Picture (left) and diagram (right) of the Deathbox and experimental setup used during day 5 of the ALF 507 and 502 tests

4.2.1.1. Diffusion-based Counters Results

The measured nvPM number reported by both the MPEC+ and the Pegasor-DT, when sampling either raw or diluted aircraft exhaust, were compared to the regulatory nvPM number measured by the APC in the EUR reference nvPM system. The regulatory number was corrected for dilution and for losses to the MPEC/DT locations using DMS500 measurements with method PSD_B [20]. The results are shown in Figure 63, where the MPEC was operated with a trap voltage of 10V and the data is presented both with and without counting efficiency correction (the counting efficiency is reported in Figure 64).

The Pegasor-DT showed good correlation with a factor bias when sampling diluted exhaust. Both instruments under-reported the corrected regulatory nvPM number by approximately 50%. The corrected MPEC+ values typically aligned within +/- 20% of the regulatory nvPM number for particles with a GMD >20 nm. After the engine test, a check of the Pegasor-DT sample inlet flow showed 2 slpm compared to the factory calibrated 3.5 slpm. This would have caused a significant under reporting (almost half) of particle number concentration. Thus, the correlation would have been much improved and shows the importance of performing nvPM instrument in-field checks.

When comparing raw exhaust sampling to diluted exhaust sampling, the MPEC+ performed similarly in both cases, indicating that it can handle fluctuations in inlet temperatures and pressures when sampling raw exhaust. As expected, due to the eductor pump sampling system in the Pegasor-DT, the instrument under-reported particle concentration at negative sample inlet pressures (i.e., low thrust/small GMD) and over-reported concentration at positive sample inlet pressures (i.e., high thrust/large GMD).

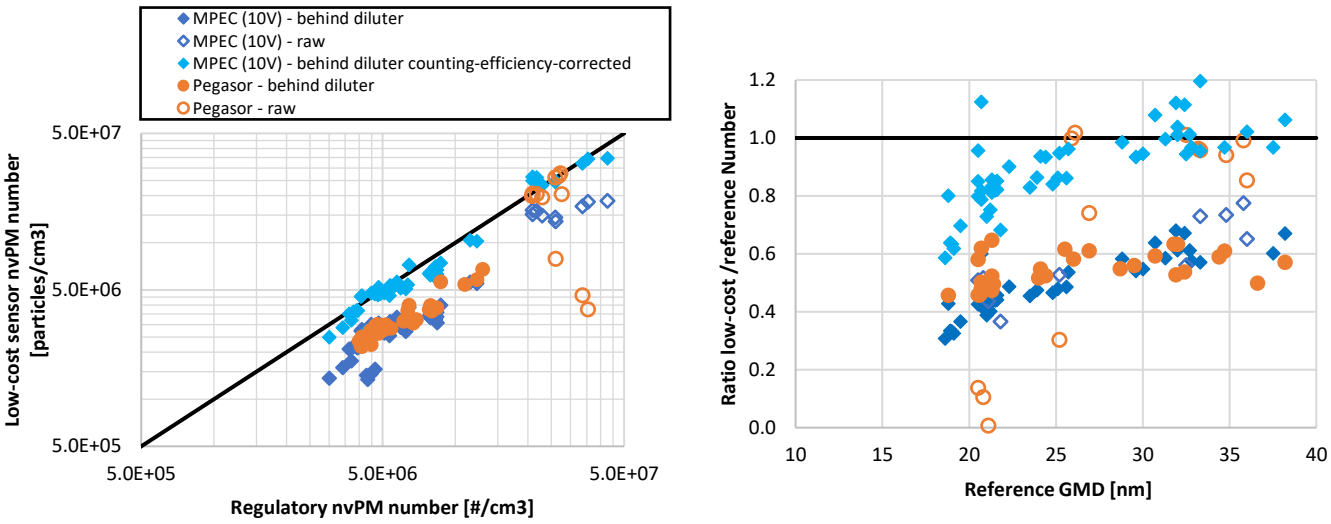

Figure 63: Regulatory nvPM number (corrected to low-cost sensor location) Vs low-cost sensor nvPM number (a) and ratio between low-cost and regulatory nvPM number Vs GMD at low-cost sensor location (b)

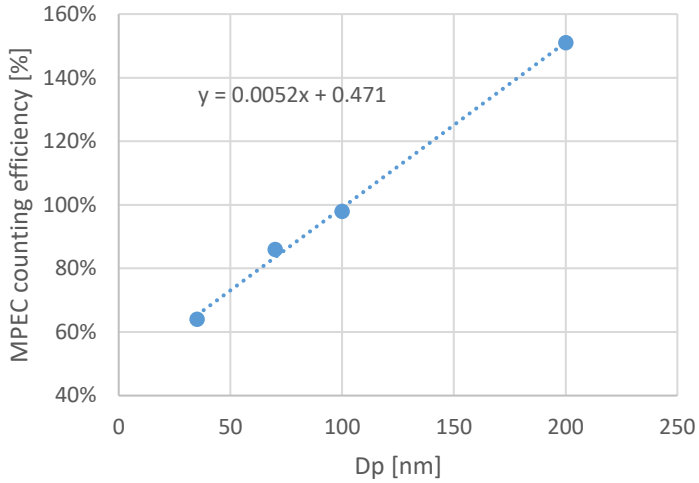

Figure 64: Dekati MPEC+ calibrated counting efficiency

The GMD reported by the Pegasor-DT was compared to that measured by the DMS500, with the DMS500 data corrected to the Pegasor-DT's sampling location. The comparison results, shown in Figure 65, indicate that the Pegasor-DT typically overpredicted the reference GMD. However, a clear trend was observed, suggesting that the Pegasor-DT size data could be adjusted to better match the DMS500 measurements. Furthermore, the good comparison between Pegasor-DT measurements for raw and diluted exhaust samples indicates that the sample inlet pressure only affected the instrument sample flow, with minimal impact on the particle size measurements.

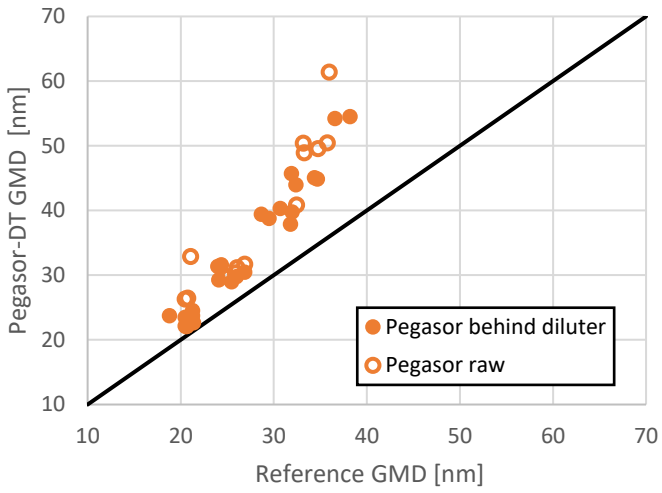

Figure 65: GMD comparison between Pegasor-DT and DMS500 when sampling aircraft exhaust (corrected to same location)

The GMD could theoretically be derived from MPEC measurements by varying the trap voltage, similar to the approach used with the Pegasor-DT. To test this concept, the MPEC+ trap voltage was adjusted between 10V and 110V at stable conditions, with the uncorrected results (not accounting for counting efficiency) displayed in Figure 66. The MPEC/reference number ratio is seen to increase with decreasing trap voltage, indicative of a higher counting efficiency at smaller sizes.

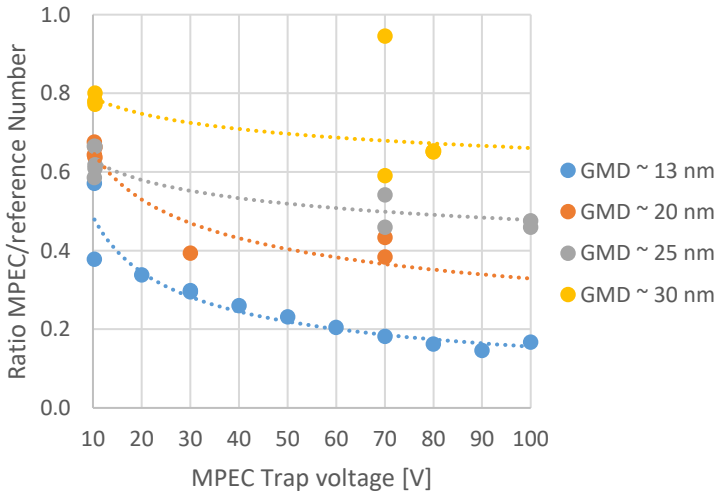

Figure 66: Ratio of MPEC number to reference number Vs MPEC trap voltage at different engine conditions (i.e., different GMDs)

4.2.1.2. ELPI+ HT results

Raw exhaust particle size distribution measurements were attempted using a High Resolution (HR) and High Temperature (HT) ELPI+, set at 180°C. Figure 67 below shows how the measured PSD from the ELPI+ compared to that measured near the nvPM number and mass instruments and demonstrates that it is possible to make such measurement on raw aircraft exhaust with this equipment. As the ELPI+ reports in aerodynamic space when compared to the SMPS which report in electrical mobility space, differences in GMD are symptomatic of particle effective density not being 1 g/cm^3. For example, as the ELPI+ measured a smaller GMD than that of the SMPS, it is expected that the density of the exhaust nvPM is < 1 g/cm^3. However, unfortunately it should be noted that the ELPI+ HT was experiencing a leak for most of this test, therefore further validation would be required.

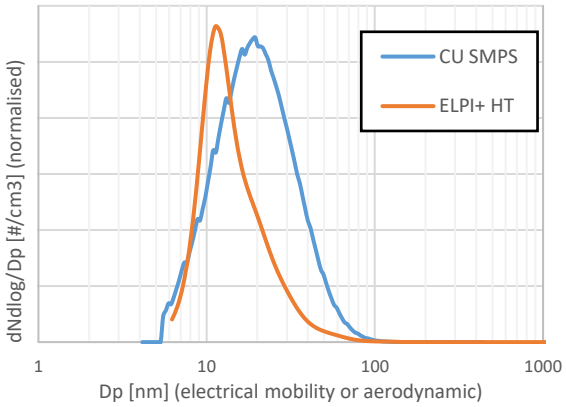

Figure 67: ALF502 exhaust particle size distribution measured raw (ELPI+) and diluted (SMPS) at idle

4.2.1.3. Particle charge and electrostatic loss

The engine exhaust aerosol charge state was quantified while sampling behind e-diluter within 4 m of the probe inlet using a TSI CPC (3756), an SMPS and an electrometer sampling in parallel behind a Cambustion electrostatic precipitator (ESP), as detailed in Figure 61.

By alternating the ESP on and off, the charge fraction, the charge distribution and the charge per particle can be determined. Preliminary results are shown in Figure 68, and highlight that as particle size increases, so does the charge fraction and as the power increases, there is an increase in charge fraction, especially at smaller diameters.

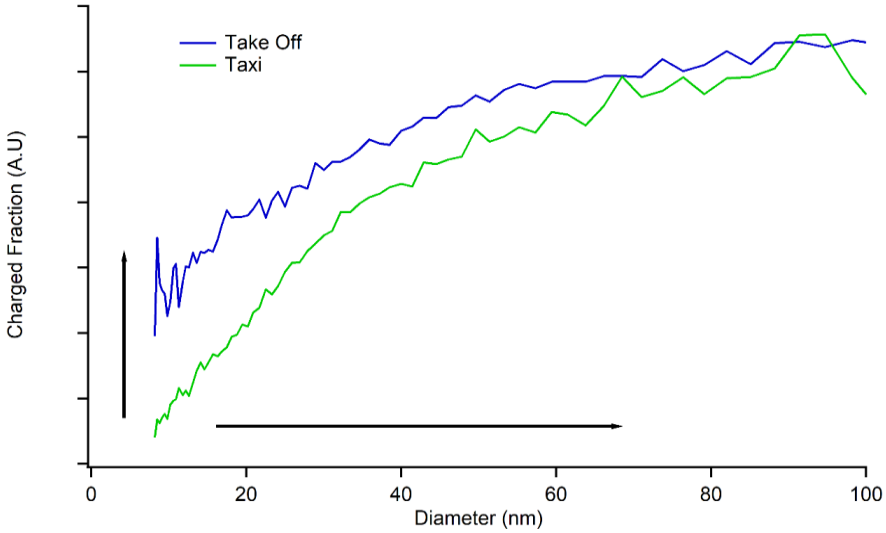

Figure 68: Preliminary data showing the size-dependent charge fraction of the nvPM as a function of thrust

The results also showed a slight positive bias in the charge state (i.e., more positively charged particles than negative) was present at high engine power. The importance of charge bias was highlighted in Lidstone-Lane et al. [42], which predicts that if a bias exists, additional electrostatic losses can occur within the first few metres a regulatory nvPM sampling system. This work forms a paper by Lidstone-Lane et al. (in prep) and his thesis, submitted 2024.

This work highlights the need to better understand the role of particle charge and electrostatic losses across a range of engine powers and particle concentrations to determine if regulated reported nvPM emissions are being underestimated.

4.2.2. Additional novel measurements

4.2.2.1. LII-300 Fluence sweeps

As previously introduced (section 0), in addition to measuring nvPM mass, the LII-300 can perform fluence sweeps to provide insights into changes in particle morphology, for example, with variations in engine thrust or fuel type. In Figure 69, the fluence of the EUR LII-300 shows significant variation with thrust, with the closest alignment occurring at a Q-switch of 165 µs, close to the default setting of 160 µs for this LII-300. The sweeps can be classified into three categories, low power (e.g., idle); medium power (e.g., 30% thrust); and high power (60% thrust and above), with each category indicating a change in particle morphology. When comparing SAF and jet-A at idle, the fuel type appears to have no measurable effect on the LII-300 fluence. Note that due to time available on test point, only limited sweeps were able to be performed which resulted in noisy fluence data. The sweeps were 5-minute long, with the Q-Switch Delay varying every 10 seconds between 139 and 220 µs by steps of 20-40 µs.

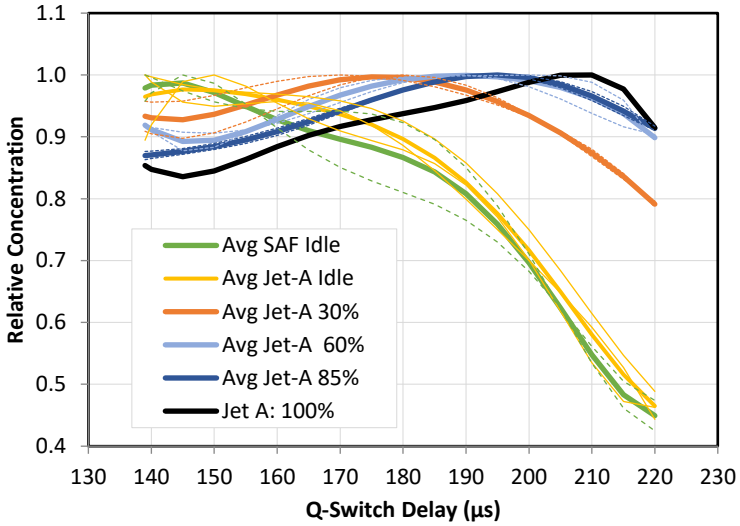

Figure 69: Fluence sweeps (i.e., ratio of maximum mass concentration to that at a different Q-switch delay) from the EUR LII-300 when sampling ALF502R exhaust with the EUR nvPM reference system ("Avg" corresponds to the average of two sweeps)

4.2.3. Differences Between LII-300 and MSS nvPM Mass Measurements

As previously introduced in section 2.3.1, a change in the ratio between the LII-300 and the MSS could indicate variation in the particle morphology or composition (e.g. elemental composition). Therefore, this ratio was compared for different fuels and different engines against engine T30 (Figure 70) and measured GMD (Figure 71).

The ratio between the EUR LII-300 and MSS is seen to fluctuate around 1.3 at low power (T30 ~120°C and GMD~20 nm) and then decreases with increasing power/GMD down to ~1.05. These trends suggest that particle morphology is a function of power for the engines tested, with better agreement between the nvPM mass instrument at high power (highest concentration and largest particle size). Changes in exhaust gas composition (e.g., humidity, NOx) may also affect the signal detection of the MSS. When looking specifically at the fuel effect, the SAF blends typically correspond to a higher LII-300/MSS ratio at a given T30 at medium and high power (Figure 70), however no fuel effect is observed when plotted against GMD (Figure 71), suggesting that the LII-300/MSS or the particle morphology is best correlated with measured GMD.

As seen in Figure 69, different engine powers and fuels result in different fluence responses of the EUR LII-300 instrument which may explain some of the observed variation in LII-300/MSS ratio. Similarly, it has been observed that the MAC (mass absorption cross-section) shows an increase of 25% from small particle sizes to larger ones for nvPM emissions from a small gas turbine engine, when measured with an MSS which uses a wavelength of 808 nm [16]. Given mass concentration is inversely proportional to the MAC, the reported mass concentrations from the MSS were shown to decrease with increasing size. The literature study covered a

wider size range than in this report, but the trend is in the same direction. It should also be noted that previous work [43], compared LII-300 and MSS on four large Rolls-Royce engine types (six total engines) with particle size. Scatter was observed (within ±15%) but with no size dependency reported.

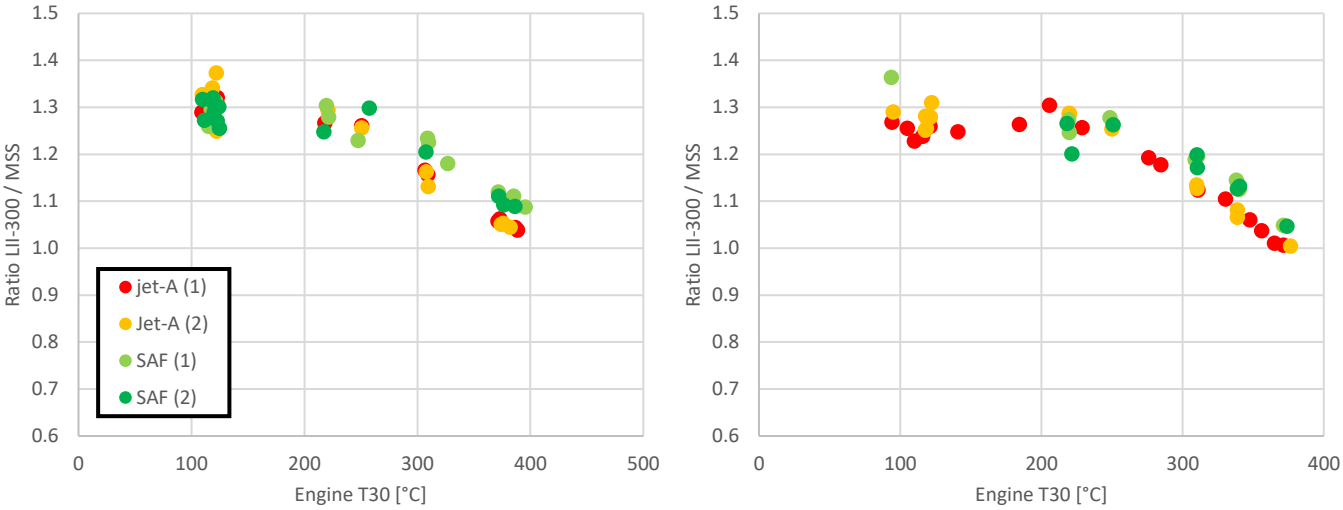

Figure 70: Measured nvPM mass ratio between the EUR LII-300 and MSS plotted against engine T30 when sampling exhaust from the ALF 507 (a) and 502 (b) burning different aviation fuels

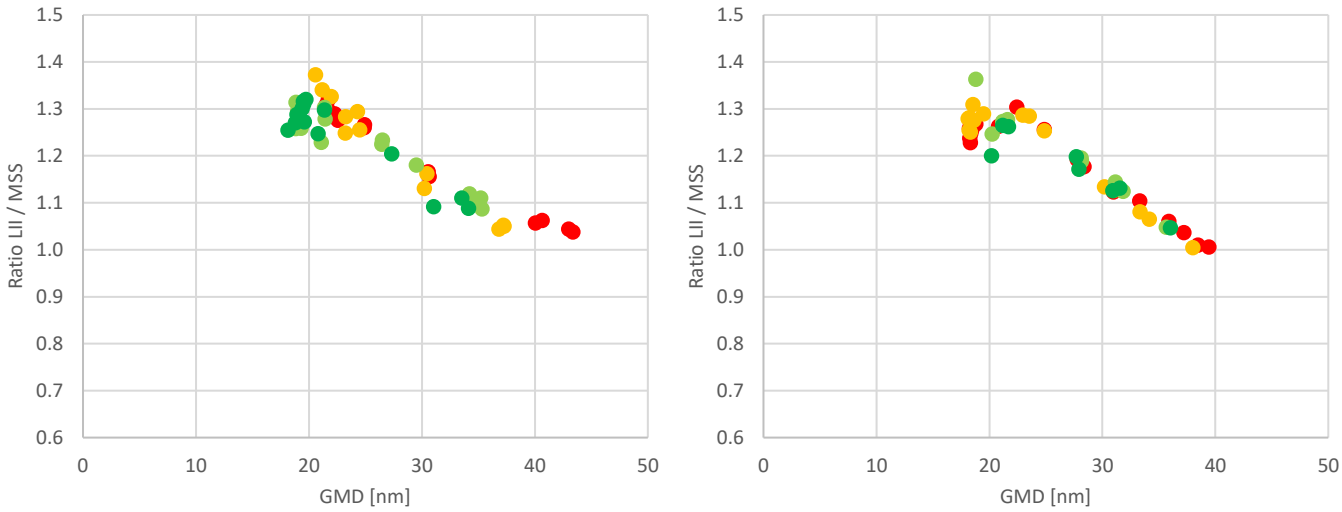

Figure 71: Measured nvPM mass ratio between the EUR LII-300 and MSS plotted against measured GMD when sampling exhaust from the ALF 507 (a) and 502 (b) burning different aviation fuels

4.3. Estimating nvPM Number and Mass from Particle Size Distribution measurements

Beyond PSD use for system loss correction calculation, where only the distribution shape is relevant (see Section 3), measured PSDs, with given knowledge of particle effective density could also be used to derive nvPM number and mass. This approach would significantly simplify nvPM measurement systems[24], with a single instrument measuring both nvPM number and mass.

PSDs measured by a Grimm SMPS 5420 during the ALF 507-1H and ALF 502R-5 emissions measurement campaigns were system loss corrected to the inlet of the regulatory nvPM number instrument (i.e., APC),

[24] Further discussed in SAMPLE IV Deliverable Report 2

enabling direct comparison and quantification of the uncertainty in deriving nvPM number from PSD measurements, with results shown in Figure 72. Additional corrections applied to the PSD-based number for comparison included STP conditions, differences in sample lines between instruments (e.g., additional thermophoretic loss to SMPS). The number concentrations obtained from a Cambustion DMS500 PSD with the aggregate inversion matrix applied were also compared to regulatory nvPM numbers. However, a significant bias was observed, and no scientific explanation has been identified to date. As a result, these findings are not presented and will require further investigation.

Figure 72 shows that the SMPS-based number agrees within 6% of the regulatory nvPM number on average, consistent with the results of the RAPTOR project, which reported an average agreement of 3% between a TSI SMPS and the Swiss reference system APC after correction for RQL exhaust sampling [5]. Significant discrepancies in PSD-derived number have been documented: Kittelson et al. [7] reported a ±30% agreement when comparing the total number concentration from five TSI SMPS' on different sources (diesel, silver, DES, PSL), and differences of up to 40% were observed when comparing two TSI SMPS, a DMS500, and an EEPS on laboratory-generated aerosols (see section 3.2.1).

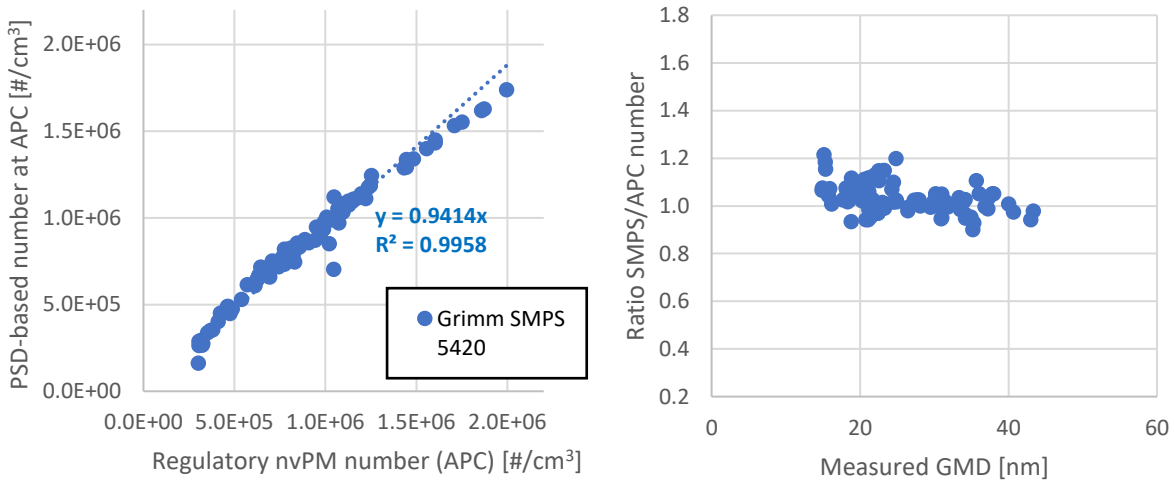

Figure 72: Comparison between regulatory (APC) and measured-PSD-based nvPM number (left) and their ratio against the measured GMD (right) when sampling the ALF 502 and 507 engines in parallel within the EUR nvPM reference system

Deriving nvPM mass from PSD measurements offers the potential to overcome some of the uncertainties in current nvPM mass definition and calibration discussed in section 2.4. This approach, already employed in previous studies [23], [44], is not limited to nvPM, offering the potential to measure total PM, including volatile components. However, assumptions are required to convert from number to mass, such as particle sphericity and effective density, which has been observed to vary between 0.3 and 1.3 g/cm^3 for aircraft nvPM [2].

As a result, this study initially focused on investigating nvPM number from PSD measurements. Follow-up work is already underway to expand on this work, incorporating novel DMA-ELPI+ measurements of particle effective density [43], as depicted within Figure 61. These measurements, combined with PSD data, will be used to derive nvPM mass and compare it with regulatory measurements.

4.4.Summary and future work of 'Novel' measurements

Novel advanced measurement techniques for nvPM number and mass were successfully tested as part of this programme.

The Dekati e-diluter pro was successfully used to sample raw aircraft exhaust close to the probe, demonstrating its potential as a viable alternative to single ejector diluters commonly used in regulatory nvPM sampling systems. The e-diluter pro offers adjustable dilution between 5:1 and 225:1 and is pressure-insensitive between 960 and 1500 mbar inlet pressure, potentially eliminating the need for a diluted CO_2 measurement. The successful deployment of the Dekati e-diluter pro for sampling aircraft PM near the probe, along with previous SAMPLEIII.3 experiments that demonstrated high-fidelity raw measurement of nvPM number, mass and size with the Artium LII-300 and Cambustion DMS500 [5], warrants further investigation and comparison with regulatory nvPM number and mass measurements.

Both the Dekati MPEC and Pegasor-DT were shown as promising instruments for measuring aircraft nvPM number (and size) near the probe inlet. The MPEC proved capable of sampling raw exhaust, typically agreeing within ±20% of regulatory nvPM number. additional work is needed to quantify the uncertainty in the nvPM number, mass and size reported by diffusion-chargers and other novel concepts.

While both certified and regulatory compliant, the LII-300 and MSS exhibited different responses (up to 30%) to aircraft engine mixed exhaust nvPM mass at varying thrust levels, further highlighting the uncertainty associated with current nvPM mass calibration and definition [19].

It should also be noted that recent engine combustion technologies, such as lean burn, have been shown to produce nvPM mass levels below the current limit of quantification for nvPM mass (3 $\mu g/m^3$ [5]), which includes sampling and measurement limits.

Deriving nvPM number and mass from a particle size measurement is emerging as a promising approach to simplify regulatory nvPM systems by removing the need for EC-based calibration and enabling a single instrument to provide nvPM number, size, and mass measurements. Good agreement (within ±10%) between PSD-based and regulatory nvPM number has been observed; however, larger uncertainties have also been witnessed for specific instrument-types. Further research is needed to quantify this uncertainty and to develop best practices for aircraft nvPM PSD measurements. More work is needed to better understand and quantify nvPM effective density from different aircraft engines and thrust regimes towards PSD-based nvPM mass.

Acknowledgements

The authors would like to thank Dr. Christos Dardiotis, the application engineer for Particle Number (PN) exhaust emission measurement devices at AVL, Dr. Mohsen Kazemimanesh, Senior Scientist in the Air Quality and Aerosol Metrology Group at the UK National Physical Laboratory (NPL) and Dr. Greg Smallwood, Principal Research Officer at National Research Council Canada (NRC), for their invaluable technical input and critical review of the relevant sections of this report.

REFERENCES

[1] ICAO, 'Annex 16 - Environmental Protection - Volume II - Aircraft Engine Emissions', Fifth edition, Jul. 2023. Accessed: May 08, 2024. [Online]. Available: https://store.icao.int/en/annex-16-environmental-protection-volume-ii-aircraft-engine-emissions

[2] L. Durdina *et al.*, 'Characterizing and Predicting nvPM Size Distributions for Aviation Emission Inventories and Environmental Impact', *Environ. Sci. Technol.*, vol. 58, no. 24, pp. 10548–10557, Jun. 2024, doi: 10.1021/acs.est.4c02538.

[3] B. Giechaskiel and A. Bergmann, 'Validation of 14 used, re-calibrated and new TSI 3790 condensation particle counters according to the UN-ECE Regulation 83', *J. Aerosol Sci.*, vol. 42, no. 3, pp. 195–203, Mar. 2011, doi: 10.1016/j.jaerosci.2011.01.002.

[4] 'UN Regulation No. 154 - Rev.1 | UNECE'. Accessed: Nov. 06, 2024. [Online]. Available: https://unece.org/transport/documents/2021/08/standards/un-regulation-no-154-rev1

[5] A. Crayford, E. Durand, D. Delhaye, L. Durdina, I. K. Ortega, and P. Williams, 'RAPTOR Work Package 4: PM Measurements Deliverables Report', 2022. Accessed: Oct. 07, 2022. [Online]. Available: https://zenodo.org/records/7385796

[6] A. Crayford and M. Johnson, 'SAMPLE III SC.01- Studying, sAmpling and Measuring of aircraft ParticuLate Emission', 2011, doi: https://www.easa.europa.eu/document-library/research-reports/easa2010fc10-sc01.

[7] B. Giechaskiel, M. Cresnoverh, H. Jörgl, and A. Bergmann, 'Calibration and accuracy of a particle number measurement system', *Meas. Sci. Technol.*, vol. 21, no. 4, p. 045102, Feb. 2010, doi: 10.1088/0957-0233/21/4/045102.

[8] B. Giechaskiel and A. Melas, 'Impact of Material on Response and Calibration of Particle Number Systems', *Atmosphere*, vol. 13, no. 11, Art. no. 11, Nov. 2022, doi: 10.3390/atmos13111770.

[9] E. Durand, 'Towards improved correction methodology for regulatory aircraft engine nvPM measurement', Thesis (PhD), Cardiff University, 2019. Accessed: Jan. 28, 2020. [Online]. Available: http://orca.cf.ac.uk/126400/

[10] B. Giechaskiel, X. Wang, D. Gilliland, and Y. Drossinos, 'The effect of particle chemical composition on the activation probability in n-butanol condensation particle counters', *J. Aerosol Sci.*, vol. 42, no. 1, pp. 20–37, Jan. 2011, doi: 10.1016/j.jaerosci.2010.10.006.

[11] J. Kangasluoma *et al.*, 'Sub-3 nm particle size and composition dependent response of a nano-CPC battery', *Atmospheric Meas. Tech.*, vol. 7, no. 3, pp. 689–700, Mar. 2014, doi: 10.5194/amt-7-689-2014.

[12] P. J. Wlasits *et al.*, 'Counting on chemistry: laboratory evaluation of seed-material-dependent detection efficiencies of ultrafine condensation particle counters', *Atmospheric Meas. Tech.*, vol. 13, no. 7, pp. 3787–3798, Jul. 2020, doi: 10.5194/amt-13-3787-2020.

[13] T. A. Sipkens and J. C. Corbin, 'Effective density and packing of compacted soot aggregates', *Carbon*, vol. 226, p. 119197, Jun. 2024, doi: 10.1016/j.carbon.2024.119197.

[14] J. C. Corbin *et al.*, 'Systematic experimental comparison of particle filtration efficiency test methods for commercial respirators and face masks', *Sci. Rep.*, vol. 11, no. 1, p. 21979, Nov. 2021, doi: 10.1038/s41598-021-01265-8.

[15] P. Lobo *et al.*, 'Comparison of standardized sampling and measurement reference systems for aircraft engine non-volatile particulate matter emissions', *J. Aerosol Sci.*, p. 105557, Mar. 2020, doi: 10.1016/j.jaerosci.2020.105557.

[16] J. C. Corbin *et al.*, 'Size-dependent mass absorption cross-section of soot particles from various sources', *Carbon*, vol. 192, pp. 438–451, Jun. 2022, doi: 10.1016/j.carbon.2022.02.037.

[17] R. Yuan *et al.*, 'Measurement of black carbon emissions from multiple engine and source types using laser-induced incandescence: sensitivity to laser fluence', *Atmospheric Meas. Tech.*, vol. 15, no. 2, pp. 241–259, Jan. 2022, doi: 10.5194/amt-15-241-2022.

[18] Cambustion Ltd, 'DMS500 User Manual (V4.26)'. 2022.

[19] T. A. Sipkens *et al.*, 'Quantifying the uncertainties in thermal–optical analysis of carbonaceous aircraft engine emissions: an interlaboratory study', *Atmospheric Meas. Tech.*, vol. 17, no. 14, pp. 4291–4302, Jul. 2024, doi: 10.5194/amt-17-4291-2024.
[20] E. Durand *et al.*, 'Correction for particle loss in a regulatory aviation nvPM emissions system using measured particle size', *J. Aerosol Sci.*, vol. 169, p. 106140, Mar. 2023, doi: 10.1016/j.jaerosci.2023.106140.
[21] J. Harper, E. Durand, P. Bowen, D. Pugh, M. Johnson, and A. Crayford, 'Influence of alternative fuel properties and combustor operating conditions on the nvPM and gaseous emissions produced by a small-scale RQL combustor', *Fuel*, vol. 315, p. 123045, May 2022, doi: 10.1016/j.fuel.2021.123045.
[22] L. Durdina, B. T. Brem, M. Elser, D. Schönenberger, F. Siegerist, and J. G. Anet, 'Reduction of Nonvolatile Particulate Matter Emissions of a Commercial Turbofan Engine at the Ground Level from the Use of a Sustainable Aviation Fuel Blend', *Environ. Sci. Technol.*, vol. 55, no. 21, pp. 14576–14585, Nov. 2021, doi: 10.1021/acs.est.1c04744.
[23] J. C. Corbin *et al.*, 'Aircraft-engine particulate matter emissions from conventional and sustainable aviation fuel combustion: comparison of measurement techniques for mass, number, and size', *Atmospheric Meas. Tech.*, vol. 15, no. 10, pp. 3223–3242, May 2022, doi: 10.5194/amt-15-3223-2022.
[24] E. Durand, P. Lobo, A. Crayford, Y. Sevcenco, and S. Christie, 'Impact of fuel hydrogen content on non-volatile particulate matter emitted from an aircraft auxiliary power unit measured with standardised reference systems', *Fuel*, vol. 287, p. 119637, Mar. 2021, doi: 10.1016/j.fuel.2020.119637.
[25] SAE International, 'ARP 6481A- Procedure for the Calculation of Sampling Line Penetration Functions and Line Loss Correction Factors', 2024, doi: https://doi.org/10.4271/ARP6481.
[26] R. Giannelli *et al.*, 'Evaluation of methods for characterizing the fine particulate matter emissions from aircraft and other diffusion flame combustion aerosol sources', *J. Aerosol Sci.*, vol. 178, p. 106352, May 2024, doi: 10.1016/j.jaerosci.2024.106352.
[27] D. B. Kittelson *et al.*, 'Experimental verification of principal losses in a regulatory particulate matter emissions sampling system for aircraft turbine engines', *Aerosol Sci. Technol.*, vol. 56, no. 1, pp. 63–74, Jan. 2022, doi: 10.1080/02786826.2021.1971152.
[28] A. Singh and C. Kuang, 'Scanning Mobility Particle Sizer (SMPS) Instrument Handbook', DOE/SC-ARM-TR--147, 1245993, Apr. 2024. doi: 10.2172/1245993.
[29] TSI Incorporated, 'Scanning mobility particle sizer spectrometer (SMPS) MODEL 3938'. 2019. Accessed: May 01, 2019. [Online]. Available: https://www.tsi.com/getmedia/3705a532-8dd8-46eb-832d-0bce6ab2921b/SMPS-3938_A4_5001532_RevE_Web?ext=.pdf
[30] A. Wiedensohler *et al.*, 'Mobility particle size spectrometers: Calibration procedures and measurement uncertainties', *Aerosol Sci. Technol.*, vol. 52, no. 2, pp. 146–164, Feb. 2018, doi: 10.1080/02786826.2017.1387229.
[31] A. Wiedensohler *et al.*, 'Mobility particle size spectrometers: harmonization of technical standards and data structure to facilitate high quality long-term observations of atmospheric particle number size distributions', *Atmospheric Meas. Tech.*, vol. 5, no. 3, pp. 657–685, Mar. 2012, doi: 10.5194/amt-5-657-2012.
[32] V. Perraud, J. N. Smith, and J. Olfert, 'High-accuracy effective density measurements of sodium methanesulfonate and aminium chloride nanoparticles using a particulate calibration standard', *Aerosol Sci. Technol.*, vol. 57, no. 4, pp. 355–366, Apr. 2023, doi: 10.1080/02786826.2023.2176739.
[33] A. Charvet, S. Bau, N. E. Paez Coy, D. Bémer, and D. Thomas, 'Characterizing the effective density and primary particle diameter of airborne nanoparticles produced by spark discharge using mobility and mass measurements (tandem DMA/APM)', *J. Nanoparticle Res.*, vol. 16, no. 5, p. 2418, Apr. 2014, doi: 10.1007/s11051-014-2418-y.
[34] L. Peng *et al.*, 'A review of measurement techniques for aerosol effective density', *Sci. Total Environ.*, vol. 778, p. 146248, Jul. 2021, doi: 10.1016/j.scitotenv.2021.146248.
[35] A. Awasthi, B.-S. Wu, C.-N. Liu, C.-W. Chen, S.-N. Uang, and C.-J. Tsai, 'The Effect of Nanoparticle Morphology on the Measurement Accuracy of Mobility Particle Sizers', *MAPAN*, vol. 28, no. 3, pp. 205–215, Sep. 2013, doi: 10.1007/s12647-013-0068-7.

[36] D. Delhaye *et al.*, 'The MERMOSE project: Characterization of particulate matter emissions of a commercial aircraft engine', *J. Aerosol Sci.*, vol. 105, pp. 48–63, Mar. 2017, doi: 10.1016/j.jaerosci.2016.11.018.
[37] J. Xue *et al.*, 'Comparison of Vehicle Exhaust Particle Size Distributions Measured by SMPS and EEPS During Steady-State Conditions', *Aerosol Sci. Technol.*, vol. 49, no. 10, pp. 984–996, Oct. 2015, doi: 10.1080/02786826.2015.1088146.
[38] T. J. Johnson, R. T. Nishida, M. Irwin, J. P. R. Symonds, J. S. Olfert, and A. M. Boies, 'Measuring the bipolar charge distribution of nanoparticles: Review of methodologies and development using the Aerodynamic Aerosol Classifier', *J. Aerosol Sci.*, vol. 143, p. 105526, May 2020, doi: 10.1016/j.jaerosci.2020.105526.
[39] A. Wiedensohler *et al.*, 'Mobility particle size spectrometers: Calibration procedures and measurement uncertainties', *Aerosol Sci. Technol.*, vol. 52, no. 2, pp. 146–164, Feb. 2018, doi: 10.1080/02786826.2017.1387229.
[40] 'TSI Advanced Aerosol Neutralizer (Model 3088) Brochure'. Accessed: Oct. 19, 2023. [Online]. Available: https://tsi.com/getmedia/85d6abad-a56a-4a1f-a61d-1c73983c7e7a/Aerosol%20Neutralizers%203088_A4_5001321_RevE_Web?ext=.pdf
[41] R. Gopalakrishnan, P. H. McMurry, and Jr. Hogan Christopher J., 'The Bipolar Diffusion Charging of Nanoparticles: A Review and Development of Approaches for Non-Spherical Particles', *Aerosol Sci. Technol.*, vol. 49, no. 12, pp. 1181–1194, Dec. 2015, doi: 10.1080/02786826.2015.1109053.
[42] F. O. N. Lidstone-Lane, E. F. Durand, P. I. Williams, M. Johnson, and A. Lea-Langton, 'Experimental characterization of electrostatic loss relevant to aviation nvPM sampling', *Aerosol Sci. Technol.*, vol. 0, no. 0, pp. 1–17, 2024, doi: 10.1080/02786826.2024.2390100.
[43] M. Johnson, 'DP17 SAE E31 Florida - "Update on mass comparison data"', Jan. 2018.
[44] L. Durdina *et al.*, 'Determination of PM mass emissions from an aircraft turbine engine using particle effective density', *Atmos. Environ.*, vol. 99, pp. 500–507, Dec. 2014, doi: 10.1016/j.atmosenv.2014.10.018.

Appendix

METAS APC Calibration report

Schweizerische Eidgenossenschaft
Confédération suisse
Confederazione Svizzera
Confederaziun svizra

Federal Institute of Metrology METAS

Certificate of Calibration No 235-13034

Object	**Particle CPC** Model : AVL489 APC Advanced Manufacturer : AVL Serial number : 409C & 507
Order	Measurement of the size-dependent counting efficiency with monodisperse, thermally treated combustion particles between 10 nm and 55 nm at a concentration of 2'500 cm^{-3}.
Applicant	**Zürcher Hochschule für Angewandte Wissenschaften** Technikumstrasse 71 CH - 8400 Winterthur Switzerland
Traceability	The reported measurement values are traceable to national standards and thus to internationally supported realisations of the SI units.
Date of Calibration	05.02.2024
Marking	Calibration label METAS 02.2024

3003 Bern-Wabern, 05 February 2024

For the Measurements	Kevin Auderset
Approved by	Dr. Konstantina Vasilatou, Head of Laboratory, Laboratory Particles and Aerosols

CIPM MRA

Mutual recognition
This certificate is consistent with Calibration and Measurement Capabilities (CMCs) that are included in Appendix C of the Mutual Recognition Arrangement (MRA) drawn up by the International Committee for Weights and Measures. Under the MRA, all participating institutes recognize the validity of each other's calibration certificates and measurement reports for the quantities, ranges and measurement uncertainties specified in Appendix C (for details see www.bipm.org).

*Valid for soot particles in the size range 23 nm to 500 nm at concentrations 500-60'000 cm^{-3}.

METAS
Lindenweg 50, 3003 Bern-Wabern, Switzerland, phone +41 58 387 01 11, www.metas.ch

Extent of the Calibration

The device under test DUT was compared with an aerosol electrometer. The comparison was carried out with size-selected and thermally treated combustion particles with a mobility diameter of 10 nm and 55 nm. Based on these measurements, the size-dependent counting efficiency of the DUT could be determined.

Measurement Procedure

The aerosol source was the Combustion Aerosol Standard "bigCAST" (Jing Ltd, Inv. No. 4276). The aerosol was thermally treated with a thermodiluter (Palas PMPD 100, S/N 5535) and diluted by a factor of 10. A blower transported the aerosol to a dilution bridge (custom made) through the electrostatic classifier (TSI Electrostatic Classifier 3080, S/N 71201060 with TSI DMA 3081, S/N 3081140501 or TSI DMA 3085, S/N 3085112702) which selected the required particle size. The DMA had been previously calibrated with size-certified PSL-particles and was used as *reference standard for the particle size*. The sheath-air-to-aerosol flow ratio was generally adjusted to >8.2:1.

The selected, monodisperse aerosol was then mixed with filtered compressed air in a mixing volume, diluted to the required concentration and distributed to the devices using a flow splitter. All tubes downstream of the classifier were made of conductive material, and the length of the tubes from the flow splitter to the devices was adapted to the respective flow rate to ensure equal diffusion losses. A schematic illustration of the experimental setup is shown in Figure 1.

The *reference standard for the particle concentration* consisted of an electrometer (TSI Aerosol Electrometer 3068B, S/N 70701106) with 1.5 L min^{-1} sample flow and an external flow meter (Vögtlin red-y smart GSM-B4TA-BN00, S/N 122021). The current measured by the electrometer was converted to the particle number concentration under ambient conditions by means of external flow measurement. The ambient pressure and temperature measured in the laboratory were used for the conversion of the flow and therefore the number concentration to the ambient conditions during measurement.

The measurement and calculation of the counting efficiency of the DUT was performed according to the ISO 27891 standard. The measurement was carried out alternately at the DMA voltage of zero (particle-free air), a voltage for the desired particle diameter, followed by a 2-fold voltage, if necessary. The latter are required for the multiple charge correction of the measured number concentration values. This cycle was measured 6 times. The results of the electrometer were corrected with respect to the drift of the zero point and the presence of multiply charged particles, the results of the DUT with respect to the multiply charged particles. The particle size distribution at the inlet of the DMA was adjusted so that the fraction of multiply charged particles at the outlet of the DMA was below 1 %.

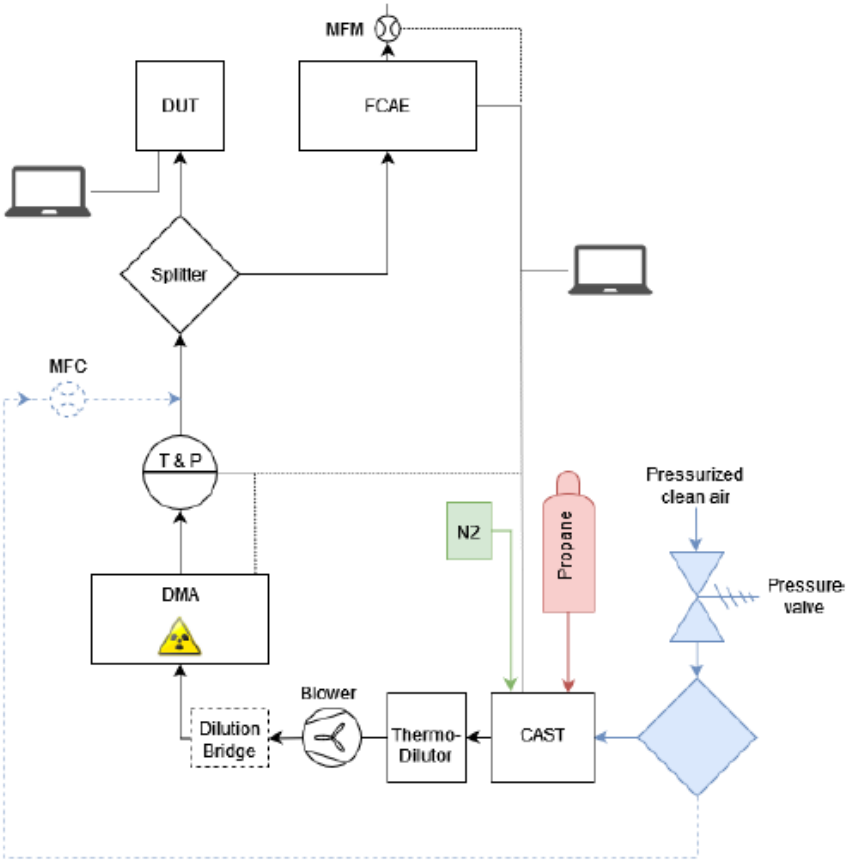

Figure 1: Schematic representation of the setup used for the measurements.

For the calculation of the multiple charge correction, pressure and temperature were measured at the outlet of the DMA.

The coefficient of variance (CV) averaged over the 6 cycles was determined for each measuring point as a test for generator stability. According to the ISO 27891 standard, the CV of the generator should be less than or equal to 3 %. The CV of the condensation particle counter was largely dominated by its dilution unit fluctuations while the CV of the reference electrometer at low concentrations contained also significant contributions from the electrical noise. The CV of the reference electrometer was less than 3 % for all measurements. The CV of the DUT was less than 5 % for all measurements.

The flow splitter bias β was determined for all particle sizes at at nominal concentrations of 2'500 cm^{-3} according to the ISO 27891 standard. Due to the different flows of the reference

electrometer and the DUT, β was assumed to be equal to 1 and the associated uncertainty was determined according to section G.3 of ISO 27891. As long as the flow conditions in the flow splitter remain the same, β can be regarded as concentration independent. The values determined were then taken into account in the respective calculations of the counting efficiencies.

Measurement Conditions

Date	*Temperature*	*Ambient pressure*
05.02.2024	(23.1…24.1) °C	(960…963) hPa

Measurement Results

d (nm): nominal el. mobility diameter of the combustion particles
C (cm $^{-3}$): mean particle number concentration
E: counting efficiency of the DUT; $C_{DUT}/C_{Reference}$
β: flow splitter bias
Q (L min^{-1}): volumetric flow of the aerosol
U: expanded measurement uncertainty

Counting efficiency

El. mobility diameter d (nm)	Nominal particle number concentration (cm^{-3})	Reference particle number concentration $C \pm U$ (cm^{-3})	Counting efficiency of the DUT $E \pm U$
10*	2'500	4'230 ± 90	0.102 ± 0.009
55	2'500	3'230 ± 110	0.772 ± 0.041

*) measurement point beyond the CMC range.

The uncertainty of the particle size was estimated to be up to 10 % for particles with a nominal diameter of 10 nm and 5-8 % for particles with a nominal diameter of 55 nm.

Flow splitter-bias

The flow splitter bias was assumed to be β = 1 and the associated uncertainty was calculated according to section G.3 of the ISO 27891 standard.

El. mobility diameter d (nm)	Flow splitter bias $\beta \pm U$
10	1.000 ± 0.037
55	1.000 ± 0.028

Certificate of Calibration No 235-13034

Sample flow

The sample flow of the DUT was determined at the inlet of the DUT using a calibrated volumetric flow meter (Gilian, Gilibrator, S/N1005075-S).

time	Nominal sample flow Q_{nom} (L min^{-1})	Effective sample flow $Q \pm U$ (L min^{-1})
Start of calibration	4.50	4.70 ± 0.05
End of calibration	4.50	4.70 ± 0.05

Uncertainty of Measurement

The reported uncertainty of measurement is stated as the combined standard uncertainty multiplied by a coverage factor $k = 2$. The measured value (y) and the associated expanded uncertainty (U) represent the interval ($y \pm U$) which contains the value of the measured quantity with a probability of approximately 95 %. The uncertainty was estimated following the guidelines of the JCGM 100:2008 (GUM).

The measurement uncertainty contains contributions originating from the measurement standard, from the calibration method, from the environmental conditions and from the object being calibrated. The long-term characteristic of the object being calibrated is not included.

NPL AVL APC calibration certificate

NATIONAL PHYSICAL LABORATORY
Teddington Middlesex UK TW11 0LW Telephone +44 20 8977 3222
NPL Management Ltd – Registered in England and Wales No 2937881

Test Report

Volatile Particle Remover Testing

FOR:	IESA A&D Limited
ON BEHALF OF:	Rolls Royce Plc P.O. Box 31 Derby DE24 8BJ United Kingdom
CUSTOMER ORDER NO:	QC 1200-00742327
NPL QUOTATION NO:	2024030002
DESCRIPTION:	Measurement of dilution factor and particle penetration efficiency of a Volatile Particle Remover according to ICAO 2017 Annex 16 Vol II Appendix 7.
VPR MODEL:	AVL APC Plus Advanced
VPR SERIAL NUMBER:	382C
DATE(S) OF TEST:	16 – 29 May 2024

Date of Issue: 2 July 2024 **Signed:** N S Brown **(Authorised Signatory)**

Checked by: Dr M Kazemimanesh **Name:** Dr A S Brown **on behalf of NPLML**

1. VPR dilution factor

The method described in NPL Procedure TECHPRO0269 was followed.

An NPL-certified gas standard of nominally 50 mmol mol^{-1} carbon dioxide in nitrogen was used as input gas to the VPR. Nitrogen gas (BIP grade 6.0, 99.9999 % purity) was used as diluent gas. Measurements were performed using a cavity enhanced absorption spectrometer (LI-COR Environmental, Model LI-7815), calibrated with ISO 17025 certified gas standards. For this measurement, the VPR inlet pressure was set to be 60 mbar less than ambient pressure.

Nominal dilution setting of VPR	69
Nominal inlet minus ambient pressure / mbar	**–60**
CO_2 amount fraction in reference gas / (µmol mol^{-1})	51,240
Measured CO_2 amount fraction / (µmol mol^{-1})	758
Measured dilution factor	68
Inlet pressure / mbar	943
Ambient pressure / mbar	1003

2. Particle concentration reduction factor

The method described in NPL Procedure TECHPRO0269 was followed. The particles were size-selected using a calibrated DMA (TSI, Model 3081) and two calibrated CPCs (TSI, Model 3752) were used to perform the particle number concentration measurements.

Measurements were conducted at nominal dilution setting of VPR equal to 69, with a controlled inlet pressure, using gold nanoparticles of nominal diameters of 15 nm, 30 nm, 50 nm and 100 nm. For all measurements, the inlet and ambient pressure difference was set to be nominally 60 mbar. The CPC at the inlet operated at the VPR inlet pressure and the CPC at the outlet operated at the VPR outlet pressure as stated in the results table below.

The minimum particle number concentration of 5,000 cm^{-3} at the VPR inlet (specified by ICAO 2017 Annex 16 Vol II Appendix 7) was met.

Nominal particle size	15 nm	30 nm	50 nm	100 nm
Estimate of multiply charged particles fraction / %	0.5	3.4	5.5	6.0
Particle number concentration at inlet / cm^{-3}	5379	6821	7099	6100
Particle number concentration at outlet / cm^{-3}	35.2	64.5	75.7	69.5
Particle concentration reduction factor	**153**	**106**	**94**	**88**
Inlet pressure / mbar	947	948	947	947
Ambient pressure / mbar	1007	1008	1007	1007

3. Penetration efficiency

The penetration efficiency was calculated as described in NPL Procedure TECHPRO0269 and in accordance with ICAO 2017 Annex 16 Vol II Appendix 7.

Nominal dilution setting of VPR	69			
Nominal particle size	15 nm	30 nm	50 nm	100 nm
Calculated penetration efficiency / %	44 ± 3	64 ± 5	72 ± 5	77 ± 6
Minimum required penetration efficiency / %*	30	55	65	70

* Specified by ICAO 2017 Annex 16 Vol II Appendix 7

The reported expanded uncertainty is based on a standard uncertainty multiplied by a coverage factor $k = 2$, providing a coverage probability of approximately 95 %.

Example AVL APC calibration certificate

AVL 489 Particle Counter Aviation Calibration Certificate

Date:	30-Sep-2020
Device: GH0965	382
Chopper Diluter	460

Makro	XF0339	V1.30

Used Instruments	Type	Serial No.
DMA	TSI 3080	71124079
Master CPC	TSI TSI 3772	3772121004
Mass Flow Meter	Vögtlin GCR-B5SA-BA25	141570
Calibration aerosol: APG combustion soot		

Measured Inlet Flows of Instruments		
Device	Vol. Flow	Normalization Cond.
APC Chopper Dil. low	4791 ml/min	25°C; 1013.25mbar
Master CPC	1021 ml/min	ambient conditons

Zero Concentration with HEPA-Filter		
APC	0.29 #/cm³	at pcrf=10*10=100
Master CPC	0.000 #/cm³	

Nr	values set: Diluter 1 low/high	Diluter 1	Diluter 2	set pcrf	Flows: Dilution Factor	Measured Penetrations: 100nm (>70%)	50nm (>65%)	30nm (>55%)	15nm (>30%)
1	low	10	10	**100**	**73**	76.3%	72.9%	68.8%	51.4%
2	low	25	10	**250**	**187**	77.6%	76.3%	70.5%	50.4%
3	low	50	10	**500**	**376**	79.0%	77.0%	70.8%	50.6%
4	low	100	10	**1000**	**762**	81.2%	78.5%	69.8%	49.9%
5	low	150	10	**1500**	**1153**	84.0%	77.5%	70.5%	47.2%

***Only calibrated at Stages 1-5. One of those stages MUST be used for ICAO Annex 16: Environmental Protection, Vol. II, Appendix 7 compliant measurements.**

Volatile Particle Removal Efficiency for Tetracontane 30nm:	**99.76%**

Signature

(Armin Sejdic)

88

Kalibrierung - Zähleffizienz - **außerhalb des akkreditierten Partikelgrößenbereichs**
*Calibration - Counting efficiency - **not within the accredited particle size range***

Partikelgröße* *Particle size** [nm]	Nom. konzentration *Nom. concentration* [#/cm³]	Gem. Konzentration *Meas. Concentration* [#/cm³]	Referenzkonz. *Reference conc.* [#/cm³]	Zähleffizienz *Counting eff.* []	rel. Messunsicherheit *rel. meas. uncertainty* []
15	7000	6318	*7034*	*0.898*	*5.9%*
10	3000	2395	*3192*	*0.750*	*7.9%*

* Die Messunsicherheit für die Partikelgröße beträgt 4% laut Kalibrierung des DEMC bei einem Nationalen Metrologischen Institut.
* *The measurement uncertainty for the particle size is 4% according to the calibration of the DEMC at a National Metrological Institute.*

Evaluierung* der Limits entsprechend UN/ECE GRPE-PMP Sub23nm draft
Limit evaluation according UN/ECE GRPE-PMP Sub23nm draft*

Kalibrierung - Linearität
Calibration - Linearity

Nr. *No.*	Nom. Konz. *Nom. Conc.* [#/cm³]	Ref. Konz. *Ref. Conc* [#/cm³]	Gem. Konz. *Meas. Conc* [#/cm³]	Zähleffizienz *Counting eff.* []	Limit *Limit* []	Status *Status* []	Residuum abw. *Residual dev.* [%]
1	10000	9375	9081	*0.969*	0.9-1.1	*passed*	*0.3%*
2	8000	7765	7504	*0.966*	0.9-1.1	*passed*	*0.1%*
3	6000	5907	5663	*0.959*	0.9-1.1	*passed*	*-0.7%*
4	4000	4117	3954	*0.960*	0.9-1.1	*passed*	*-0.5%*
5	2500	2569	2462	*0.958*	0.9-1.1	*passed*	*-0.7%*
6	0	0	0	-	<0.5#/cm³	*passed*	-

Berechnung des k-Faktors bei 55nm
k-factor calculation at 55nm

	Wert *Value*	Limit *Limit*
Steigung/Slope	0.965	0.9-1.1
R^2	1.000	>0.97
k-Faktor	1.036	-

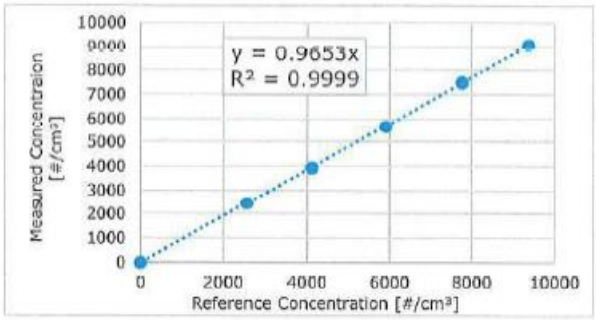

Zähleffizienz bei 10nm und 15nm mit angewandtem k-Faktor
Counting efficiency at 10nm and 15nm with k-factor applied

Partikelgröße *Particle size* [nm]	Zähleffizienz *Counting eff.* []	Limit *Limit* []	Status *Status* []
10	0.777	0.5-0.8	*passed*
15	0.930	≥0.9	*passed*

Example Cambustion DMS500 calibration certificate

Cambustion

DMS500 Certificate of Calibration

after Service and Adjustment

Company Name: NRC	Instrument Serial №: M125
Company Location: Canada	Calibration № (matrix):m2cqw747
Ship Date: October 2021	Date Calibrated: 8th October 2021

The DMS500 system is certified as meeting or exceeding the Test Specifications, when tested prior to dispatch. The calibration standards used for these measurements are traceable to relevant international standards. The results refer to measurements made at the time of test and not to the instrument's ability to maintain calibration. *The reported measurement uncertainties are based upon a standard uncertainty multiplied by a coverage factor k = 2, which for a normal distribution provides a level of confidence of approximately 95%. The standard uncertainties are a consolidation of the uncertainty in the standard and the uncertainty in performing the measurement.*

(a) Size and Gain: against Differential Mobility Analyser Sized Aerosol, with concentration indicated with a standard aerosol electrometer
Electrometer filter flow = 8.0 slpm

Aerosol	DMA Size (nm)	DMS Size (nm)	Electrometer Concentration (#/cc)	DMS Concentration (#/cc)
H_2SO_4	15.0 ± 1.5	15.1	43200 ± 8630	41400
NaCl	50.0 ± 5.0	49.9	31100 ± 6220	30300
NaCl	100 ± 10	102	20400 ± 4070	20500

(b) Size Only: Nebulised, dried and neutralised suspension of NIST Traceable Certified NanoSpheres (PSL), Thermo Scientific

PSL Size (nm)	DMS Size (nm)	Lot No	Expiry Date
303 ± 30	306	238629	01/03/2024
600 ± 60	602	230585	01/09/2023
903 ± 90	887	239389	01/04/2024

Standards used for part (a)

Function		Mfr and Model	Serial Number	Calibrated By	Calibration Reference	Calibration Date	Calibration Due
DMA		TSI 3082	3082001912001	Cambustion	3082001912001/2021	22/03/2021	22/03/2022
Aerosol Electrometer	Electrometer	Keithley 6514	1247513	Keithley Instruments	0500131	08/01/2021	08/01/2022
	Mass flow meter	Aalborg GFC171	224526-1	Aalborg	210524224526-1	24/05/2021	24/05/2022

Calibrator: J.Evans

Approved By: JPRS

Dr J.P.R. Symonds

Director

CAMBUSTION LTD

J6 The Paddocks
347 Cherry Hinton Road
Cambridge CB1 8DH
United Kingdom
Tel: +44 1223 210250
Fax: +44 1223 210190
E-mail: *cambustion@cambustion.com*

Cambustion

DMS500 Certificate of Calibration with Soot Agglomerates

after Service and Adjustment

Company Name: *NRC*	Instrument Serial №: M125
Company Location: Canada	Calibration № (matrix): m2cqs747
Ship Date: October 2021	Date Calibrated: *8th October 2021*

In addition to the standard spherical calibration (m2cqw747), an additional calibration is provided for measurement from highly fractal aerosols, e.g. Diesel. This applies only to the accumulation mode lognormal fit output given by the *Diesel* aerosol description file (.dmd).

The calibration standards used for these measurements are traceable to relevant international standards. The results refer to measurements made at the time of test and not to the instrument's ability to maintain calibration. *The reported measurement uncertainties are based upon a standard uncertainty multiplied by a coverage factor k = 2, which for a normal distribution provides a level of confidence of approximately 95%. The standard uncertainties are a consolidation of the uncertainty in the standard and the uncertainty in performing the measurement.*

Size and Gain: against Differential Mobility Analyser Sized Aerosol, with concentration indicated with a standard aerosol electrometer
Electrometer filter flow = 8.0 slpm

Aerosol	DMA Size (nm)	DMS Size (nm)	Electrometer Concentration (#/cc)	DMS Concentration (#/cc)
Soot	50.0 ± 5.0	49.3	17400 ± 3480	17000
Soot	100 ± 10	101	26300 ± 5270	25200
Soot	200 ± 20	204	35000 ± 7000	34000

Standards used:

Function		Mfr and Model	Serial Number	Calibrated By	Calibration Reference	Calibration Date	Calibration Due
DMA		TSI 3082	3082001912001	Cambustion	3082001912001/2021	22/03/2021	22/03/2022
Aerosol Electrometer	Electrometer	Keithley 6514	1247513	Keithley Instruments	0500131	08/01/2021	08/01/2022
	Mass flow meter	Aalborg GFC171	224526-1	Aalborg	210524224526-1	24/05/2021	24/05/2022

Calibrator: J.Evans

Approved By: JPRS

Dr J.P.R. Symonds

Director

CAMBUSTION LTD

J6 The Paddocks
347 Cherry Hinton Road
Cambridge CB1 8DH
United Kingdom
Tel: +44 1223 210250
Fax: +44 1223 210190
E-mail: *cambustion@cambustion.com*

Example TSI EEPS calibration certificate

Sample Data Sheet

Date/Time: 7/02/2020 9:11:54 AM
Instrument Label: Model 3090AK, SN: 30900196
Firmware: MCU: 3.15, DSP: 3.02

Read Status Record	Units	Nominal	3090/3091
Status Code			0x77
Error Code 1		0x0	0x0
Error Code 2		0x0	0x0
Sheath Flow	LPM	39.4±.20	39.4
Sample Flow	LPM	8.0±0.08	8.0
Charger Flow	LPM	0.60±0.02	0.6
Extraction Flow	LPM	2.00±0.02	2.0
Absolute Pressure	mBar	968±40	951.0
Voltage Top	V	85±2	85.1
Voltage Middle	V	470±10	468.7
Voltage Bottom	V	1200±4	1199.3
Sheath Flow Temp	°C	25±5	24.2
Sample Flow Temp	°C	25±5	24.2
Charger Flow Temp	°C	25±5	25.8
Extraction Flow Temp	°C	25±5	25.5
Neg. Charger Current	nA	35±0.5	34.8
Pos. Charger Current	nA	31±0.5	30.9
Neg. Charger Voltage	V	2000±500	1736.9
Pos. Charger Voltage	V	2000±500	2178.8

Zero Electrometer Table	Units	Offset Range	Offset	RMS Range	RMS
Channel 1	fA	< 750	8.6	< 15	1.2
Channel 2	fA	< 750	10.2	< 15	1.0
Channel 3	fA	< 750	10.2	< 50	2.7
Channel 4	fA	< 750	19.2	< 50	2.9
Channel 5	fA	< 750	26.9	< 50	6.5
Channel 6	fA	< 750	29.8	< 50	6.6
Channel 7	fA	< 750	28.1	< 50	3.9
Channel 8	fA	< 750	31.8	< 50	3.2
Channel 9	fA	< 750	32.5	< 50	4.3
Channel 10	fA	< 750	34.1	< 50	5.0
Channel 11	fA	< 750	61.8	< 50	10.9
Channel 12	fA	< 750	64.1	< 50	6.0
Channel 13	fA	< 750	61.2	< 50	6.2
Channel 14	fA	< 750	65.2	< 50	12.7
Channel 15	fA	< 750	61.5	< 50	3.2
Channel 16	fA	< 750	69.2	< 50	4.1
Channel 17	fA	< 750	62.9	< 50	3.9
Channel 18	fA	< 750	58.3	< 50	3.7
Channel 19	fA	< 750	61.6	< 50	6.7
Channel 20	fA	< 750	59.1	< 50	6.5
Channel 21	fA	< 750	76.1	< 50	4.5
Channel 22	fA	< 1000	56.7	< 125	5.6

External Checks	Units	Nominal	3090/91	Nominal	3090/91	Nominal	3090/91
Analog Input (Ch1)	V	1±0.5	0.99	5±0.5	4.98	9±0.5	8.95
Analog Input (Ch2)	V	1±0.5	1.00	5±0.5	4.99	9±0.5	9.00
Pump Voltages (sheath, sample, extract)	V	6.0-9.5	7.70	11.0-14.0	11.70	6.0-9.0	7.49
Check Trigger (input #1, #2, output)	V	Pass/Fail	PASS	Pass/Fail	N/A	Pass/Fail	PASS
Flow (inlet, outlet / both without cyclone)	LPM	9.6-10.2	9.87	±0.3 inlet	9.72		
Final system leak check	" h2O	< 10 per 5 min	PASS				
Heater Check (output)	A	1±0.3	1.0				

Aerosol Checkout	Units	Standard	3090/3091	% Diff	Tolerance
100nm Classified Emery Oil vs SMPS	nm	98.2	93.06	-5.2%	+/- 10% of Standard
100nm Classified Emery Oil vs CPC 3776	#/cm3	4.40E+04	4.25E+04	-3.4%	+/- 20% of Standard
Polydisperse Emery Oil vs SMPS	nm	98.2	93.06	-5.2%	+/- 10% of Standard
Polydisperse Emery Oil vs CPC 3776	#/cm3	6.63E+03	6.70E+03	1.1%	+/- 20% of Standard

Final Checkout	☑		☑
Inspect Charger Needles	YES	Hi Pot Test	YES
Add Caps to Inlet & Outlet	YES	Visual Inspect Cabinet for Blemishes	YES
Check Power Cord for Destination Country	YES	Clean & Grease Cyclone	YES

Technician: Patrick Abe

Figure 73: Example of theoretical particle loss in a scientifically optimum nvPM sampling system

European Union Aviation Safety Agency

Konrad-Adenauer-Ufer 3
50668 Cologne
Germany

Environmental Research - Engine Emissions | EASA

Mail EASA.research@easa.europa.eu
Web www.easa.europa.eu

An Agency of the European Union